8-1-1994

Development of sensitometric techniques for the characterization of stereolithographic resins

Rudd Matthew Hardesty

Development of Sensitometric Techniques for the Characterization of Stereolitographic Resins.

by

Rudd Matthew Hardesty

B.S. University of South Carolina (1991)

A thesis submitted in partial fulfillment of the requirements for the degree of Master of Science in the Center for Imaging Science in the College of Imaging Arts and Sciences of the Rochester Institute of Technology

July 1994

Signature of Author Rudd M. Hardesty

Accepted by Dana G. Marsh August 29, 1994

Coordinator, M.S. Degree Program

College of Imaging Arts and Sciences
Rochester Institute of Technology
Rochester, New York

Certificate of Approval

M.S. Degree Thesis

The M.S. Degree Thesis of Rudd Matthew Hardesty has been examined and approved by the thesis committee as satisfactory for the thesis requirement of the Master of Science degree.

Dr. Jonathan Arney, Thesis Advisor: _____

Dr. Dana Marsh: _____

Dr. Richard Hailstone: _____

Date: August 29, 1994

Thesis Release Permission
Rochester Institute of Technology
College of Imaging Arts and Sciences

Development of Sensitometric Techniques for the Characterization of Stereolitographic Resins.

I, Rudd Matthew Hardesty, hereby grant permission to the Wallace Memorial Library of R.I.T to reproduce my thesis in whole or in part. Any reproduction will not be for commercial use of profit.

Date: August 29, 1994

Development of Sensitometric Techniques for the Characterization of Stereolitographic Resins.

by

Rudd Matthew Hardesty

Submitted to the Center for Imaging Science in partial fulfillment of the requirements for the Master of Science Degree at the Rochester Institute of Technology.

Abstract:

Four desktop sensitometers of stereolithographic resins were created and tested against the characteristic curves of the resins produced under exposure conditions used with a Stereolithographic Apparatus. Two sensitometers measure the percent conversion as a function of exposure, one measures the optical density, and the fourth is an attempt to reproduce the characteristic curve with an alternate exposure source. It was concluded that the slopes of the characteristic curves can be determined by measuring the optical density of the resins. However, the slopes cannot be determined by measuring the percent conversion of the resins as a function of exposure. The critical exposures of the resins can be determined from the induction periods measured by the percent conversion sensitometers. The characteristic curves produced with the fourth sensitometer have no correlation with the actual characteristic curves.

Acknowledgments

I wish to acknowledge Dr. Jon Arney for his help, enthusiasm and insights in all portions of this project. Thanks to Dr. Marsh and Dr. Hailstone for much help in the completion of my thesis. Thanks to Mr. Lee Sanders for a lot of help with the research and lab work that was involved.

Dedication

This thesis is dedicated to my parents, Richard and Judy Hardesty, for their endless love, their infinite patience and their never ending support.

Table of Contents

List of Figures

List of Tables

Nomenclature

From the working curves:

E_c	=	Critical Exposure
D_p	=	The slope of the working curve (Depth of Polymerization)
100 mW D_p	=	The slope of the working curve determined from using only data points with the laser power set to 100 mW.
800 mW D_p	=	The slope of the working curve determined from using only data points with the laser power set to 800 mW.
C_d	=	Cure Depth

From the Shrinkage Sensitometer:

%S	=	Percent Shrinkage
T_{is}	=	Induction period, in seconds, measured with the shrinkage sensitometer.
T_{hs}	=	Time taken to reach the half shrinkage point.
Γ_s	=	The shrinkage gamma

From the Rate Sensitometer:

H_p	=	The peak height measured from the output of the rate sensitometer
T_{iq}	=	Induction period, in seconds, measured with the rate sensitometer.
T_{hq}	=	Time taken to reach the peak rate.
Γ_{q1}	=	The first rate gamma
Γ_{q2}	=	The second rate gamma

From the Flash Sensitometer:

E_{cf}	=	Critical Exposure, as measured with the flash sensitometer
D_{pf}	=	The slope of working curve as produced with the flash sensitometer.

From the Absorbancy Sensitometer:

O.D.	=	Optical Density

1 Introduction and Summary

1.1 Introduction:

Stereolithography, or Rapid Prototyping, is a three dimensional printing process which uses light sensitive photopolymer resins in the formation of solid images. In 1982, Alan Herbert (Herbert, 1982) introduced the archetype rapid prototyping device. With the first commercially available systems produced in 1988, Rapid Prototyping is still in it's infancy (Jacobs, 1992). Since it's introduction, Rapid Prototyping has seen great advancements in it's technology, both hardware and software, and now, with over 300 StereoLithographic Apparatuses (SLA's) in 17 countries in use today (Jacobs, 1992), it is conceivable that stereolithography may become an indispensable component in design by CAD (Computer Aided Design) software (André, 1993).

The stereolithographic process consists of first designing the prototype part using CAD software. Then the CAD design is entered into an SLA which forms the prototype, layer by layer, by using a laser to solidify a liquid (or in some cases, a powdered) resin. Figure 1.1 shows a schematic drawing of the basic operation of a SLA. In laminated object manufacturing (LOM), a CO_2 laser carves each layer of the prototype in an adhesive material. Although there are many different approaches to the actual formation of the prototype, only one method will be described here, and it should be noted that all the other methods have some similarity to

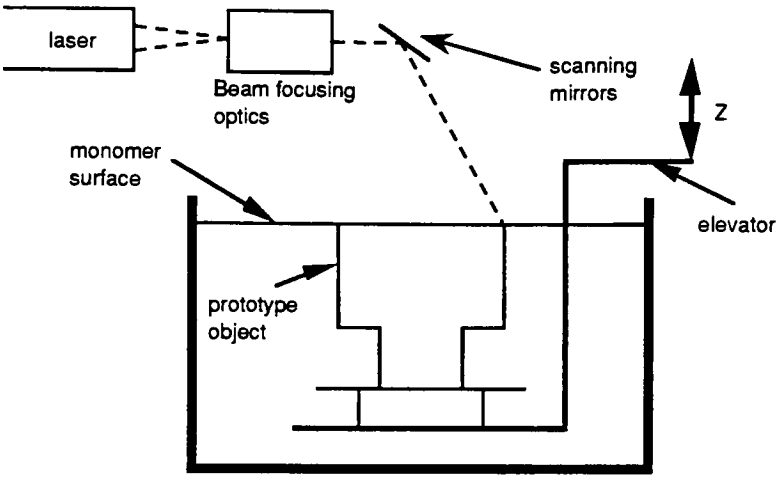

Figure 1.1: Schematic drawing of a SLA device.

this one method. For a more complete listing of alternate rapid prototyping methods, see Rapid Prototyping & Manufacturing, Fundamentals of Stereolithography by Paul F. Jacobs, Ph.D. The examples of time and money saved by using rapid prototyping over conventional methods of part design and manufacture are numerous (See Jacobs, 1992, Chapters 12-15). Designers can now complete in three weeks, from initial design to completed prototype object, what used to take almost six months (Park, 1993).

Along with all the rapid advancements of the hardware and software used in stereolithography, there has been just as many alterations to the photopolymer resins used in the SLA's. After exposure, some resins form hard and brittle objects, while others are soft and, in some cases, flexible. The amount of exposure necessary to induce a reaction varies from resin

to resin, as well as the depth of cure of a resin at a given exposure. Needless to say, the properties of the resin play an important role in the proper development of a prototype object.

For the photopolymers used in rapid prototyping, an understanding of the working curve (depth of cure versus ln(exposure)) is fundamental (Jacobs, 1992). The working curve of any imaging system is necessary for the understanding of how that imaging system responds under a given set of exposure conditions. The working curve for a stereolithographic resin is analogous with the density versus log(exposure) working curve for photographic film. In both cases, the working curve is a property of the material that is measured. Characteristics of the resins can be measured from the stereolithographic working curve, such as the critical exposure necessary to induce any reaction (E_c) and the slope of the working curve (Depth of polymerization, D_p). Figure 1.2 is a typical working curve of a stereolithographic resin, taken from Jacobs' book on rapid prototyping.

A method for determining the characteristics of the resin is called the WINDOWPANE™ diagnostic method, described in detail in Jacobs' book on rapid prototyping. Although the WINDOWPANE™ diagnostic method is extremely precise, it can be rather time consuming and impractical in that the entire vat must be emptied and cleaned before any new resin can be added (250^3 mm^3 for a SLA-250 or approximately 500^3 mm^3 for a SLA-500). This uses a lot of resin to generate a diagnostic part that is just a little larger than a penny. The WINDOWPANE™ diagnostic method would prove to be a burden if, for example, the D_p and E_c values

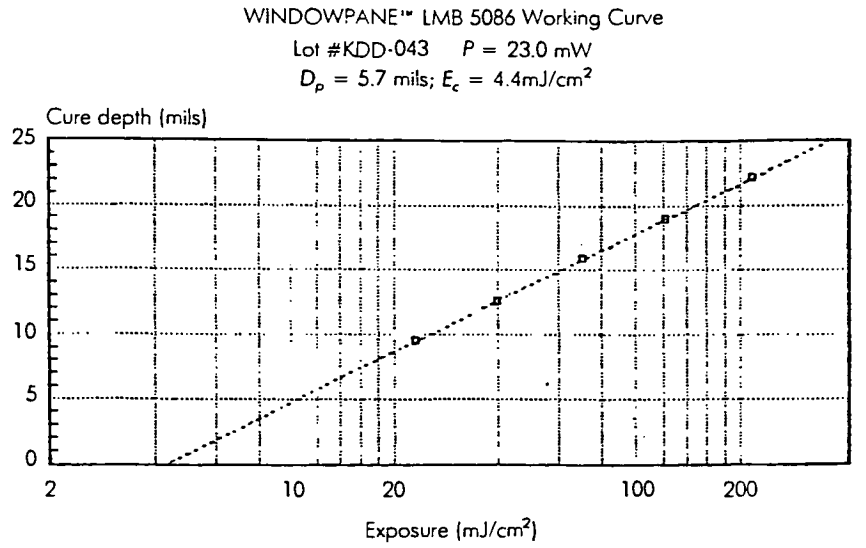

Figure 1.2: Working curve as produced by the WINDOWPANE™ method, (Jacobs, 1992 p.276).

of many different photopolymer resins were to be found. It would be beneficial if a diagnostic method could be devised such that the D_p and E_c values of a resin could be measured external to the SLA, in a minimal amount of time, using a small amount of photopolymer resin.

For this project, four simple and inexpensive methods of measuring the sensitometric properties of stereolithographic resins are used. Two of these methods, the measurement of volume shrinkage and the measurement of the reaction rate, are based on the Reiser model of measuring the sensitometric properties of the resins. The third method is based on the Jacobs model of measuring the optical density of the resins, and the fourth method is an attempt to reproduce the working curves of the resins by using a camera flash as an alternate exposure source. These

four sensitometers are evaluated in terms of their ability to correlate with the D_p and E_c data measured from the working curves of the resins. The working curves will be produced by measuring depth versus ln(exposure) using an ultraviolet laser and General Dynamics laser scanning device, controlled by our own software.

1.2 Reiser Model

We know that the depth of cure of a polymer sample varies with exposure because polymerization occurs. Therefore, by monitoring polymerization versus exposure, an indirect measure of depth versus exposure can be made. Two convenient and inexpensive methods of measuring polymerization are 1) measuring the volume shrinkage during polymerization (the shrinkage sensitometer) and 2) measuring the rate of heat output during polymerization (the rate sensitometer).

According to Reiser (Reiser, 1989), the fundamental measurement of the sensitometric properties of a photopolymer is the percentage of monomer converted to polymer (%C) as a function of exposure (E), where exposure is intensity multiplied by time. The final output of the imaging process (depth of cure, refractive index change, etc.) is a function of the percent conversion. (See figure 1.3). As an indirect measure of conversion, the first two sensitometers will measure 1) the percent shrinkage as a function of exposure time and 2) the rate of heat generation during polymerization as a function of exposure time, where two different

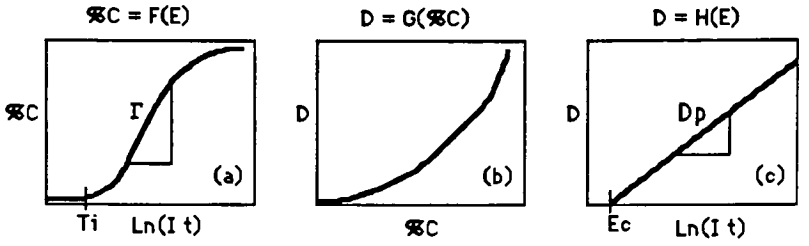

Figure 1.3: (a) Percent conversion as a function F of exposure, the chemical kinetic curve, %C = F(E). (b) Depth as a function G of percent conversion, D = G(%C). (c) Depth as a function H of exposure, D = H(E).

constant intensity ultraviolet lamps are used as exposure sources in both sensitometers. This gives a total of four experiments for monitoring the polymerization of the resins, two different intensity ultraviolet lamps used with both the shrinkage and the rate sensitometer. It will be shown that both shrinkage and rate are directly related to chemical conversion.

If, in figure 1.3, function G is known, then by measuring conversion as a function of exposure, depth as a function of exposure can be easily determined. The assumption is that for similar resins, the function G is similar, and the major factor governing differences in the sensitometric behavior of the resins is due to the fundamental percent conversion versus exposure curve, or the chemical kinetics of the photopolymerization process. The first two sensitometers will determine if, by measuring conversion as a function of exposure, an indirect measure of depth as a function of exposure can be made.

With the hopes of rejecting our null hypothesis (H_0), and thus accepting our alternate hypothesis (H_1), we will hypothesize that there is no correlation between the induction period measured with the conversion sensitometers (T_i) and the critical exposure (E_c) measured from the working curve.

$$H_0: \quad \rho = 0, \text{ for } T_i \propto E_c \qquad (1.1)$$
$$H_1: \quad \rho \neq 0, \text{ for } T_i \propto E_c \qquad (1.2)$$

According to Dougherty (Dougherty, 1990), with the hypothesis test designed in this way, a rejection of H_0, and thus the acceptance of H_1, "not only determines that there is some partial linear relationship between the variables, but also that they are not independent."

The second null hypothesis regarding the two conversion sensitometers is that there will be no correlation between the slope of conversion versus ln(time) graph (G in figure 1.3a) and the slope of the working curve, D_p. Again, we hope that the data will show that we can reject the null hypothesis, and thus accept the alternate hypothesis, that there is a correlation between Γ and D_p.

$$H_0: \quad \rho = 0, \text{ for } \Gamma \propto D_p \qquad (1.3)$$
$$H_1: \quad \rho \neq 0, \text{ for } \Gamma \propto D_p \qquad (1.4)$$

1.3 Jacobs Model

The third sensitometer is a test of Jacobs' model of the working curve, in which the optical density of the resins is inversely proportional to D_p. According to Jacobs, the working curve of stereolithographic resins can be derived from the Beer-Lambert law of absorption, in which the optical density is inversely proportional to D_p. The absorbancy sensitometer will measure the optical density of the resins. Again we state our null hypothesis in the hopes that we can reject the null hypothesis in favor of the alternate hypothesis. Our null hypothesis for the absorbancy sensitometer is that there will be no correlation between the optical density (OD) and the inverse of the slope of the working curve ($1/D_p$).

$$H_0: \quad \rho = 0, \text{ for } OD \propto 1/D_p \qquad (1.5)$$

$$H_1: \quad \rho \neq 0, \text{ for } OD \propto 1/D_p \qquad (1.6)$$

1.4 Alternate Exposure Source Working Curves

The fourth sensitometer, called the flash sensitometer, is an attempt to reproduce the working curve for stereolithographic resins by using an alternative exposure source. Like the working curve produced with the laser, a slope and an exposure axis intercept can be found to give D_{pf} and E_{cf}, where the f indicates the values were obtained with the flash sensitometer. As with the previous sensitometers, we will design our hypothesis with the hopes of rejecting the null hypothesis and thus

accepting the alternate hypothesis. The first null hypothesis is that the critical exposure measured with the flash sensitometer (E_{cf}) will not correlate with the critical exposure measured from the working curve (E_c).

$$H_0: \quad \rho = 0, \text{ for } E_{cf} \propto E_c \qquad (1.7)$$
$$H_1: \quad \rho \neq 0, \text{ for } E_{cf} \propto E_c \qquad (1.8)$$

The second null hypothesis is that the slope of the flash sensitometer's working curve (D_{pf}) will not correlate with D_p, the slope of the working curve.

$$H_0: \quad \rho = 0, \text{ for } D_{pf} \propto D_p \qquad (1.9)$$
$$H_1: \quad \rho \neq 0, \text{ for } D_{pf} \propto D_p \qquad (1.10)$$

1.5 Summary of Results:

The results of these experiments show that the shrinkage and the rate sensitometers are capable of measuring the critical exposure of the resins. However, the slope (Γ) of the chemical kinetic curve as measured by the shrinkage and rate sensitometers does not correlate with the slope of the working curve (D_p), in contrast to what is predicted by Reiser's fundamental measurement of the sensitometric properties of a photopolymer. The only exception to this was when Γ was measured with the rate sensitometer using a high intensity UV lamp as the exposure source.

The optical density of the resins as measured with the absorbancy sensitometer shows a high correlation with the inverse of the slope of the

working curves, as is predicted by the Jacobs model of the working curves. The optical density of the resins could be used as a predictor of the slope of the working curves. If the characteristics of a resin were to be measured external to a SLA, two devices would be needed. One to measure an induction period, and the other to measure the optical density.

The flash sensitometer is a simple attempt to reproduce the working curves of the resins using an alternate exposure source. The results of the flash sensitometer experiment show that this sensitometer is capable of measuring the critical exposure of the resins. However, the slope (D_{pf}) of the flash working curve does not correlate with the slope (D_p) of the laser scanner working curve.

The results indicate that the shrinkage sensitometer, rate sensitometer and the flash sensitometer are capable of measuring the critical exposure of the resins. Before they could do so, however, they would have to be calibrated for greater precision. These three sensitometers could not be used as an indirect measure of D_p. The optical density of the resins as measured by the absorbancy sensitometer is capable of determining the D_p value of the resins.

2 Background

2.1 The Reiser Model

In brief, when a resin polymerizes, the individual monomer molecules that make up the resin join together to form large polymer chains. To start the reaction, however, it is necessary to include a light sensitive initiator, called a photoinitiator. A photoinitiator is a molecule, or a molecular system, that is capable of forming free radicals upon irradiation with light (Reiser, 1989). Free radicals are molecules that have an unpaired electron in a molecular orbital. Photoinitiators are included in the design of photopolymer resins as they 'jump start' the reaction.

$$I_n + h\nu \longrightarrow 2R\cdot \qquad (2.1)$$

$$R\cdot + O_2 \longrightarrow (\text{inert}) \qquad (2.2)$$

$$R\cdot + M \longrightarrow RM\cdot + (\text{heat}) \qquad (2.3)$$

$$RM\cdot + M \longrightarrow RMM\cdot + (\text{heat}) \qquad (2.4)$$

$$R\cdot + R\cdot \longrightarrow RR\ (\text{inert}) \qquad (2.5)$$

$$R\cdot \longrightarrow (\text{inert}) \qquad (2.6)$$

The polymerization process consists of four major parts. The sequence of reactions is outlined above, where I_n stands for initiator, $R\cdot$ for a free radical with the available electron, and M stands for monomer. First is the generation of free radicals by the initiator (2.1). Second is the induction

period that results from the radical's consumption of dissolved oxygen in the system (2.2). The third step is the formation of large polymer chains (2.3 and 2.4), and the fourth is termination of the reaction. Termination of the reaction can occur when two radicals react to form an inert molecule (2.5), or when a polymer chain doubles back on itself and the free radical becomes trapped (2.6).

The fundamental measurement of the sensitometric properties of a photopolymer is the percentage of monomer converted to polymer as a function of exposure, %C = F(E) (Reiser, 1989). For the shrinkage and the rate sensitometers, the intensity of the exposure source is held constant, so we can simplify percent conversion to a function of the time of exposure, %C = F(t). The method of determining the percent conversion from the measurement of shrinkage and rate is given in the next two sections, 2.1.1 "Finding Percent Conversion from the Measurement of Shrinkage" and 2.1.2 "Finding Percent Conversion from the Measurement of Rate."

2.1.1 Finding Percent Conversion from the Measurement of Shrinkage

In 1950, Frank S. Nichols used the molecular size of a monomer molecule as a predictor of the percent shrinkage observed during polymerization. Specifically, he found that molecular size was inversely proportional to the observed shrinkage (Nichols, 1950). The compensation for shrinkage in photopolymer resins that are used in Rapid Prototyping is of major concern to the users of this technology.

During the polymerization process, the initial volume that the monomer occupies decreases; the photopolymer resin shrinks. The total volume that a monomer occupies before exposure is made up of the molecular size of the molecule added to the free volume of the molecule. The free volume is the volume the molecule occupies due to it's vibrational, rotational and translational degrees of freedom (Flory, 1964; van Krevelen, 1990). Before exposure, the monomer has three translational degrees freedom, three rotational degrees of freedom and many vibrational degrees of freedom. When large polymer chains are formed during exposure, the molecules cannot rotate, translate and vibrate as they once did, and this loss of some degrees of freedom means a loss of volume.

Each monomer molecule that is added to the polymer chain causes some loss of volume. Therefore, by measuring the shrinkage of the monomer, an indirect measure of the number of molecules that reacted to form polymer chains is made. In reference back to figure 1.3, a measure of conversion as a function of exposure is being made. Correlations of this sensitometric measurement with the depth versus exposure working curves can be made.

In a paper by J. G. Kloosterboer (Kloosterboer, 1988(a)), the idea of measuring linear shrinkage as an indicator of total volume shrinkage is made. Volume shrinkage is the change in volume divided by the initial volume, expressed as a percentage, as given in equation 2.7.

$$\%S = \frac{\Delta V}{V_0} \qquad (2.7)$$

If the resins were to shrink equally in each direction (X, Y, Z as given in figure 2.1), then for a very thin sample with a large surface area, we would expect to see some lateral movement in the X and Y direction. However, this is not observed. For a sample that is much thinner than it is wide, the majority of the shrinkage will occur in the smallest direction, Z, as shown in figure 2.1. Therefore, by measuring the linear shrinkage, a measure of the total volume shrinkage is being made.

$$\boxed{\%S = \frac{\Delta Z}{Z_0}} \qquad (2.8)$$

Kloosterboer measured shrinkage using a linear displacement transducer, as was done in this research. According to Kloosterboer, volume shrinkage can be measured by monitoring the decrease in thickness of a sample composed of two glass plates with a thin layer of resin in between. Kloosterboer also assumes, as is assumed here, that the

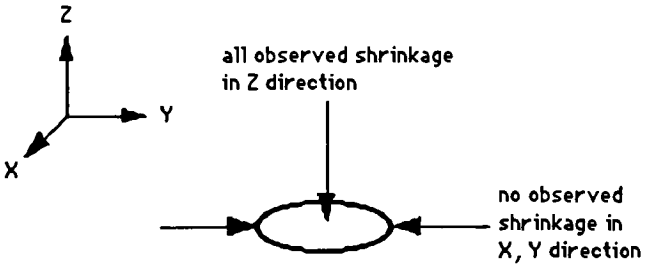

Figure 2.1: Schematic drawing of a drop of resin, showing where the majority of shrinkage occurs.

majority of the volume change will occur as a decrease in thickness of sample, provided that there is good adhesion of the polymer to the glass plates.

J. DeBoer (DeBoer,1992), in a paper on measuring volume change during polymerization, states "the large area-to-thickness ratio of the sample justifies the assumption that, although the measurement is one dimensional, a volume shrinkage is determined." DeBoer used a different method of measuring shrinkage than the method used in this research (he used an interferometer to monitor the displacement of the surface of the resin as it shrinks). However his assumptions about linear shrinkage as a measure of total volume shrinkage for thin samples applies to this research.

Another article employing the use of a linear displacement transducer to measure shrinkage in thin layer monomer samples is authored by D.C. Watts (Watts,1991). Watts states that "the fractional linear shrinkage measured is approximately equivalent to the fractional volumetric shrinkage." The method of measuring shrinkage employed in this research is strongly supported in the literature. Provided the samples are thin enough, the shrinkage measured in a linear direction will give an accurate measurement of the total volume change that occurs during polymerization.

An example output from the shrinkage sensitometer is shown in figure 2.2. The graph shows the characteristic induction period (T_{is}) that results from the consumption of oxygen dissolved in the resin. Once the

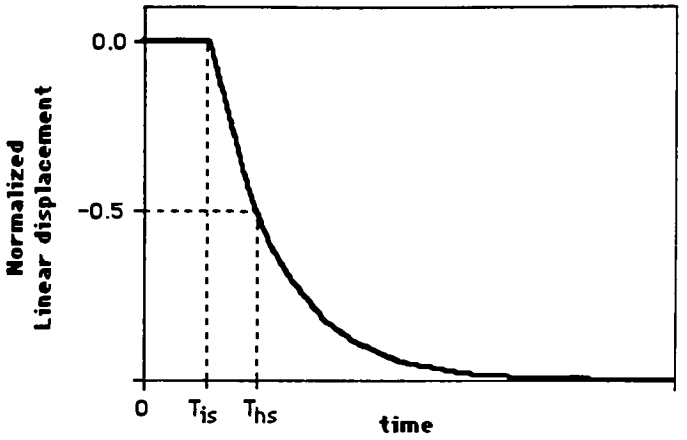

Figure 2.2: An example output from the Shrinkage Sensitometer.

oxygen is consumed, the resin begins to polymerize, and shrinkage occurs. The linear displacement, ΔZ, is shown as a negative displacement because in the experimental setup, the pin of the positional transducer is moving down, the conventionally negative direction. Linear displacement and shrinkage are, however, expressed as positive values for ease of use and calculations.

Figure 2.2 shows the displacement of the positional transducer as a function of time, and should not be confused with a plot of shrinkage versus time. Shrinkage increases as a function of time, and can be found from the graph of displacement versus time by simply dividing the initial thickness of the sample into $\Delta Z(t)$.

Figure 2.3 is an example of the normalized shrinkage as a function of the logarithm of time. Recalling that shrinkage is a measure of the percent conversion of the monomer, we see that figure 2.3 represents

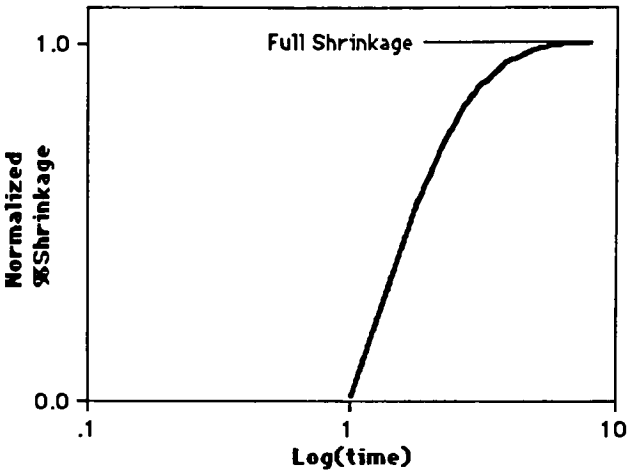

Figure 2.3: An example of shrinkage as a function of the logarithm of time.

Reiser's fundamental measurement of the sensitometric properties of a photopolymer (See figure 1.3(a)). Then, according to the Reiser model, the induction period measured by the shrinkage sensitometer should be proportional to the critical exposure as measured from the working curves produced by the laser scanner. Also, the slope of figure 2.3 should be proportional to the slope of the working curve, D_p.

Along with the induction period and percent shrinkage measured from the output of the shrinkage sensitometer, the slope of the shrinkage as a function of log(time) graph (figure 2.3) will also be measured. This slope is referred to as the shrinkage gamma, Γ_s.

$$\Gamma_s = \frac{\Delta S}{\Delta \log(t)} \qquad (2.9)$$

The logarithm of the time is used for two reasons. First, the slope of the working curve is expressed as Δ(Depth) divided by ΔLog(Exposure), so one would expect a higher correlation between Γ_s and D_p if they are in the same format. Secondly, if ΔZ decreases exponentially, as is hinted at in figure 2.3, then shrinkage will increase as a logarithmic function. Therefore a plot of shrinkage as a function of log(time) will be linear.

To simplify the calculation of Γ_s, it will be evaluated at the same point for each resin, the half shrinkage point, ΔS = 0.5. Because we are interested in the relative measure of the Γ_s values, not in the actual value itself, the numerator can be normalized to one. At the half shrinkage point, the denominator in equation 2.9 becomes $\log(T_{hs}) - \log(T_{is})$ where T_{hs} is the time taken to reach half shrinkage and T_{is} is the shrinkage induction period. Both T_{hs} and T_{is} are measured from the moment the exposure source is turned on. The equation for the slope of the shrinkage curve then becomes:

$$\boxed{\Gamma_s = \frac{1}{\log(T_{hs}/T_{is})}} \qquad (2.10)$$

2.1.2 Finding Percent Conversion from the Measurement of Rate

In the measurement of the kinetic rate of photopolymerization, Gozzelino (1992), employs an experimental setup similar to the one used in this research. A thin layer of monomer is applied to the surface of a thermopile, and exposed. The heat flow through the detector is a measure

of the rate of the reaction. This is also supported through work done by Kloosterboer (1988).

In the formation of polymer, each monomer bond that breaks and reattaches to another monomer releases a certain amount of energy in the form of heat (Hoyle, 1992). Therefore, the rate of heat production is directly proportional to the rate of polymerization (Reiser, 1989). By measuring the rate of heat production, a direct correlation can be made to the rate of polymerization.

The rate that a monomer converts into polymer is dependant on the initial concentration of the monomer molecules, the concentration of free radicals and the intensity of the light used in exposure. Polymer chains can only be built as fast as free radicals are formed. Termination of the polymerization reaction can occur through two methods, two radicals can react and form an inert molecule, or long polymer chains can enclose a free radical leaving it unreachable. These reaction equations are shown as equations 2.11 through 2.14 below where the square brackets indicate concentration. In the equations below, I_n is the initiator, K is the rate constant for the formation of free radicals, I_0 is the intensity of the exposure source, k_p is the propagation constant, k_{t1} and k_{t2} are termination constants, and q is a unit of heat.

Reaction Equation:	Reaction Rate:	
$I_n \longrightarrow R\cdot$	KI_0	(2.11)
$R\cdot + M \rightarrow RM\cdot + (q)$	$k_p[R\cdot][M]$	(2.12)
$R\cdot + R\cdot \rightarrow RR$ (inert)	$k_{t1}[R\cdot]^2$	(2.13)
$R\cdot \rightarrow$ (inert)	$k_{t2}[R\cdot]$	(2.14)

We are interested in the formation of polymer where the rate of formation of polymer is the negative of the rate of disappearance of monomer. The formation rate of polymer was given above in equation 2.12. Then, the rate of disappearance of monomer is:

$$-\frac{d[M]}{dt} = k_p[R\cdot][M] \qquad (2.15)$$

To simplify this equation, the concentration of radicals needs to be found. When the system is in a steady state, the formation rates and termination rates of radicals are the same. There is one method of forming free radicals and two methods that the free radical concentration can be depleted. Each case will be considered separately. First, if free radicals can only be terminated by reacting with another free radical, then in an equilibrium state, we can equate the formation rate and the termination rate of free radicals.

$$KI_0 = k_{t1}[R\cdot]^2 \qquad (2.16)$$

$$[R\cdot] = \sqrt{\frac{KI_0}{k_{t1}}} \qquad (2.17)$$

Note that for this case, a doubling of intensity would not double the free radical concentration. In other words, the system would fail reciprocity.

In the second case, we assume that the termination of free radicals can only occur when a free radical becomes trapped in a long polymer chain. Then in equilibrium, the rate of formation of free radicals is equal to the rate of termination of free radicals.

$$KI_0 = k_{t2}[R\cdot] \qquad (2.18)$$

$$[R\cdot] = \frac{KI_0}{k_{t2}} \qquad (2.19)$$

In this situation, a doubling of the intensity yields a doubling of the free radical concentration, i.e., there is no reciprocity failure. In realistic situations, the termination of the reaction occurs at some combination of the two termination rates discussed above. Depending on the monomer's molecular structure, one of the two termination rates discussed above will be favored. A general form for the equilibrium state of the free radical concentration is given as equation 2.20.

$$[R\cdot] = \left[\frac{KI}{k_t}\right]^n \text{ where } \frac{1}{2} \leq n \leq 1 \qquad (2.20)$$

The concentration of free radicals is now known, and is a collection of constants and a function of the intensity of source. As long as the exponent n remains constant, the free radical concentration remains constant. This can be plugged back in to equation 2.15 equating the rate of disappearance of monomer with the rate of formation of polymer.

$$-\frac{d[M]}{dt} = k_p\left[\frac{KI}{k_t}\right]^n [M] \qquad (2.21)$$

To find the monomer concentration as a function of time of exposure, the above equation needs to be integrated. Separating the equation into

monomer concentration on the left and time on the right yields an easily integratable equation. Assuming n is constant and collecting the constants k_p, k_t, K and I into one observed constant, k_{obs}, results in:

$$-\frac{d[M]}{[M]} = k_{obs}\, dt \qquad (2.22)$$

Integration of each side then yields the monomer concentration as a function of time, plus some constant of integration.

$$-\ln([M]) = k_{obs}\, t + (\text{const.}) \qquad (2.23)$$

To find the value of the constant of integration, the above equation is evaluated at time (t) equal to zero ($k_{obs}\, t = 0$). Also realizing that at $t = 0$, the concentration of monomer is the initial monomer concentration, [M] = $[M_0]$. So then:

$$-\ln([M_0]) = (\text{const.}) \qquad (2.24)$$

Plugging this back into equation 2.23, we arrive at:

$$-\ln([M]) = k_{obs}\, t - \ln([M_0]) \qquad (2.25)$$

This can be further simplified by moving $\ln([M_0])$ to the left hand side of the equation. Further simplification results from the properties of the logarithmic function.

$$\ln([M_0]) - \ln([M]) = k_{obs}\, t \qquad (2.26)$$

$$\boxed{\ln\left[\frac{[M_0]}{[M]}\right] = k_{obs}\, t} \qquad (2.27)$$

$$[M] = \frac{[M_0]}{\exp(k_{obs}t)} \qquad (2.28)$$

A plot of equation 2.28, monomer concentration as a function of time, is shown in figure 2.4 as the solid line. The disappearance of monomer is directly proportional to the appearance of heat, so it is expected that the total heat output as a function of time will increase while the monomer concentration decreases. This is also shown in figure 2.4 as the dotted line.

To measure the rate of disappearance of the monomer, we measure the rate of generation of heat (dQ/dt). An example output from the Rate Sensitometer is shown in figure 2.5. Notice the curve shows an induction period (T_{iq}) due to the consumption of oxygen in the system. The

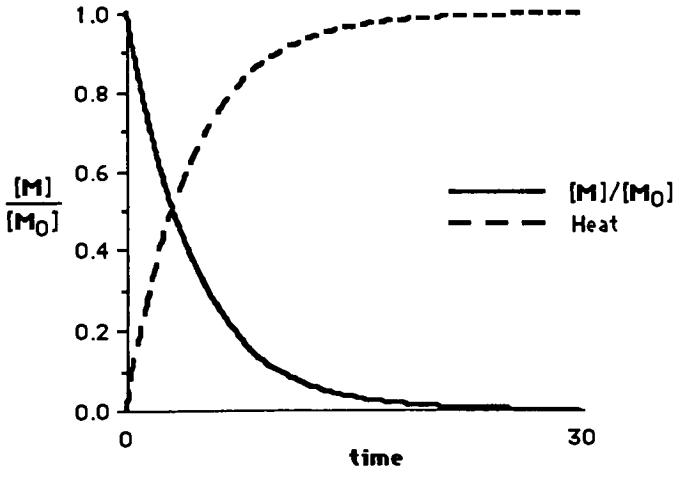

Figure 2.4: The exponential decay of the monomer concentration (solid line) and the cumulative heat output during polymerization (dotted line).

generation of heat quickly reaches a peak when the greatest number of monomers are forming polymer chains. The reaction slowly tapers off, as more and more free radicals are terminated either by colliding with each other or by becoming entrapped within a large polymer chain.

Integration of the rate curve with respect to time will give the total amount of chemistry done in the reaction. If each radical - monomer reaction that occurs generates one unit of heat, then the total heat output is a measure of the total number of bonds that broke and reattached to form polymer chains. This is an indirect measure of the percent conversion as a function of exposure. It is expected that each photopolymer resin will react at different rates, thus allowing the rate sensitometer to be a good tool in differentiating between photopolymer resins.

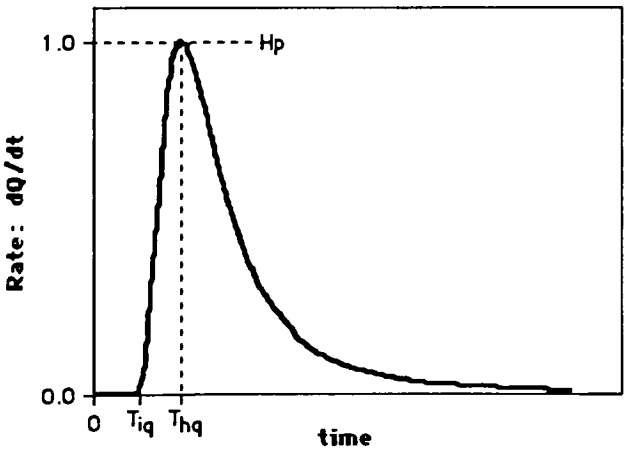

Figure 2.5: Example output from the Rate Sensitometer showing the rate of reaction as a function of time.

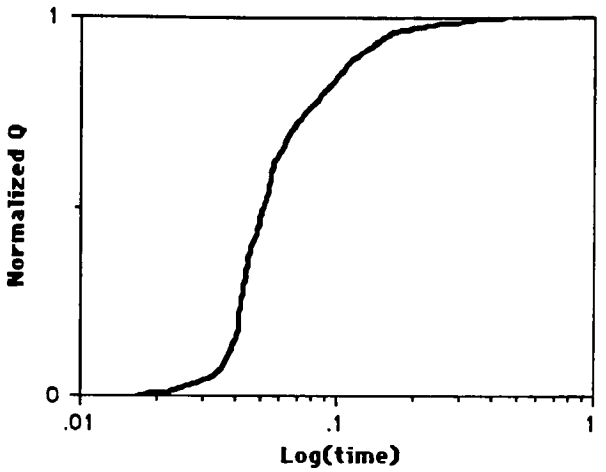

Figure 2.6: An example of the total heat output as a function of the logarithm of time.

Figure 2.6 is a graph of the total heat output as a function of the logarithm of time. Recalling that the cumulative heat output is an indirect measure of the percent conversion of the monomer as it converts to polymer, we see that figure 2.6 represents Reiser's fundamental measurement of the sensitometric properties of a photopolymer (See figure 1.3a). Then, according to the Reiser model, the induction period measured by the rate sensitometer should be proportional to the critical exposure as measured from the working curves produced by the laser scanner. Also, the slope of figure 2.6 should be proportional to the slope of the working curve, D_p. The slope of figure 2.6 is found by taking the derivative of Q(t) with respect to the logarithm of time. The first rate gamma, Γ_{q1} equation 2.29, is defined to be this derivative.

$$\Gamma_{q1} = \frac{dQ}{d[\log(t)]} \qquad (2.29)$$

To simplify this equation, recall that the output of the rate sensitometer measures dQ/dt as a function of time (figure 2.5). At any particular time t, the height of the output, H, from the rate sensitometer is equal to dQ/dt.

$$H = \frac{dQ}{dt} \qquad (2.30)$$

$$H\,dt = dQ \qquad (2.31)$$

Substituting equation 2.31 into equation 2.29 results in:

$$\Gamma_{q1} = \frac{H\,dt}{d[\log(t)]} \qquad (2.32)$$

Further simplification comes from recognizing that d[log(t)]/dt can be easily calculated. The derivative of a logarithm can be simplified as follows:

$$\frac{d[\log(t)]}{dt} = \frac{\log(e)}{t} = \frac{0.4343}{t} = \frac{1}{2.303\,t} \qquad (2.33)$$

Substituting the end result of equation 2.33 into equation 2.32, results in the time dependent form of Γ_{q1}.

$$\Gamma_{q1} = 2.303\,H\,t \qquad (2.34)$$

At $t = T_{hq}$ (from figure 2.5), $H = H_p$, the peak rate measured from the rate sensitometer. The final form of Γ_{q1}, in terms of constants easily measured from the output of the rate sensitometer, is given as equation 2.35.

$$\boxed{\Gamma_{q1} = 2.303\, H_p\, T_{hq}} \qquad (2.35)$$

It is known from pretesting of known resins, that there is a lot of variability in the value of H_p. Therefore, a second rate gamma, Γ_{q2}, is used that is formulated to closely resemble the gamma obtained for the shrinkage sensitometer, Γ_s. Without any mathematical or physical justification the second rate gamma is based only on values that contain little variability in their measurements, T_{iq} and T_{hq}.

$$\boxed{\Gamma_{q2} = \frac{1}{\log(T_{hq}/T_{iq})}} \qquad (2.36)$$

2.2 Jacobs Model of the Working Curve

The best procedure to measure cure depth as a function of exposure is the WINDOWPANE™ method as discussed in Jacobs' book on Rapid Prototyping. The LADDER method that is employed in this research is very similar to the WINDOWPANE™ method, and is also based on the development of any imaging system's working curve. The working curve, or characteristic curve, is the curve that results from measuring a characteristic response of an imaging system at various exposures. For

stereolithography, this characteristic response is the depth of cure measured as a function of exposure.

To derive the stereolithographic working curve equation from the fundamental properties of an imaging system, it is necessary to examine the relationship between depth and exposure. In the stereolithographic process, a laser beam strikes the surface of the photopolymer resin with some intensity, I_0. The exposure at the surface of the resin, E_0, is given by the intensity of the laser multiplied by the time of exposure: $E_0 = I_0 t$. According to the Beer-Lambert exponential law of absorption, the intensity at a given depth x falls off with an exponential decay:

$$I_x = I_0 e^{-K x} \qquad (2.37)$$

where K is a constant, to be discussed later, intrinsic to the material. By multiplying each side of the above equation by time, and recalling that exposure is intensity multiplied by time, we have:

$$E_x = E_0 e^{-K x} \qquad (2.38)$$

Solving this equation for x results in equation 2.39.

$$x = \frac{1}{K} \ln\left(\frac{E_0}{E_x}\right) \qquad (2.39)$$

For the photopolymer to solidify, the exposure it receives needs to exceed some critical exposure, E_c. As the exposure decreases depthwise into the resin, there will be a particular cure depth, C_d, at which the exposure is equal to E_c. All of the monomer above C_d (closer to the

surface) will exceed the critical exposure (E_c) to convert to polymer, and all the monomer below C_d will not reach the critical exposure and remain monomer. Plugging C_d in for x, and noting that E_x is now equal to E_c:

$$C_d = \frac{1}{K} \ln\left(\frac{E_0}{E_c}\right) \qquad (2.40)$$

Equation 2.40 gives the maximum depth that can be polymerized at a given laser exposure E_0. By varying the laser exposure, the cure depth, C_d, can be calculated as a function of laser exposure. A semilog plot of equation 2.40 is shown in figure 2.7. The similarities of figure 2.7 to figure 1.2 is evident. It is important to note from figure 2.7 that the value of K, or rather, 1/K, controls the slope of the plot. The slope of the working curve

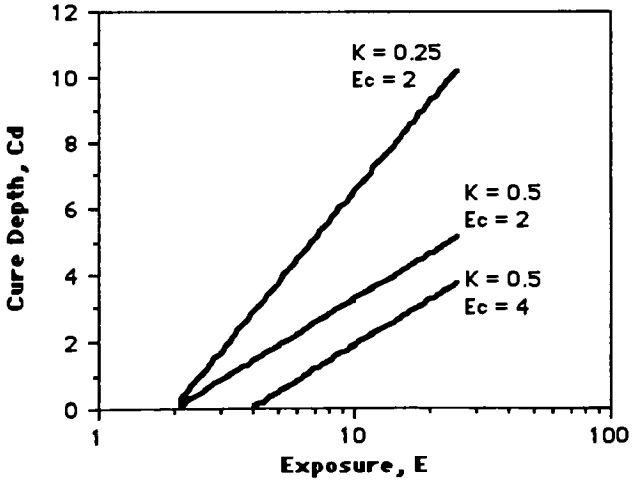

Figure 2.7: A plot of the Working Curve Equation, graphed with arbitrary units of exposure and depth.

is commonly referred to as D_p, or Depth of Polymerization. The value of E_c, the critical exposure, is the intercept of the line with the exposure axis.

The constant K is an intrinsic property of the resin, determined by the Beer-Lambert law of absorption. This constant is the product of the extinction coefficient of the material, denoted by ε (epsilon), and the concentration, C, of the solution, ($K = \varepsilon C$). As was shown previously, D_p is inversely proportional to K, so at a fixed thickness of the resin (x), D_p is inversely proportional to the optical density of the resin, where the optical density is the product of ε, C and x. Resins that have a very low optical density will have a high D_p value, and will also have a deeper cure depth for a given exposure than a resin with a high optical density.

As an indirect measure of the D_p value of a resin, the fourth sensitometer will measure the absorbancy of the resins in the ultraviolet range of light. The terms absorbance and optical density refer to the same measurement, and will be used interchangeably. Optical density is defined as the logarithm of the ratio of the reference irradiance to the sample irradiance.

$$\text{Optical Density} = \log\left[\frac{I_0}{I}\right] \qquad (2.41)$$

To measure absorbancy, an ultra-violet spectrophotometer will be used. The instrument uses a wavelength tunable source, which shines light through a vial containing the sample. A detector then measures the intensity of light that makes it through the vial. When the vial contains a reference material (acetone, for this experiment) with no sample, the

measured intensity is referred to as I_0. When the resin sample is added (diluted by the reference material), the intensity of light reaching the detector is I, the sample intensity.

This experiment is valid for only those resins that obey the Beer-Lambert law of absorption. Resins that contain light scattering materials will not obey the Beer-Lambert law of absorption, and the experimentally measured absorption of such resins may not follow the Jacobs model, which is based on the Beer-Lambert law. The resins at working strength, are too thick and viscous to be used in the spectrophotometer (they absorb all the light), so they are diluted with acetone. Acetone is used because it does not absorb in the part of the UV spectrum where measurements are taken.

2.3 Flash Exposure Working Curves

The third sensitometer is an attempt to reproduce the working curves of the resins by using an alternative source for exposure. Rather than have to produce working curves on an SLA, a small, convenient, desk top method of measuring the working curves was designed. A flash source (Vivitar 285 HV) intended for use with a camera, was used as the exposure source. The plastic, UV absorbing cover was removed from in front of the bulb, and the flash unit was mounted above a dish of resin. Depth is then measured as a function of the number of flashes that the resin receives. A pseudo working curve is produced, and the D_{pf} and E_{cf} values are

measured, where the f indicates that the values were found using the flash sensitometer.

The flash sensitometer produces working curves that are in units of Depth versus log(#Flashes). The actual amount of exposure that the resin receives is unknown, so therefore, the units of D_{pf} and E_{cf} are arbitrary. There should be a high correlation of D_p to D_{pf} and E_c to E_{cf} if the flash sensitometer is reliable at reproducing the working curve made with a UV laser.

3.1 LADDER Method of producing working curves

The WINDOWPANE™ method of measuring the working curves of the resins is described in detail in Jacobs book on rapid prototyping (Jacobs, 1992). Figure 3.1 is a diagram of the WINDOWPANE™ diagnostic part as given in Jacobs book (Jacobs, 1992 p. 271), where CD1 through CD5 are the different cure depths obtained at increasing exposures. The design of the LADDER diagnostic part used in this experiment is based on the WINDOWPANE™ method, using a General Dynamics laser scanning device, driven by our own software.

The LADDER method of determining the working curves of the resins

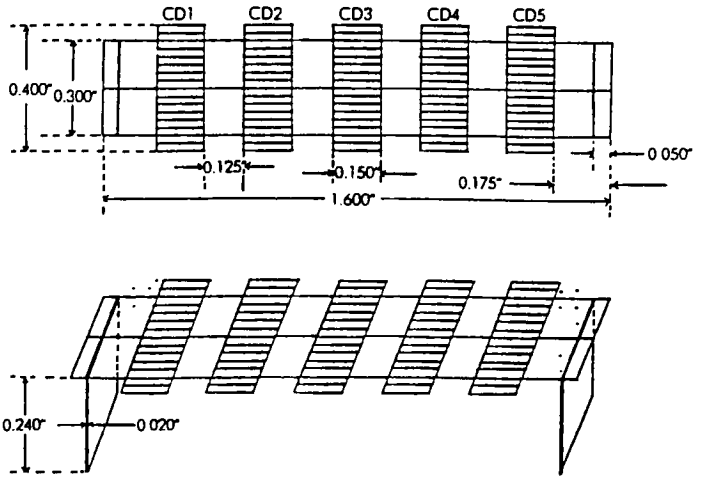

Figure 3.1: Schematic drawing of the WINDOWPANE™ diagnostic part, as developed by 3D Systems, Inc. (Jacobs, 1992 p. 271)

was accomplished using a high powered laser, which emits several bands of wavelengths from 333.6 nm to 363.8 nm in the ultra-violet range of the spectrum. Scanning mirrors reflect the laser downward toward the sample resin, and the motion of the mirrors controls the motion of the laser spot on the surface of the resin sample. The speed and the position of the mirrors is controlled through the computer program.

The laser is scanned onto the surface of the resin in the form of a five rung ladder, where each rung of the ladder is twice the exposure of the previous. Figure 3.2 shows an example of a LADDER output, where the grey areas are support structure and the white areas are the measurable rungs. The resin is contained in a small, approximately 10 centimeter diameter, glass petri dish. The dish itself sits on a piece of black paper to absorb any stray light.

After the step wedge is built, it is removed from the dish of resin and washed in alcohol to remove any excess, unexposed monomer. Once the

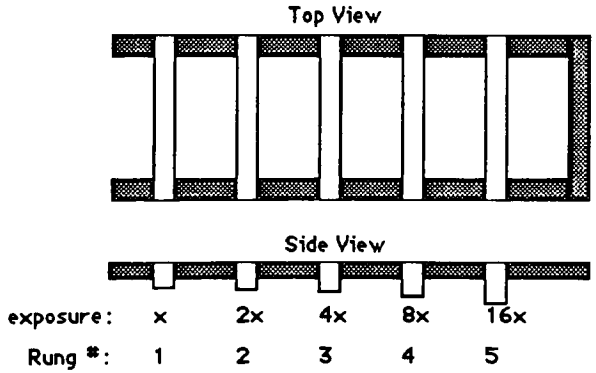

Figure 3.2: Top and side view of the LADDER diagnostic part.

ladder is cleaned, it is placed under an ultraviolet lamp for a final curing. Measurements of the step wedges are made with a digital micrometer, sensitive to 1 micrometer.

Six different programs were designed to control the speed of the laser over the surface of the resin. The programs are referred to by their number, and the ladders are referred to by the program that made them. Therefore program two creates ladder two, with five rungs of different exposure. Program six has the fastest scan times (lowest exposure) and program one has the slowest scan times (highest exposure). LADDERs are made for each of the eighteen stereolithographic resins under two laser powers, 100 milliwatts (mW) and 800 mW, for a total of 36 working curves. If D_p and E_c are independent of the laser intensity (no reciprocity failure) we expect the working curves produced at 100 mW and 800 mW to overlap.

The exposure that a spot of resin on the surface of the petri dish receives is a function of the intensity of the laser, the surface area of the laser beam, and the speed at which the laser passes over the spot. The program that controls the mirrors is designed to scan a set distance in a set time. The rung with the highest exposure is designed so that the laser takes four seconds to travel 4.63 cm. The scan times for every rung of every ladder is given in table 3.1. The velocity of the laser beam is then the scanned distance (4.63 cm) divided by the scan time (4 seconds), or 1.16 cm/second.

The exposure of a spot of resin is the intensity of the laser multiplied by

	Ladder #1	Ladder #2	Ladder #3	Ladder #4	Ladder #5	Ladder #6
Rung #1	0.25	0.125	0.0625	0.0313	0.0156	0.00781
Rung #2	0.5	0.25	0.125	0.0625	0.0313	0.0156
Rung #3	1.0	0.5	0.25	0.125	0.0625	0.0313
Rung #4	2.0	1.0	0.5	0.25	0.125	0.0625
Rung #5	4.0	2.0	1.0	0.5	0.25	0.125

Table 3.1: Time to scan 4.63 centimeters for each rung of each ladder (in seconds).

the time the spot is under the laser beam. The time that a spot of resin is under the laser beam is the diameter of the laser beam divided by the velocity of the laser beam. The velocity of the laser beam can easily be found by dividing the scan times of table 3.1 into 4.63 cm. However, the diameter of the laser beam is not known at this point.

To find the diameter of the laser beam it is necessary to know the value of D_p. To find a resin's D_p value, it is necessary to determine the exposure, and to determine exposure, it is necessary to know the diameter of the laser beam. Although this seems circular, it will be shown that the slope of the working curve, D_p, is independent of the actual exposure values. Because of this, an assumed diameter of the laser beam can be used to find the exposure, and then the calculated D_p values can be used to find the actual laser beam diameter. For the purpose of these calculations, a diameter of 0.2 cm will be assumed for the laser beam when used at 100 mW, and 0.3 cm at a laser power of 800 mW. These values come from a best guess by measuring the spot size of the laser beam on a piece of paper.

The exposure time for an individual spot of resin is then the diameter of the laser beam divided by the velocity of the laser beam, where the velocity of the laser can easily be determined from table 3.1. The total exposure is then the laser intensity multiplied by the time of exposure. The exposure per unit area is the total exposure divided by the area of the laser beam spot size. Tables 3.2 and 3.3 list the exposure per unit area for laser power settings of 100 mW and 800 mW, respectively. These are the units of exposure used in finding the working curves of the stereolithographic resins.

The first plots of the working curves are made with the assumed value

	Ladder #1	Ladder #2	Ladder #3	Ladder #4	Ladder #5	Ladder #6
Rung #1	34.38	17.19	8.59	4.30	2.15	1.07
Rung #2	68.75	34.38	17.19	8.59	4.30	2.15
Rung #3	137.51	68.75	34.38	17.19	8.59	4.30
Rung #4	275.02	137.51	68.75	34.38	17.19	8.59
Rung #5	550.68	275.02	137.51	68.75	34.38	17.19

Table 3.2: Exposure per unit area for a spot of resin. The assumed beam diameter is 0.2 centimeters, and the laser intensity is 100 mW.

	Ladder #1	Ladder #2	Ladder #3	Ladder #4	Ladder #5	Ladder #6
Rung #1	183.3	91.7	45.8	22.9	11.5	5.7
Rung #2	366.7	0.0162	0.0081	0.0040	0.0020	0.0010
Rung #3	733.3	0.0324	0.0162	0.0081	0.0040	0.0020
Rung #4	1466.7	0.0648	0.0324	0.0162	0.0081	0.0040
Rung #5	2933.3	0.123	0.0648	0.0324	0.0162	0.0081

Table 3.3: Exposure per unit area for a spot of resin. The assumed beam diameter is 0.3 centimeters, and the laser intensity is 800 mW.

of the laser beam diameter. The effect of the laser beam diameter on the working curve needs to be verified to continue. Figure 3.3 is a plot of depth as a function of exposure, where exposure is found from the process outlined above. For figure 3.3, three different values for the beam diameter were assumed, 0.1 cm, 0.2 cm and 0.3 cm. The results are identical, except that the increase in the assumed magnitude of the beam diameter causes a shift toward the lower exposure levels. The slope of the working curve does not change with an increase or decrease in laser beam diameter, so therefore, the D_p values of the resins can be found using the assumed laser beam diameter. The critical exposure values (E_c), however, cannot. To find the critical exposure, the actual diameter of the laser beam has to be found.

According to Jacobs (Jacobs, 1992), the measured width of a polymer

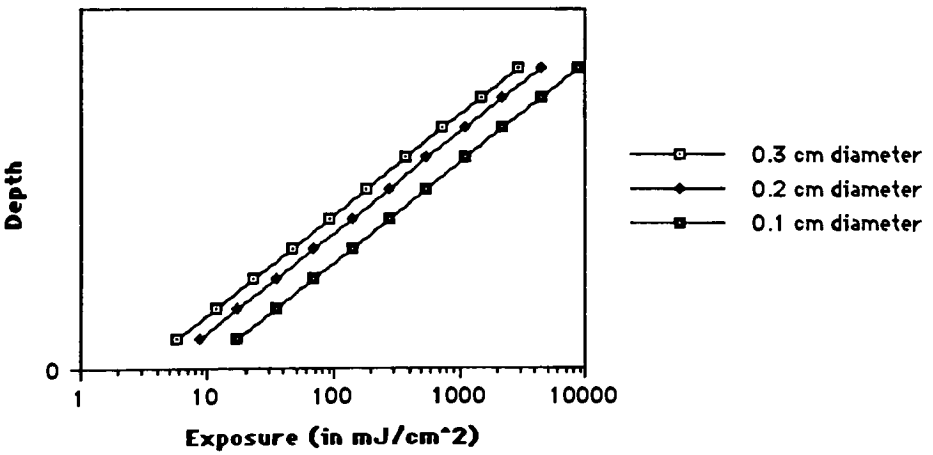

Figure 3.3: The effect of changing the assumed value of the laser beam diameter on the working curve.

sample (cured line width, L_w) is directly proportional to the laser beam diameter (B), and is also directly proportional to the square root of the cure depth (C_d) divided by twice the depth of polymerization (D_p).

$$L_w = B\sqrt{\frac{C_d}{2D_p}} \qquad (3.1)$$

The cure depth (C_d) and the line width (L_w) are easily measured from the step wedges of the LADDER output. The D_p values are measured as the slope of the working curves using simple linear regression. To find the laser beam diameter, B, a plot of L_w versus $\sqrt{C_d/2D_p}$ is made. The slope of the line that best fits the data points, with a zero intercept, is the laser beam diameter, B.

The derivation of equation 3.1 is based on three assumptions (Jacobs, 1992). First, is that the distribution of the laser irradiance is Gaussian. Second, the photopolymer resin obeys the Beer-Lambert law of absorption. The third assumption is that the photopolymer resin has some critical exposure, E_c, corresponding to the transition from the liquid phase to the solid phase. This second assumption would seem to eliminate three resins from the analysis. The Somos resins 2100, 4100 and 5100 all contain light scattering materials, and thus they do not obey the Beer-Lambert law of absorption. These resins will not be eliminated from the determination of the laser beam diameter at this time.

3.2 Polymerization Kinetics: Method of Measuring Shrinkage

The shrinkage sensitometer consists of a linear displacement transducer connected to a strip chart recorder. The linear displacement transducer (XDER) measures the displacement of a cover slip, resting on the surface of a resin sample, as the resin shrinks during exposure. The linear displacement of the XDER is a measure of the total volume shrinkage the resin undergoes in the process of changing from a liquid to a solid.

Figures 3.4 and 3.5 are schematic drawings of the shrinkage sensitometer. Two different intensity UV exposure sources were used with the shrinkage sensitometer. The low intensity UV lamp was used with ten resins: Cubital 5601, Loctite 8100, SLA 5081-1, SLR 804, Somos

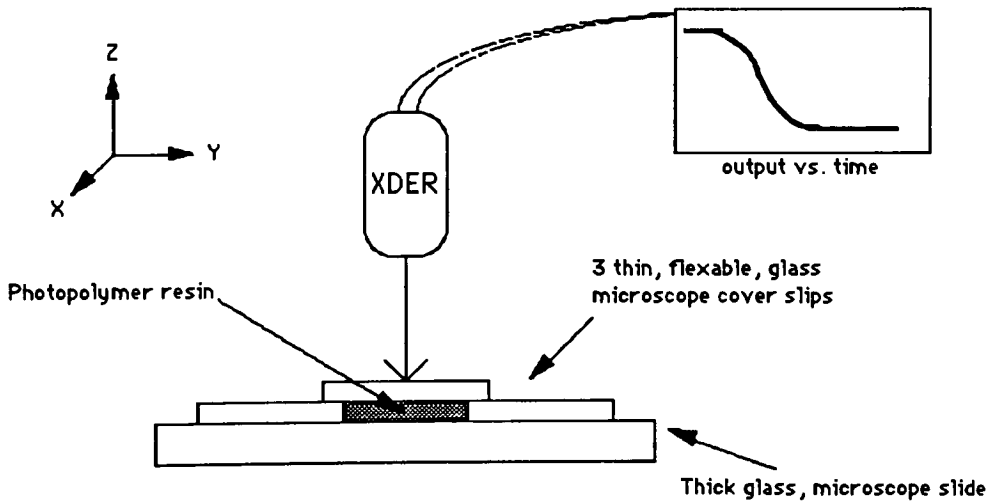

Figure 3.4: Schematic drawing of the Shrinkage Sensitometer.

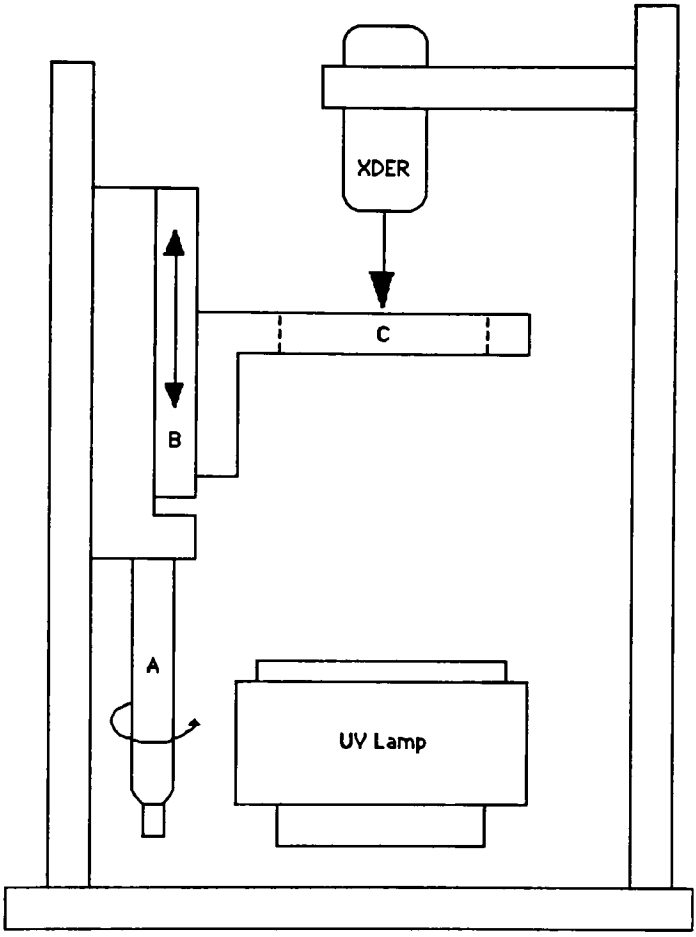

Figure 3.5: View of the entire shrinkage sensitometer. Turning of micrometer A raises and lowers platform B, attached to platform C. Light from the UV lamp exposes resin through hole in platform C.

2100, Somos 3100, XB 5131, XB 5143, XB 5149 and XB 5154. All resins were run using the high intensity UV lamp. Exposure of the resin samples is from below. The distance between the lamp and the resin sample is 14 centimeters for the low intensity lamp and 7.5 centimeters for the high intensity lamp. Two lamps were used because the low intensity lamp proved to be of insufficient strength to induce any measurable reaction in some of the proprietary resins.

Before any measurements on the resins can be made, the displacement transducer has to be calibrated to known distances. This is done by moving the XDER known, small distances and measuring the output on the chart recorder. The support base for the resin samples in the shrinkage sensitometer is attached to a micrometer, accurate to 10 mm (see figure 3.5). Without any sample in place, the micrometer is moved 10 mm, and the distance is measured on the chart recorder in millimeters. On average, for each mm moved by the XDER, the chart recorder will measure 6.4 mm with a 95% confidence interval of $\pm$ 0.14 mm.

To prepare a sample for exposure, two thin, glass cover slips are placed on a thick glass microscope slide, approximately one and one-half centimeters apart. Between the two cover slips, a drop of the resin to be tested is placed and is covered with a third glass cover slip, overlapping the edges of the previous two. As the resin shrinks during exposure, it adheres to the top cover slip, drawing it down.

At the instant the lamp is turned on to expose the resin sample, the chart recorder is started. An example output of the linear displacement of

the XDER versus time of exposure is shown as figure 3.6. When the output of the shrinkage sensitometer has leveled off, and no further displacement of the XDER is recorded, the UV lamp is turned off and the recorder is stopped.

The induction period, T_{is}, and the time to reach half shrinkage, T_{hs}, are measured from the instant the lamp is turned on. T_{hs} is measured at half the total displacement of the liner XDER. T_{is} and T_{hs} are indicated on figure 3.6. To measure the percent shrinkage, %S, the final thickness of the exposed polymer sample has to be measured. The final thickness of the polymer sample, X_f, is measured using a digital micrometer, sensitive to 1 mm. The shrinkage sensitometer has already been calibrated, so the distance recorded by the chart recorder, in millimeters, can be converted to

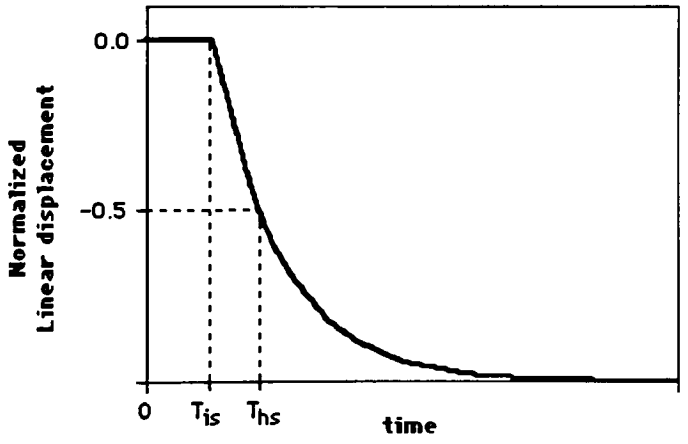

Figure 3.6: Example output from the shrinkage sensitometer showing the induction period (T_{is}) and the time taken to reach half shrinkage (T_{hs}).

actual distance, in micrometers, moved by the XDER (ΔX). The percent shrinkage is then the final thickness of the polymer sample divided by the initial thickness of the polymer sample:

$$\%S = \frac{X_f}{(X_f + \Delta X)} \qquad (3.2)$$

To determine the shrinkage gamma, Γ_s, the induction period, T_{is}, and the time to reach half shrinkage, T_{hs}, are needed. These values, expressed in seconds, are plugged into the equation for Γ_s determined in section two.

$$\Gamma_s = \frac{1}{\log(T_{hs}/T_{is})} \qquad (3.3)$$

Testing the shrinkage sensitometer for repeatability was done using the photopolymer resin HDDA (1,6-Hexanediol diacrylate). HDDA is a widely used monomer (Kloosterboer, 1988(a)), and it's properties are well studied. To induce a reaction, 4.75 grams of HDDA were mixed with 0.25 grams of photoinitiator (Irgacure 651, Ciba-Geigy) for a solution of 5% Initiator, by weight. A total of 25 samples were run using the high intensity UV lamp, placed 7.5 centimeters away from the sample. For each sample, the induction period (T_{is}), half shrinkage time (T_{hs}), percent shrinkage (%S), and the shrinkage gamma (Γ_s) were measured. Table 3.4 is a summary of the average values for each measurement. The raw data is in appendix B.

The small confidence intervals shown in table 3.4 indicate that the shrinkage sensitometer produces very repeatable results. The %Error column of table 3.4 is found by dividing the 95% confidence interval by the

	Average	95% Confidence Interval	% Error
T_{is}	2.717 sec	± 0.272 sec	± 10.03 %
T_{hs}	6.941 sec	± 0.413 sec	± 5.96 %
%S	14.289 %	± 0.203 %	± 1.42 %
Γ_s	2.472	± 0.166	± 6.70 %

Table 3.4: Average values of measurements for monomer HDDA when used with the shrinkage sensitometer. (See appendix B).

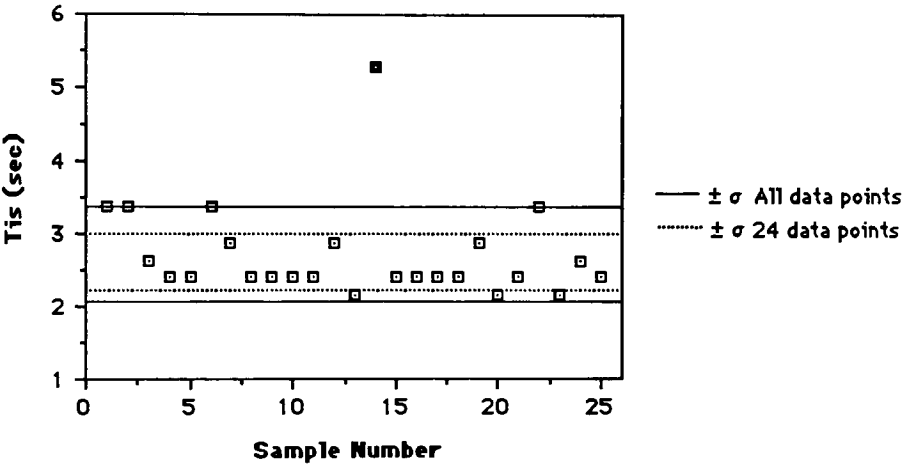

Figure 3.7: Induction Periods for the 25 samples of HDDA used with the shrinkage sensitometer. Sample #14 is shown as a shaded square.

mean, and expressing the result as a percentage. The smaller this percentage, the more precise the value of that reading.

If, in the calculation of the confidence intervals, one extraneous point (the fourteenth sample in appendix B) with an extremely long induction

period is excluded from the analysis, then the 95% confidence intervals for both T_{is} and T_{hs} (and consequently Γ_s) improve, and the %Errors for those measurements decrease. The justification for the removal of this data point is in it's distance from the mean of the remaining 24 data points. Figure 3.6 shows the values of the induction period (T_{is}) for each sample tested. The single data point (#14) with the extremely long induction period is the data point removed from the analysis. The induction period of the fourteenth data point is almost seven standard deviations away from the mean of the data when only the 24 remaining data points are considered.

The confidence intervals of the data, using only the remaining 24 data samples are given in table 3.5. Removal of the errant data point results in a reduction of the %Error for the T_{is} from ±10.03% to ±6.39%. The %Error for the time taken to reach half shrinkage (T_{hs}) is also reduced, from ±5.96% to ±3.32%. The percent errors for %S and Γ_s remain unchanged, within the measurement capabilities of the shrinkage sensitometer.

	Average	95% Confidence Interval	% Error
T_{is}	2.610 sec	± 0.167 sec	± 6.39%
T_{hs}	6.770 sec	± 0.225 sec	± 3.32%
%S	14.311 %	± 0.206 %	± 1.44%
Γ_s	2.445	± 0.162	± 6.64%

Table 3.5: Average values of measurements for monomer HDDA when used with the shrinkage sensitometer, excluding a single point. (See appendix B).

3.3 Polymerization Kinetics: Method of Measuring Rate

The rate sensitometer measures heat flow through a thin foil thermopile. As the resin sample is exposed, it releases heat, and the heat flows into a large, colder, aluminum block. The faster the heat is released from the resin, the faster the heat flow through the thermopile, and the larger the output recorded by the strip chart recorder.

Figure 3.8 is a schematic drawing of the rate sensitometer. The rate sensitometer consists of a large aluminum block with a thin foil thermopile taped to it's surface with a plastic, heat conductive tape. The output of the thermopile is fed into to an amplifier and then to a strip chart recorder. Once the sample is in place on the thermopile, an aluminum cover is placed over the sample and the thermopile, and is clamped into place on opposite sides. The clamps provide a repeatable

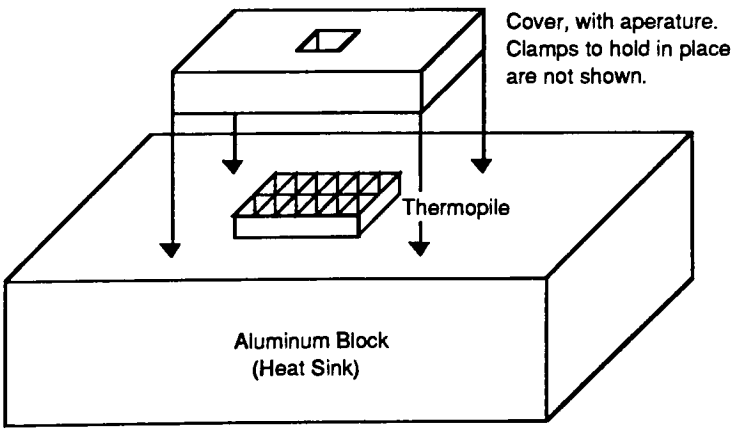

Figure 3.8: Schematic drawing of the rate sensitometer.

pressure to the sample, and spreads the resin sample out to a uniform thin layer. An aperture in the cover provides a uniform exposure area. Two different intensity UV lamps were used to expose the resins. The lower intensity lamp was placed 14 cm from the surface of the sample, and the high intensity lamp was placed 7.5 cm from the sample. Two lamps were used because the low intensity lamp proved to be of insufficient strength to induce any measurable reaction in some of the proprietary resins.

The resin samples are built upon a square plastic microscope coverslip. Plastic is used because any heat generated from the exposure of the resin sample will flow easily through the plastic. A square piece of thin lens paper is placed on the plastic to hold the resin in place. Not only does the lens tissue keep the resin from squishing out the sides of the sensitometer, it also spreads the resin out to a very repeatable thickness. After a drop of resin has been placed on top of the tissue, it is covered with a small glass microscope slide. The glass is transparent to the UV light, however it does not allow heat to flow through. Therefore, all the heat will flow downward, through the thermopile and into the large aluminum block.

Once the sample is in place on the thermopile, it is covered and clamped down on opposite sides with two constant pressure hinge clamps. A shutter is placed over the aperture to block any light and the UV lamp is turned on. The shutter is removed once the sensitometer has reached an equilibrium temperature. The shutter is removed from the sensitometer at the same instant that the chart recorder is started.

Figure 3.9 is an example output from the rate sensitometer. T_{iq} and

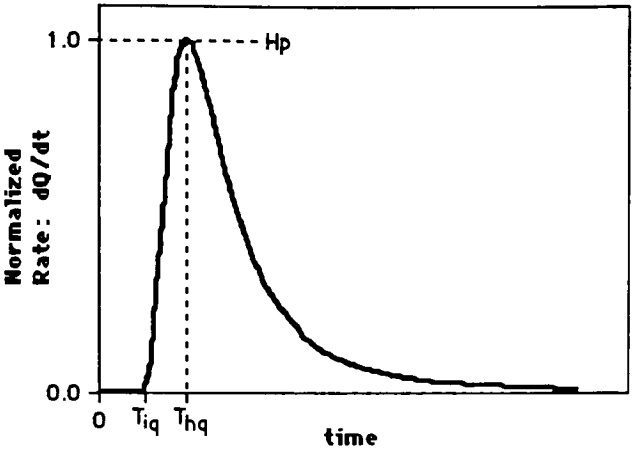

Figure 3.9: Example output from the shrinkage sensitometer showing the induction period (T_{iq}), the time taken to reach half shrinkage (T_{hq}), and the peak rate (H_p).

T_{hq} are measured from the instant the shutter is opened. H_p is measured from the base line in units of centimeters, as a result of never having the rate sensitometer calibrated to actual heat units. Also measured from the output of the rate sensitometer are the rate gammas, Γ_{q1} and Γ_{q2}. The derivations of Γ_{q1} and Γ_{q2} were given in section 2 and the formulas are reprinted here as equations 3.4 and 3.5. The units of Γ_{q1} are in centimeter seconds, and Γ_{q2} is unitless.

$$\Gamma_{q1} = 2.303\, H_p\, T_{hq} \qquad (3.4)$$

$$\Gamma_{q2} = \frac{1}{\log(T_{hq}/T_{iq})} \qquad (3.5)$$

	Average	95% Confidence Interval	% Error
T_{iq}	2.292 sec	± 0.345 sec	± 15.03 %
T_{hq}	5.886 sec	± 0.564 sec	± 9.59 %
H_p	13.998 cm	± 1.075 cm	± 7.68 %
Γ_{q1}	184.052 (cm sec)	± 11.95 (cm sec)	± 6.49 %
Γ_{q2}	2.405	± 0.128	± 5.31 %

Table 3.6: Average values of measurements for monomer HDDA when used with the rate sensitometer. (See Appendix B).

Table 3.6 shows the average values obtained for the induction period (T_{iq}), the time to reach the peak rate (T_{hq}), the peak height (H_p) and the shrinkage gammas (Γ_{q1} and Γ_{q2}) obtained by running 25 samples of monomer HDDA in the rate sensitometer. The raw data of these measurements is recorded in appendix B. As with the shrinkage sensitometer, HDDA was used only to test the repeatability of measurement and the accuracy of the rate sensitometer. The third column of table 3.6 is the percent error expressed as the 95% confidence interval divided by the mean. We can see from this that there appears to be a lot of variability in the measurement of T_{iq}, T_{hq} and the peak height, H_p. The errors in these measurement are carried over into the measurements of the rate gammas, Γ_{q1} and Γ_{q2}.

If, in the calculation of the confidence intervals, five outlying points with extremely long induction periods are excluded from the analysis, then the confidence intervals for T_{iq}, T_{hq} and H_p (and consequently Γ_{q1} and Γ_{q2}) improve, and the %Errors for those measurements are markedly

smaller. The justification for the removal of these data points is their distance from the remaining data points in the measurement of the induction period. The data points with the extremely long induction periods are shown in figure 3.10 as shaded squares. The induction periods of these data points are almost 10 standard deviations away from the mean of the data when only the twenty data points are considered (see appendix B).

The confidence intervals of the data, using only the remaining 20 data samples are given in table 3.7. Removal of the errant data point results in a reduction of the %Error for the induction period from ±15.03% to ±3.6% and a reduction in the %Error for T_{hs} from ±9.59% to ±2.22%. H_p shows a little improvement, having it's %Error reduced from ±7.68% to ±4.77%. As a result of the improvement in the %Error for T_{iq} and T_{hq}, the second

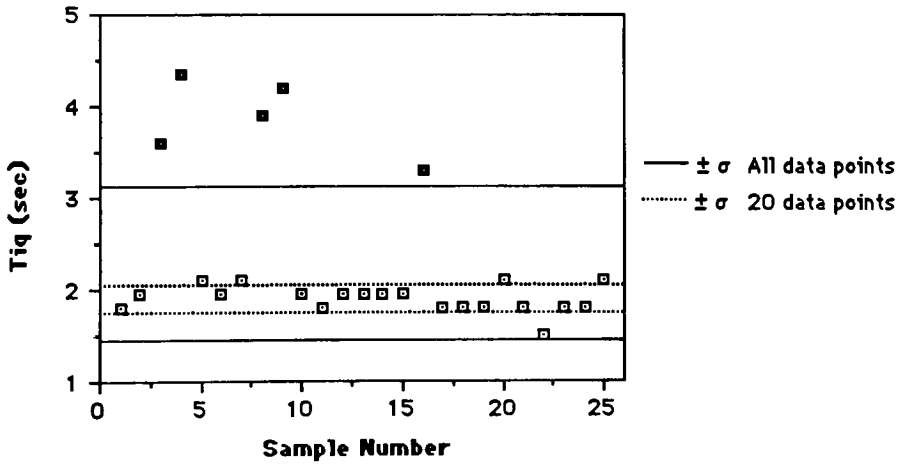

Figure 3.10: Induction Periods for the 25 samples of HDDA used with the rate sensitometer. Five outliers are shown as shaded squares.

	Average	95% Confidence Interval	% Error
T_{iq}	1.897 sec	± 0.068 sec	± 3.60 %
T_{hq}	5.243 sec	± 0.116 sec	± 2.22 %
H_p	14.957 cm	± 0.714 cm	± 4.77 %
Γ_{q1}	180.605 (cm sec)	± 9.874 (cm sec)	± 5.47 %
Γ_{q2}	2.269	± 0.070	± 3.10 %

Table 3.7: Average values of measurements for monomer HDDA when used with the rate sensitometer, excluding 5 extraneous data points. (See Appendix B).

rate gamma also shows some improvement. The percent error for the first rate gamma (Γ_{q1}) remains essentially unchanged, within the measurement capabilities of the shrinkage sensitometer.

3.4 Measurement of Optical Density

The optical density of the resins was measured using a Perkin Elmer 552A UV/VIS double beam spectrophotometer in the UV range of the spectrum. As was mentioned previously, the optical density, or absorbance, of the resins is given by the logarithm of the ratio of the initial intensity to the final intensity (equation 3.6). The optical density is wavelength dependant, and for this experiment, is measured from 325 nm to 500 nm.

$$O.D.(l) = \log\left[\frac{I_0(l)}{I(l)}\right] \qquad (3.6)$$

To be able to use the resins in the spectrophotometer, they have to be diluted. At working strength, the resins are too thick to allow any irradiation from the spectrophotometer to pass through. One gram of the resin was diluted with acetone to a volume of 10 milliliters. The total weight of the monomer and acetone solution was an average of 8.2 grams for all the samples. The average monomer concentration, expressed as a percentage of the total weight of the solution, was approximately 12.3%.

The laser employed to make the working curves of the resins uses a band of six UV lines between 333.6 nm and 363.8 nm. Table 3.8 tabulates the wavelength and relative power at the six UV lines used by the laser. Notice in table 3.8 that line numbers 1 and 2 are within 0.2 nm of each other. Also, line numbers 4 and 5 are within 0.3 nm of each other. Therefore, one measurement will be made at one of these wavelengths and applied to both. It is assumed that the absorbancy of the resins does not change much over that 0.3 nm range. The absorbancy measured at each wavelength will be scaled by the relative intensity. The total

Line Number	Wavelength	Relative Power
1	333.4 nm	10%
2	333.6 nm	10%
3	335.8 nm	6%
4	351.1 nm	31%
5	351.4 nm	13%
6	363.8 nm	30%

Table 3.8: Wavelengths and relative powers used by the laser.

absorbancy of a resin is then the sum of scaled absorbancies for the six wavelengths.

To be able to correctly measure the optical density of the resins, the resins have to obey the Beer-Lambert law of absorption. The Somos resins 2100, 4100 and 5100 contain light scattering materials, and thus do not obey the Beer-Lambert law of absorption. Therefore, these resins will not be included when correlating the optical density with the inverse of D_p. If the Jacob model of the working curves is correct, then the optical density will be directly proportional to $1/D_p$. The line that best fits the data is determined through simple linear regression.

3.5 Working Curves Produced with the Flash Sensitometer

The flash sensitometer is an attempt to measure the working curves of the resins using an alternate exposure source. A camera flash is mounted 6 cm above a petri dish of resin. The dish is one cm deep, and has been coated with black tape to avoid any reflection of light from the flash off the bottom of the dish. A cardboard screen with a 3 cm x 1 cm rectangle cut in the center is used as an aperture so only a small amount of resin is exposed at a time.

The amount of exposure is controlled through the number of flashes. It is assumed that each burst from the camera flash delivers the same amount of light to the resin, provided that the manual flash button on the camera is pressed the instant the green ready light comes on. The resin

being tested is exposed for a number of flashes, then the cardboard screen is removed and the rectangular polymer sample is taken out of the dish of resin. Excess, unexposed, resin is removed from the sample with a clean, lint free, chemical wipe. The thickness of the sample is then measured using a digital micrometer.

Three measurements of the final thickness are taken on each sample, one in the center, and one on each end. This is done because it was found that the polymer samples curl downward into the dish of resin as they gain thickness, giving the samples an inverted canoe shape. This causes error when measuring the thickness of the samples as illustrated in figure 3.11. A minimum of three samples at each number of flashes are also produced to better average the results. The number of flashes range from a minimum of two to a maximum of 12 in even increments.

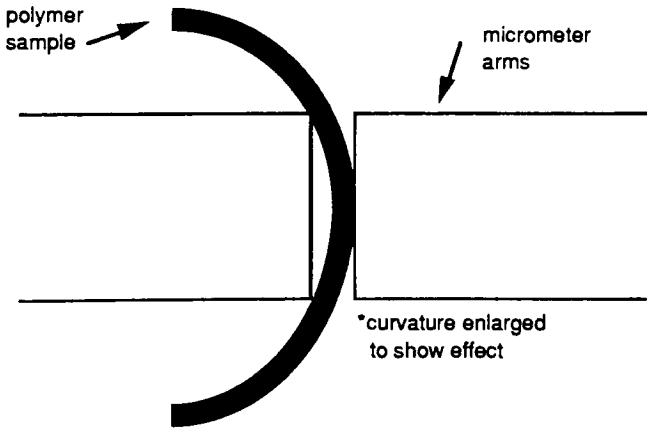

Figure 3.11: Illustration of the error in measuring the thickness of the polymer samples produced by the flash sensitometer.

The measured depth, in millimeters, is plotted as a function of the base two logarithm of the number of flashes. The slope of the line that best fits this data, using simple linear regression, is D_{pf}, and the intersection of this line with the horizontal exposure axis is E_{cf}. The subscript f indicates the values were found with the flash sensitometer, therefore, D_{pf} and Ecf should not be confused with D_p and E_c.

Not all resins were used with the flash sensitometer. Flash working curves were produced for the following ten resins: Cubital 5601, Loctite 8100, SLA 5081-1, SLR 804, Somos 2100, Somos 3100, XB 5131, XB 5143, XB 5149 and XB 5154. The camera flash used in this experiment proved to have inadequate intensity in the UV range to induce a reaction in some of the propriety resins.

4 Results

4.1 Organization of Experimental Results

Experimental results presented in this chapter are organized as follows. First, the experimental data for the depth versus log(exposure) working curves is presented in section 4.2. Next, sections 4.3 through 4.6 are the results from each of the four sensitometers, the shrinkage, rate, absorbancy and flash sensitometers, respectively. The final section in this chapter (section 4.7) is a comparison of the two sensitometers (the shrinkage and the rate sensitometers) that are used to monitor the percent conversion (%C) of the resins during polymerization. Section 4.7 is included to determine if the two sensitometers are indeed measuring the same properties of the resins as they were theorized to do.

4.2 LADDER Method of Producing Working Curves

The working curves of the resins are presented as cure depth (C_d) versus the natural log of exposure. Therefore, the units of D_p [$\Delta C_d / \Delta \ln(E)$] are in millimeters per ln(Exposure), where exposure is in units of mJ/cm^2. The D_p and E_c values resulting from the LADDER method of making working curves are determined from simple linear regression of the data.

Before the final working curves of the stereolithographic resins can be determined, the laser beam diameter has to be known at both the 100 mW

and 800 mW laser power settings. To determine the laser beam diameter, the D_p value of the resins, at that laser power, has to be known. Therefore the results will be presented in the order in which they were determined. First, three D_p values for each of the eighteen stereolithographic resins will be presented, one each for laser power settings of 100 mW and 800 mW (used in determining the laser beam diameter), and the third using the combined data of both power settings. Next, the diameter of the laser beam, at power settings of 100 mW and 800 mW, is determined from the

Resin Name	100 mW D_p	95% Confidence Interval
PR1	0.16	± 0.02
PR2	*	± *
PR3	2.17	± 0.21
PR4	0.34	± 0.05
PR5	0.34	± 0.04
PR6	0.37	± 0.07
Cubital 5601	0.32	± 0.08
Loctite 8100	0.43	± 0.07
SLA 5081-1	0.50	± 0.13
SLR 804	0.45	± 0.04
Somos 2100	0.18	± 0.01
Somos 3100	0.19	± 0.04
Somos 4100	0.22	± 0.03
Somos 5100	0.13	± 0.23
XB 5131	0.15	± 0.04
XB 5143	0.38	± 0.04
XB 5149	0.37	± 0.02
XB 5154	0.11	± 0.05

Table 4.1: Listing of the resins and their 100 mW D_p values. Only one data point was recorded for PR2, therefore no 100 mW D_p value could be calculated.

data. The two diameters are then used to determine the exposure the resin receives as the laser beam passes over. Once the correct exposures are known, the E_c values of the resins can be determined.

As a note on nomenclature, the term 100 mW D_p refers to the slope of the working curve determined from using only data points obtained with the laser power set to 100 mW. The term 800 mW D_p is then the slope of the working curve obtained when using the laser set to 800 mW. When D_p appears by itself, it is referring to the slope of the working curve

Resin Name	800 mW D_p	95% Confidence Interval
PR1	0.17	± 0.19
PR2	2.46	± *
PR3	1.90	± 0.34
PR4	0.29	± 0.07
PR5	0.31	± 0.02
PR6	0.36	± 0.07
Cubital 5601	0.33	± 0.06
Loctite 8100	0.36	± 0.07
SLA 5081-1	0.44	± 0.12
SLR 804	0.42	± 0.17
Somos 2100	0.14	± 0.03
Somos 3100	0.16	± 0.02
Somos 4100	0.29	± 0.08
Somos 5100	0.22	± 0.12
XB 5131	0.18	± 0.05
XB 5143	0.30	± 0.10
XB 5149	0.38	± 0.03
XB 5154	0.16	± 0.08

Table 4.2: Listing of the resins and their 800 mW D_p values. Only three data points were recorded for PR2, an insufficient number to calculate a 95% confidence interval.

obtained using all the data points collected.

Table 4.1 lists the tabulated 100 mW D_p values for each of the eighteen stereolithographic resins. Also listed is the 95% confidence interval for each D_p value. Table 4.2 shows the 800 mW D_p values for the eighteen stereolithographic resins. The large 95% confidence intervals are mainly a result of the few number of data points. The 95% confidence intervals do shrink when the data points from the 100 mW exposure and the 800 mW exposure are combined.

The third table, table 4.3, tabulates the D_p value of the resins when the data recorded at the separate laser power settings are combined. Also

Resin Name	D_p	95% Confidence Interval	R^2
PR1	0.16	± 0.03	0.94
PR2	2.39	± 0.68	0.99
PR3	2.07	± 0.29	0.94
PR4	0.30	± 0.04	0.93
PR5	0.31	± 0.03	0.96
PR6	0.37	± 0.04	0.96
Cubital 5601	0.33	± 0.04	0.94
Loctite 8100	0.39	± 0.05	0.95
SLA 5081-1	0.46	± 0.08	0.89
SLR 804	0.44	± 0.05	0.97
Somos 2100	0.16	± 0.02	0.95
Somos 3100	0.18	± 0.02	0.99
Somos 4100	0.26	± 0.06	0.79
Somos 5100	0.20	± 0.10	0.50
XB 5131	0.18	± 0.03	0.91
XB 5143	0.35	± 0.05	0.91
XB 5149	0.37	± 0.02	0.99
XB 5154	0.18	± 0.06	0.70

Table 4.3: Listing of the resins and their D_p values using all data points.

included in table 4.3 is the R^2 value for each resin. According to Dougherty (Dougherty, 1990), R is called the sample correlation coefficient of the data, and R^2 is called the coeficient of determination. R^2 ranges in value from zero to one, where a value near zero indicates random variation of the data, and a value near one indicates that most of the variability is attributable to regression.

Figures 4.1 and 4.2 compare each resins 100 mW D_p, 800 mW D_p and the final D_p values. Figure 4.2 is an enlargement of figure 4.1 to show more detail in the resins after exclusion of resins PR2 and PR3. We can see from these graphs that the D_p values collected under each laser power and the cumulative D_p value using all the data points are very close to each other. This confirms that the intensity of the exposure source does not have an effect on the D_p value of a resin.

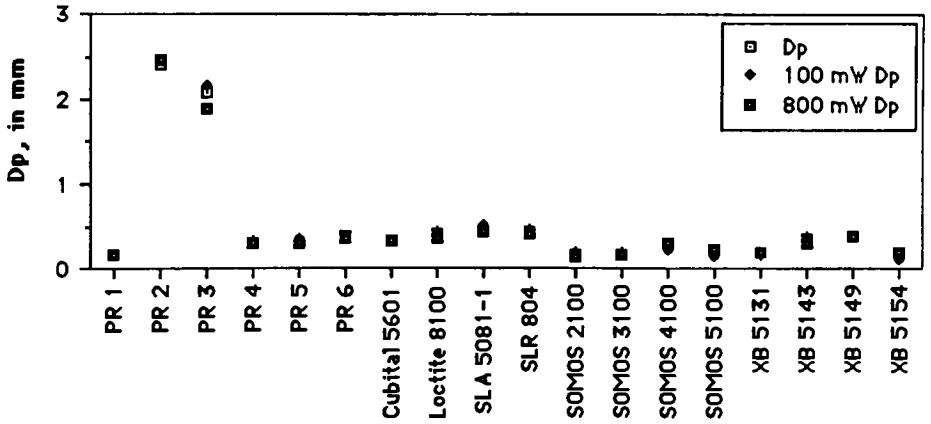

Figure 4.1: Comparison of 100 mW D_p , 800 mW D_p and the final D_p value of the resins.

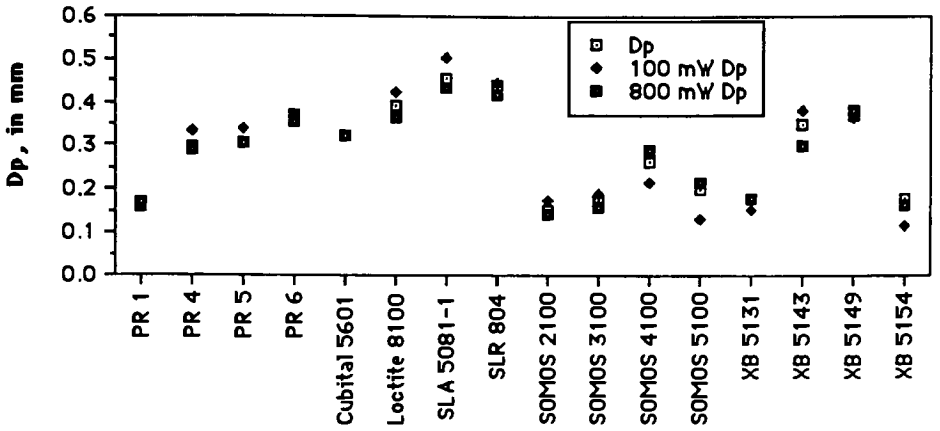

Figure 4.2: Enlargement of figure 4.1.

To determine the laser beam diameter, B, at each laser power setting, it is necessary to measure the line width (L_w) at the corresponding cure depth (C_d). L_w is measured at the deepest cure depth for each ladder to limit the number of data points. Using equation 3.1 (reprinted below), the diameter of the laser beam at both power settings can be determined.

$$L_w = B\sqrt{\frac{C_d}{2D_p}} \qquad (3.1)$$

Figure 4.3 shows the results of plotting the measured line width (L_w) as a function of $\sqrt{C_d/(2D_p)}$ with the laser set at a power of 100 mW. The diameter of the laser beam at 100 mW is then the slope of the line through the origin that best fits the data. At 100 mW, the diameter is 1.84 mm with a 95% confidence interval of ± 0.03 mm. The R^2 value of the data, assuming an intercept of the origin, is 0.80.

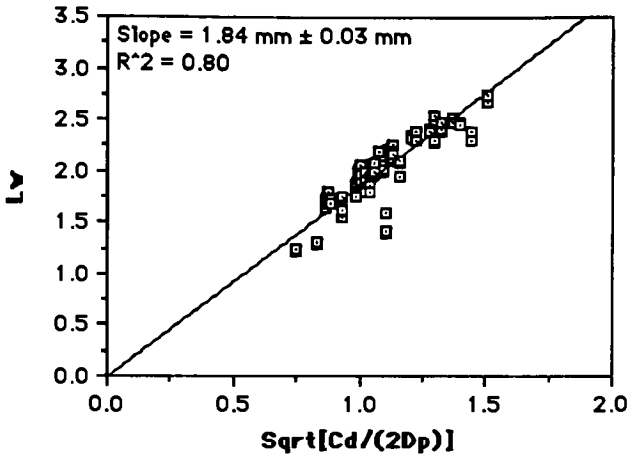

Figure 4.3: The measured line width as a function of $\sqrt{C_d/(2D_p)}$ for laser power setting of 100 mW.

Figure 4.4 shows the results for the 800 mW laser power setting. At 800 mW, the diameter is 2.40 mm with a 95% confidence interval of ± 0.04 mm. The R^2 value of the data, assuming an intercept of the origin, is 0.51. This is low because of the assumption of an intercept of the origin, when, as indicated in figure 4.10, there appears to be some positive y axis intercept of the data. The R^2 value of the data with no constraint on the intercept is 0.83.

Now that the laser beam diameters are known, the exposure at the surface of the resin can be determined. Exposure is determined by the process outlined in the previous section. Table 4.4 and table 4.5 list the exposure, in mJ/cm^2, for each rung of each ladder when the laser beam is set to a power of 100 mW and 800 mW, respectively. From the graphs of

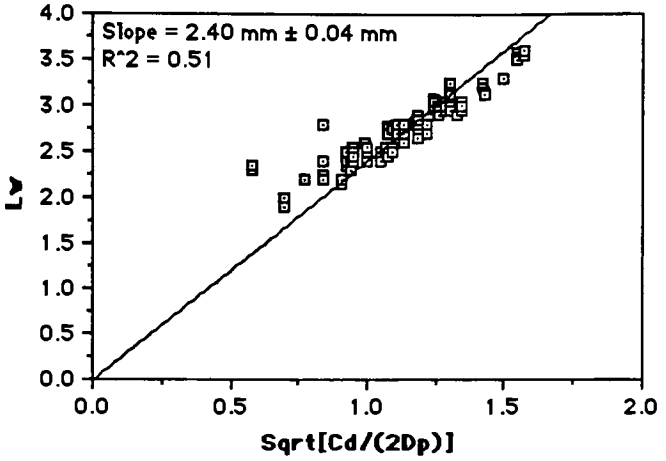

Figure 4.4: The measured line width as a function of $\sqrt{C_d/(2D_p)}$ for laser power setting of 800 mW.

Ladder:	#1	#2	#3	#4	#5	#6
Rung #1	37.27	18.62	9.31	4.65	2.33	1.16
Rung #2	74.47	37.27	18.62	9.31	4.65	2.33
Rung #3	148.95	74.47	37.27	18.62	9.31	4.65
Rung #4	298.15	148.95	74.47	37.27	18.62	9.31
Rung #5	595.80	298.15	148.95	74.47	37.27	18.62

Table 4.4: Exposure, in mJ/cm^2 calculated for a laser beam diameter of 1.84 mm and a laser power of 100 mW.

Ladder:	#1	#2	#3	#4	#5	#6
Rung #1	229.29	114.65	57.33	28.66	14.33	7.17
Rung #2	458.61	229.29	114.65	57.33	28.66	14.33
Rung #3	917.18	458.61	229.29	114.65	57.33	28.66
Rung #4	1834.45	917.18	458.61	229.29	114.65	57.33
Rung #5	3668.73	1834.45	917.18	458.61	229.29	114.65

Table 4.5: Exposure, in mJ/cm^2 calculated for a laser beam diameter of 2.40 mm and a laser power of 800 mW.

the working curves using the correct exposures, the critical exposures can be determined. The intercept of the best fit line with the ln(exposure) axis is the natural logarithm of the critical exposure of the resin, $\ln(E_c)$. The inverse logarithm of this number yields the critical exposure of the resin.

Table 4.6 lists each resin's D_p and E_c value along with the 95% confidence interval for D_p and E_c. The graphical depictions of the working curves for all of the eighteen resins are given in appendix C. The D_p values in table 4.6, and their 95% confidence intervals, are taken from table 4.3. To find the 95% confidence intervals of the E_c values, the

Resin Name:	D_p (mm)	E_c (mJ/cm2)	Lower E_c Limit	Upper E_c Limit
PR1	0.16 ± 0.03	6.89	4.03	11.77
PR2	2.39 ± 0.68	755.00	434.78	1311.07
PR3	2.07 ± 0.29	128.51	105.14	157.08
PR4	0.30 ± 0.04	68.24	50.90	91.47
PR5	0.31 ± 0.03	61.36	46.28	81.35
PR6	0.37 ± 0.04	78.33	64.48	95.15
Cubital 5601	0.33 ± 0.04	20.05	15.26	26.34
Loctite 8100	0.39 ± 0.05	17.74	12.93	24.33
SLA 5081-1	0.46 ± 0.08	21.83	14.75	32.30
SLR 804	0.44 ± 0.05	31.60	23.53	42.45
Somos 2100	0.16 ± 0.02	5.54	3.94	7.79
Somos 3100	0.18 ± 0.02	8.06	6.09	10.65
Somos 4100	0.26 ± 0.06	15.55	10.06	24.03
Somos 5100	0.20 ± 0.10	23.82	12.31	46.08
XB 5131	0.18 ± 0.03	11.93	8.07	17.63
XB 5143	0.35 ± 0.05	21.66	16.47	28.48
XB 5149	0.37 ± 0.02	28.29	24.52	32.63
XB 5154	0.18 ± 0.06	9.64	5.02	18.53

Table 4.6: The tabulated D_p and E_c values for the eighteen stereolithographic resins and the 95% confidence limits.

working curves of the resins have to be reversed, so that ln(Exposure) is plotted on the vertical y-axis, and cure depth (C_d) is plotted on the horizontal x-axis. Simple linear regression of this data will yield a line through the data with a slope equal to $1/D_p$ and a y-axis intercept equal to $\ln(E_c)$. Notice in table 4.6 that the 95% confidence range for E_c is not symmetrical about E_c. This is because the 95% confidence interval for E_c is calculated from the plot of ln(E) versus C_d, which yields a symmetrical interval around $\ln(E_c)$. When these lower and upper limits are converted to exposure units by taking the anti logarithm, they become non-symmetrical.

The results from the measurement of the working curves of the resins gives an idea of the precision of the LADDER method of producing the working curves. We can see from the working curves in appendix C that the LADDER method produces data that does exhibit some scatter, which appears in the size of the 95% confidence intervals of table 4.6.

4.3 Shrinkage Sensitometer

Two different intensity UV lamps were used as exposure sources for the measurement of shrinkage. The lower intensity lamp was not of sufficient intensity to induce polymerization in some of the proprietary resins, so therefore, the switch to the higher intensity lamp was made. While only ten of the resins were run under the lower intensity lamp, all eighteen were run under the high intensity lamp. Results from both

Resin Name:	T_{is} (sec)	σ	T_{hs} (sec)	σ	%S	σ	Γ_s	σ
Cubital 5601	110.80	2.84	175.00	4.34	4.94	0.11	5.04	0.08
Loctite 8100	98.60	1.51	141.40	2.71	5.34	0.17	6.40	0.30
SLA 5081-1	139.80	7.37	238.60	7.97	5.18	0.09	4.31	0.16
SLR 804	120.84	5.21	161.52	3.30	4.71	0.23	7.97	0.70
Somos 2100	23.28	2.17	35.62	2.05	2.38	0.11	5.46	0.70
Somos 3100	24.43	2.19	38.00	3.29	5.66	0.35	5.36	0.93
XB 5131	81.60	4.33	184.80	15.60	5.40	0.59	2.86	0.43
XB 5143	95.80	1.93	139.40	3.52	5.12	0.06	6.17	0.50
XB 5149	103.32	3.48	165.96	6.22	5.40	0.23	4.87	0.30
XB 5154	35.28	0.42	78.48	4.04	5.42	0.17	2.89	0.17

Table 4.7: The mean and standard deviation of T_{is}, T_{hs}, %S and Γ_s using the low intensity UV lamp as the exposure source.

Resin Name:	T_{is} (sec)	σ	T_{hs} (sec)	σ	%S	σ	Γ_s	σ
PR1	3.64	0.39	14.32	1.47	7.88	0.21	1.68	0.07
PR2	57.78	16.18	177.60	52.69	4.13	0.72	2.12	0.35
PR3	11.40	0.60	42.80	2.42	5.74	0.13	1.75	0.13
PR4	6.80	1.51	33.20	2.96	6.01	0.23	1.45	0.13
PR5	8.80	1.25	36.40	3.30	5.46	0.12	1.62	0.06
PR6	10.40	1.83	39.20	2.96	4.94	0.11	1.73	0.16
Cubital 5601	4.90	0.46	13.00	0.92	5.55	0.10	2.37	0.20
Loctite 8100	4.10	0.75	10.10	0.75	5.86	0.07	2.55	0.31
SLA 5081-1	7.40	0.92	20.40	1.59	6.58	0.26	2.27	0.15
SLR 804	4.50	0.30	10.80	0.30	5.31	0.02	2.64	0.24
Somos 2100	1.09	0.31	3.79	0.28	2.86	0.08	1.90	0.48
Somos 3100	1.45	0.23	3.97	0.88	6.78	0.23	2.45	0.77
Somos 4100	4.04	0.18	9.95	0.45	4.40	0.21	2.56	0.07
Somos 5100	2.56	0.55	8.16	0.63	3.18	0.12	2.04	0.47
XB 5131	2.48	0.62	14.46	1.31	6.13	0.17	1.32	0.22
XB 5143	3.50	0.17	10.40	0.62	5.69	0.03	2.12	0.09
XB 5149	3.80	0.35	12.30	0.52	6.10	0.20	1.96	0.13
XB 5154	2.20	0.17	10.00	0.46	5.90	0.14	1.53	0.12

Table 4.8: The mean and standard deviation of T_{is}, T_{hs}, %S and Γ_s using the high intensity UV lamp as the exposure source.

lamps are included. Each resin was tested a minimum of three times under each lamp.

Table 4.7 shows the tabulated results for the average values of the induction period (T_{is} in seconds), the half shrinkage time (T_{hs} in seconds), the percent shrinkage (%S), and the shrinkage gamma (Γ_s) for the ten resins run under the lower intensity UV lamp. The standard deviation (σ) of the data is also listed in table 4.7. Table 4.8 lists the average values, along with the standard deviation, of T_{is}, T_{hs}, %S and Γ_s for all eighteen resins as measured using the shrinkage sensitometer under the high intensity UV lamp.

4.4 Rate Sensitometer

As with the shrinkage sensitometer, resins exposed in the rate sensitometer were exposed using both the high intensity and the low intensity UV lamps. Again, the low intensity UV lamp did not have sufficient power to induce polymerization in some of the propriety resins. The high intensity lamp was used with all eighteen of the resins, while only ten of the resins were run with the lower intensity lamp as the exposure source. Each resin was tested a minimum of three times under both lamps.

Measurements taken with the rate sensitometer, using the low intensity UV lamp, are tabulated in table 4.9 and table 4.10. Table 4.9 lists the induction period (T_{iq}, in seconds), the time to reach the peak rate (T_{hq},

Resin Name:	T_{iq} (sec)	σ	T_{hq} (sec)	σ	H_p (cm)	σ
Cubital 5601	69.6	4.16	117.6	4.16	1.37	0.16
Loctite 8100	63.2	1.39	108.4	0.69	1.65	0.23
SLA 5081-1	101.6	1.39	167.2	0.69	0.62	0.03
SLR 804	73.2	1.20	110.0	3.02	1.72	0.20
Somos 2100	20.4	1.04	32.8	0.35	3.27	0.03
Somos 3100	16.4	0.57	26.3	1.02	11.15	1.11
XB 5131	60.8	3.67	126.0	6.24	0.60	0.09
XB 5143	58.0	1.83	95.6	4.85	1.42	0.12
XB 5149	70.0	3.86	115.6	5.00	0.85	0.15
XB 5154	19.2	0.60	41.4	1.80	1.59	0.07

Table 4.9: The mean and standard deviation of T_{iq}, T_{hq} and H_p using the low intensity UV lamp as the exposure source.

Resin Name:	Γ_{q1}(cm·s)	σ	Γ_{q2}	σ
Cubital 5601	371.96	45.04	4.39	0.20
Loctite 8100	410.92	54.40	4.27	0.12
SLA 5081-1	239.53	14.12	4.63	0.15
SLR 804	435.94	62.20	5.67	0.37
Somos 2100	246.77	4.15	4.89	0.56
Somos 3100	675.99	94.64	4.88	0.33
XB 5131	174.38	29.12	3.16	0.09
XB 5143	312.53	38.83	4.63	0.31
XB 5149	226.49	39.80	4.59	0.11
XB 5154	151.47	13.52	3.00	0.15

Table 4.10: The mean and standard deviation of Γ_{q1} and Γ_{q2} using the low intensity UV lamp as the exposure source.

in seconds) and the peak height (H_p, in centimeters). Table 4.10 lists both rate gammas (Γ_{q1} and Γ_{q2}) where the units of Γ_{q1} are cm·seconds and Γ_{q2} is unitless. Included in both of the tables are the standard deviations of the data (σ).

If Γ_{q1} and Γ_{q2} measure the same sensitometric properties of the resins, then a graph of Γ_{q1} versus Γ_{q2} should be very liner. Figure 4.5 is just such a graph, and we can see that there appears to be some type of correlation between the two rate gammas, however the linear correlation of the data is low ($R^2 = 0.33$). This could indicate one of two things. First, that there is a non-linear correlation between Γ_{q1} and Γ_{q2}, meaning that Γ_{q1} and Γ_{q2} measure different properties of the resins, or second, that the apparent non-linear correlation of the data is just due to random scatter of the data.

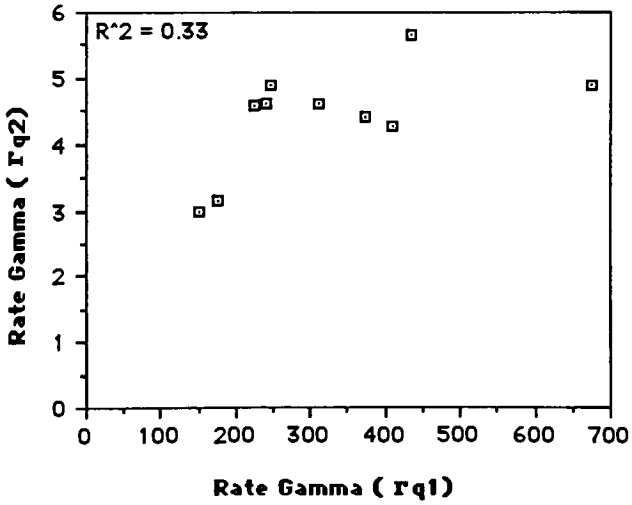

Figure 4.5: Γ_{q1} versus Γ_{q2} as measured by the rate sensitometer using the low intensity UV lamp.

If we make the null hypothesis that there is no correlation between Γ_{q1} and Γ_{q2} when using the low intensity UV lamp, then we would have to accept the null hypothesis at the 95% confidence level.

All eighteen resins were tested under the high intensity UV lamp, compared to only ten of the resins tested under the low intensity UV lamp. The data measured from both lamps is the same: induction period (T_{iq}), the time take to reach the peak rate (T_{hq}), the height of the peak rate (H_p) and the rate gammas (Γ_{q1} and Γ_{q2}). Tables 4.11 and 4.12 tabulate all the average readings of the rate sensitometer when exposing with the high intensity UV lamp. Listed also in these tables are the standard deviations

Resin Name:	T_{iq} (sec)	σ	T_{hq} (sec)	σ	H_p (cm)	σ
PR1	2.5	0.93	8.1	1.17	12.05	2.86
PR2	45.2	4.85	70.9	3.04	3.14	0.21
PR3	9.6	0.00	19.9	0.98	2.82	0.20
PR4	4.1	0.44	13.5	0.77	5.20	0.27
PR5	4.4	0.50	13.5	0.20	5.17	0.39
PR6	5.0	0.37	13.8	0.37	4.10	0.21
Cubital 5601	3.6	0.00	9.1	0.17	16.77	0.80
Loctite 8100	3.2	0.17	9.1	0.09	14.27	0.28
SLA 5081-1	5.0	0.59	13.4	0.97	9.24	0.77
SLR 804	3.9	0.30	9.5	0.15	14.52	0.89
Somos 2100	1.2	0.12	4.0	0.14	15.61	1.34
Somos 3100	1.1	0.12	3.4	0.07	38.44	3.85
Somos 4100	3.3	0.32	9.4	0.34	12.76	1.49
Somos 5100	1.5	0.14	6.1	0.12	10.94	0.44
XB 5131	2.5	0.17	8.8	0.23	9.73	0.49
XB 5143	2.9	0.23	10.2	0.15	10.32	1.08
XB 5149	4.0	0.09	11.5	0.09	7.98	0.56
XB 5154	1.2	0.09	6.3	0.17	10.52	0.14

Table 4.11: The mean and standard deviation of T_{iq}, T_{hq} and H_p using the high intensity UV lamp as the exposure source.

Resin Name:	Γ_{q1}(cm·s)	σ	Γ_{q2}	σ
PR1	219.09	29.44	1.92	0.36
PR2	511.88	13.07	5.15	0.75
PR3	129.17	14.60	3.18	0.20
PR4	161.73	3.70	1.93	0.08
PR5	160.10	10.68	2.06	0.19
PR6	130.90	10.08	2.24	0.12
Cubital 5601	351.58	23.15	2.48	0.05
Loctite 8100	297.37	8.20	2.22	0.11
SLA 5081-1	286.11	43.79	2.35	0.26
SLR 804	316.06	22.74	2.61	0.20
Somos 2100	143.55	8.04	1.91	0.12
Somos 3100	304.98	36.27	1.99	0.19
Somos 4100	275.86	31.67	2.23	0.20
Somos 5100	154.42	8.69	1.65	0.09
XB 5131	197.38	14.13	1.83	0.10
XB 5143	242.45	27.25	1.83	0.13
XB 5149	211.45	15.35	2.16	0.06
XB 5154	151.39	5.54	1.36	0.05

Table 4.12: The mean and standard deviation of Γ_{q1} and Γ_{q2} using the high intensity UV lamp as the exposure source.

of the data. There are a few data points with a standard deviation of zero, such as the induction period for resins PR3 and Cubital 5601. For the three data samples recorded for these resins, the induction period was repeated exactly, to the precision that the induction period could be measured.

As with the low intensity lamp, comparisons can be made between the two different rate gammas that were measured. Figure 4.6 seems to show some linear relation between Γ_{q1} and Γ_{q2}, however at $\Gamma_{q1} \approx 150$, there is a cluster of data points ranging in values from $\Gamma_{q2} < 1.5$ to $\Gamma_{q2} > 3.0$, almost the entire range of Γ_{q2} values. The lone data point with an extremely high

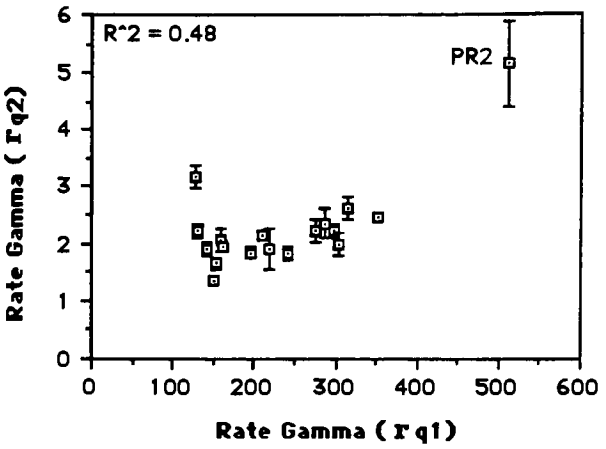

Figure 4.6: Γ_{q1} versus Γ_{q2} as measured by the rate sensitometer using the high intensity UV lamp. Error bars are plus and minus one standard deviation for Γ_{q2}.

Γ_{q1} and Γ_{q2} value belongs to the resin PR2. This comes about from the long induction period this resin has. It is interesting to note the effect of resin PR2 on the correlation of the data shown in figure 4.6. If resin PR2 were removed from the analysis, then the R^2 value of the data would drop to 0.0013. If we make the null hypothesis that there is no correlation between Γ_{q1} and Γ_{q2} without resin PR2 in the analysis, then we would accept this hypothesis at the 95% confidence level. However, we have no sufficient reason to reject resin PR2 from the analysis. By keeping resin PR2 in the analysis, we would have to reject the null hypothesis at the same confidence level, and thus accept the alternate hypothesis that there is some linear correlation between Γ_{q1} and Γ_{q2}.

It is possible that much of the scatter of the data in figure 4.6 could be attributed to the variability in the measurement process of the rate gammas. The error bars in the figure represent $\pm\sigma$ from the mean of Γ_{q2}, as listed in table 4.12. Error bars for Γ_{q1} are excluded from figure 4.6 to conserve space. The error bars for Γ_{q1} are nearly the same graphical size as those for Γ_{q2} shown in figure 4.6. From these error bars, it appears as if the variability of the measurement process could account for some of the scatter of the data, but not for all of it.

The uncorrelation of Γ_{q1} and Γ_{q2} shown in figures 4.5 and 4.6 suggest that the two rate gammas are measuring different properties of the resin. In section 4.7, we make a comparison between the shrinkage and the rate sensitometers to determine if they are measuring the same properties of the resins, as we assumed in the development of the Reiser model. If the two sensitometers correlate, then we will have a high level of confidence in both.

4.5 Absorbancy Sensitometer

The absorbancy plots of all eighteen resins are given in appendix section D. The absorbancy of all eighteen resins was recorded, but because of the light scattering properties of the Somos resins 2100, 4100 and 5100, these resins are not included in the tabulated results. The difference in absorbancy between these three resins and the remaining resins is quite evident from the absorbancy plots in appendix D. The spectrophotometer

is calibrated such that the total absorbancy, measured as the total height of the recording paper, is 3.0 absorbancy units. The height of the paper along the absorbancy scale is 249 millimeters. To find the absorbancy at a certain wavelength, the height of the output at that wavelength is measured in millimeters, then converted to absorbancy units. This absorbancy then has to be scaled by the relative power that the laser emits at each wavelength, as tabulated in table 3.8 on page 53.

Table 4.13 lists the scaled absorbancies at each of the six wavelengths emitted by the laser. The total absorbancy for a particular resin is then the sum of the absorbancies at each wavelength. This total absorbancy is given in table 4.14. The data in table 4.14 does not tell much about the resins

Resin Name:	333.4 nm	333.6 nm	335.8 nm	351.1 nm	351.4 nm	363.8 nm
PR1	0.23	0.23	0.13	0.56	0.24	0.54
PR2	0.13	0.13	0.07	0.06	0.03	0.02
PR3	0.15	0.15	0.07	0.06	0.02	0.01
PR4	0.26	0.26	0.15	0.24	0.10	0.24
PR5	0.26	0.26	0.15	0.30	0.13	0.24
PR6	0.26	0.26	0.15	0.29	0.12	0.23
Cubital 5601	0.18	0.18	0.11	0.47	0.20	0.36
Loctite 8100	0.09	0.09	0.04	0.23	0.10	0.34
SLA 5081-1	0.17	0.17	0.10	0.33	0.14	0.16
SLR 804	0.19	0.19	0.11	0.34	0.14	0.16
Somos 3100	0.24	0.24	0.15	0.69	0.29	0.47
XB 5131	0.24	0.24	0.13	0.57	0.24	0.64
XB 5143	0.21	0.21	0.12	0.45	0.19	0.20
XB 5149	0.21	0.21	0.13	0.45	0.19	0.20
XB 5154	0.14	0.14	0.15	0.71	0.30	0.77

Table 4.13: The scaled absorbancy of the resins, diluted with acetone, at the six wavelengths emitted by the UV laser.

Resin Name:	Total Absorbancy
PR1	1.92
PR2	0.44
PR3	0.46
PR4	1.25
PR5	1.34
PR6	1.30
Cubital 5601	1.48
Loctite 8100	0.88
SLA 5081-1	1.06
SLR 804	1.14
Somos 3100	2.09
XB 5131	2.06
XB 5143	1.38
XB 5149	1.39
XB 5154	2.20

Table 4.14: The total absorbancy of the resins.

when examined by itself, however, the correlation of these absorbancies with the inverse of D_p (chapter 5 section 4) reveals the relation between the absorbancy and the slope of the working curve.

4.6 Flash Sensitometer

The ten resins that were exposed in the rate and shrinkage sensitometers with the low intensity UV lamp were also tested in the flash sensitometer. The flash sensitometer proved to be of insufficient intensity to expose some of the propriety resins. The actual intensity of each flash in the flash sensitometer is not known, and it is not necessary for the determination of the reliability of the flash sensitometer to reproduce the

working curves determined from the laser scanner. Therefore, rather than have actual exposure values for the flash working curves, the exposure axis is left in units of the $\log_2$(#Flashes). If each flash delivers the same amount of light, and the time duration between flashes is unimportant, then by doubling the number of flashes, the exposure is doubled.

Table 4.15 is a summary of the data recorded from the flash working curves. The slope of the flash working curve (D_{pf}) is found from the slope of the linear regression line that best fits the depth versus $\log_2$(#Flashes) graph. The intercept of this line with the exposure axis (E_{cf}) is the flash critical exposure, expressed in units of number of flashes. Listed with the D_{pf} and E_{cf} values in table 4.15 are the 95% confidence intervals. As with the working curves, the 95% confidence intervals for E_{cf} are found from

Resin Name	D_{pf}	E_{cf} (in flashes)	Lower E_{cf} limit	Upper E_{cf} Limit
Cubital 5601	0.58 ± 0.07	1.68	1.43	1.97
Loctite 8100	0.41 ± 0.02	0.81	0.72	0.91
SLA 5081-1	0.33 ± 0.03	1.91	1.67	2.19
SLR 804	0.28 ± 0.03	1.59	1.38	1.83
Somos 2100	0.27 ± 0.03	0.71	0.58	0.86
Somos 3100	0.30 ± 0.03	1.00	0.86	1.16
XB 5131	0.22 ± 0.03	0.88	0.69	1.13
XB 5143	0.31 ± 0.03	1.62	1.39	1.89
XB 5149	0.33 ± 0.05	1.98	1.63	2.39
XB 5154	0.33 ± 0.05	1.05	0.82	1.33

Table 4.15: Summary of the D_{pf} and E_{cf} values and the 95% confidence limits.

reversing the data. The graphs of the working curves for the ten stereolithographic resins are in appendix E. Listed on each graph are the D_{pf} and E_{cf} values, along with the R^2 value of the data. Each resin shows highly correlated data, all with R^2 values over 0.90.

4.7 Correlation of the Shrinkage and Rate Sensitometers

The measurement of shrinkage and rate are indirect measures of conversion as the monomer molecules join into polymer chains. In the shrinkage sensitometer, volume change results from the loss of free volume as the individual monomer molecules join to form long polymer chains. In the rate sensitometer, heat is given off as monomer molecules join together to form polymer. As a check to see if the shrinkage and the rate sensitometers are measuring the same properties of the resins, a comparison of the results is made. The induction periods (T_{is} and T_{iq}) measured at both intensities of the exposure source are compared in section 4.7.1. Section 4.7.2 is a comparison of the shrinkage gamma (Γ_s) with the two rate gammas (Γ_{q1} and Γ_{q2}).

4.7.1 Correlation of the Induction Period Data

Figure 4.7 is a scatter plot of T_{is} versus T_{iq} when the low intensity UV lamp is used as the exposure source. As is evident in figure 4.7, T_{is} and T_{iq} are highly correlated with a R^2 value of 0.96. If we hypothesize that there

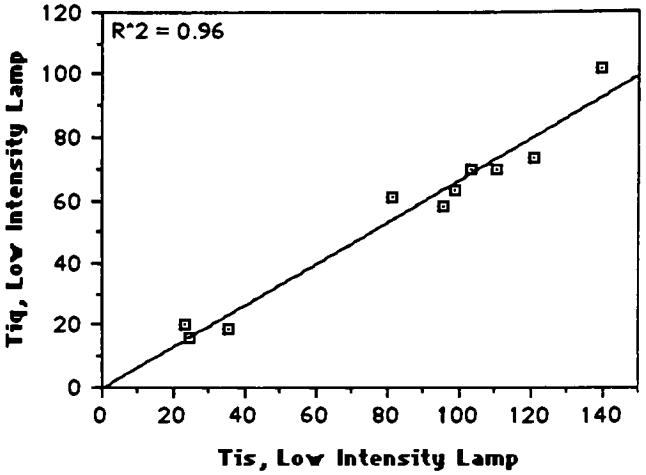

Figure 4.7: T_{iq} versus T_{is} using the low intensity UV lamp as the exposure source.

is no correlation between T_{is} and T_{iq} when the low intensity lamp is used as the exposure source, then at the 95% confidence level we can reject this hypothesis. We would thus accept the alternate hypothesis that there is a linear relationship between T_{is} and T_{iq}.

Figure 4.8 is a diagram of T_{iq} versus T_{is}, using the high intensity UV lamp as the exposure source. The data is highly correlated, with a R^2 value of 0.99. The high correlation of this data is slightly misleading, due to the data point of resin PR2 in the upper right corner. To have a better view of the correlation of the remaining resins, an enlargement of figure 4.8 is given in figure 4.9. The data for resin PR2 is not being thrown out, but is only temporary removed to show the correlation of the remaining resins. Without resin PR2 in the analysis, the R^2 value is reduced to 0.79.

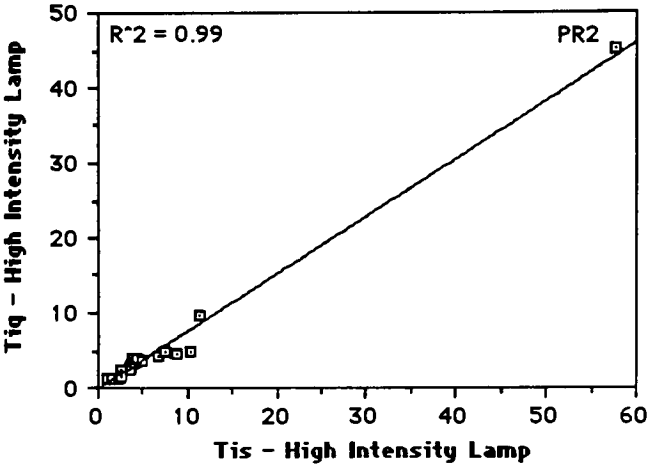

Figure 4.8: T_{iq} versus T_{is} using the high intensity UV lamp as the exposure source.

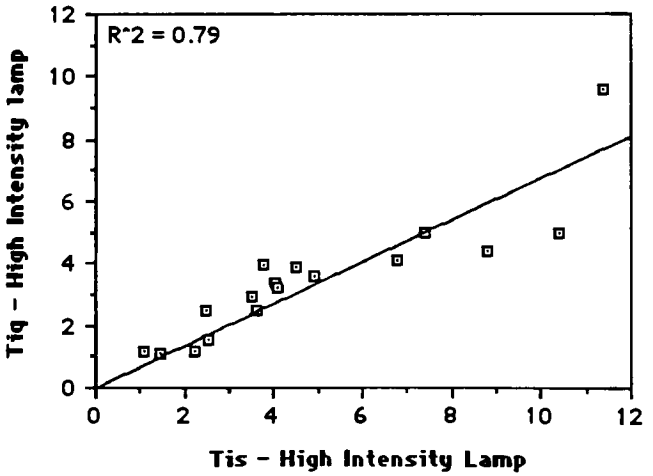

Figure 4.9: Enlargement of figure 4.8

In either case, if we hypothesize that there is no correlation between T_{is} and T_{iq} when the high intensity lamp is used as the exposure source, then at the 95% confidence level we can reject this hypothesis. We would thus accept the alternate hypothesis that there is a linear relationship between T_{is} and T_{iq}.

4.7.2 Correlation of the Shrinkage and the Rate Gammas

If shrinkage and heat are both proportional to the percent conversion, then there should be a correlation between the shrinkage gamma and the two rate gammas. Figure 4.10 is a plot of Γ_{q1} versus Γ_s with the low intensity UV lamp as the exposure source. The line in the figure is the best fit line found from simple linear regression with an intercept of the

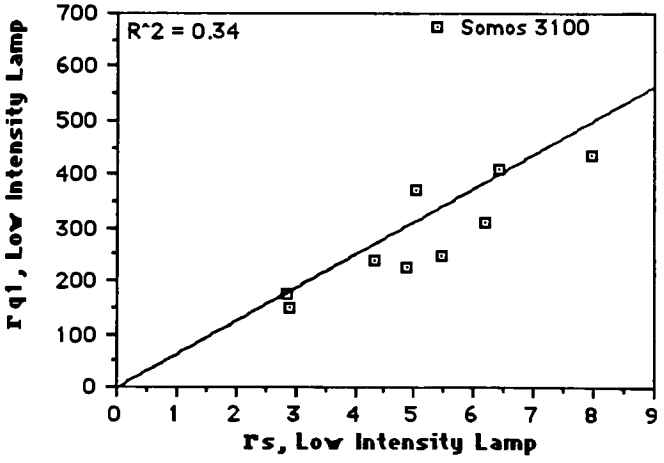

Figure 4.10: Γ_s versus Γ_{q1} using the low intensity UV lamp as the exposure source.

origin. The correlation of the data is low, (R^2 = 0.34) which is mostly due to the data point for Somos 3100. Somos 3100 has the highest Γ_{q1} value, due to it's very large peak height, H_p. It appears from the data shown in figure 4.10 that there might be a correlation between Γ_{q1} and Γ_s, except for the data point belonging to the Somos 3100 resin. However, we do not have a reason to remove Somos 3100 from the analysis, and so it must remain. If we were to make the null hypothesis that there is no correlation between Γ_{q1} and Γ_s, then at the 95% confidence level, we would have to accept that our null hypothesis is correct. We therefore conclude that there is no correlation between Γ_{q1} and Γ_s, when the low intensity UV lamp is used as the exposure source.

Figure 4.11 shows Γ_{q1} versus Γ_s when using the high intensity UV lamp as the exposure source. The slope of the line that best fits the data,

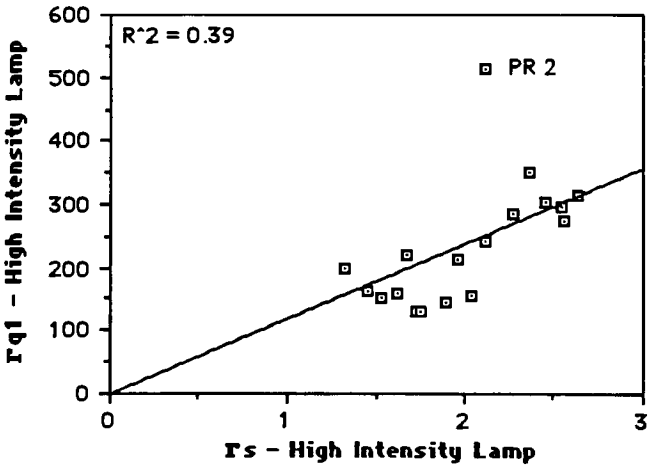

Figure 4.11: Γ_s versus Γ_{q1} using the high intensity UV lamp as the exposure source.

with an intercept through the origin, is shown in the graph. The data is not highly correlated with a R^2 value of 0.39. This low correlation could be a result of the data point for resin PR2. Again, there is no good reason to remove resin PR2 from the analysis, so it will remain. In either case, if we make the null hypothesis that there is no correlation between Γ_{q1} and Γ_s when using the high intensity UV lamp as the exposure source, then we would reject the null hypothesis at the 95% confidence level. We therefore conclude that there is a correlation between Γ_{q1} and Γ_s, when the high intensity UV lamp is used as the exposure source.

Figure 4.12 is a plot of Γ_{q2} versus Γ_s when using the low intensity UV lamp as the exposure source. The data is moderately correlated with a R^2 value of 0.75. The line in figure 4.12 is the best fit line of the data with an intercept of the origin. If we make the null hypothesis that there is no

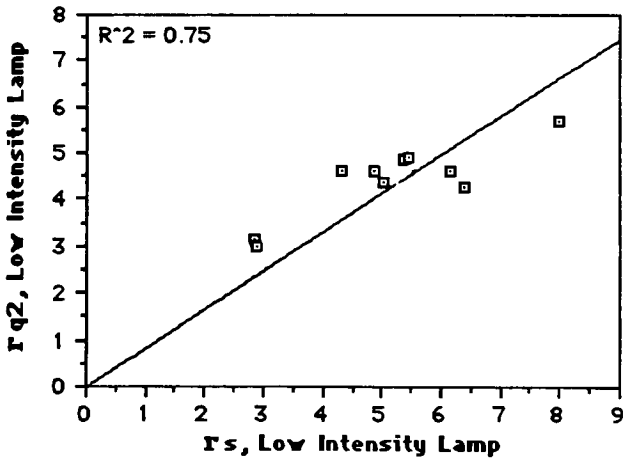

Figure 4.12: Γ_s versus Γ_{q2} using the low intensity UV lamp as the exposure source.

correlation between Γ_{q2} and Γ_s, then at the 95% confidence level, we can reject the null hypothesis, and thus accept the alternate hypothesis that Γ_{q2} and Γ_s are correlated. Out of all the correlations between the shrinkage gamma and the rate gammas presented in this section, the highest correlation comes about when comparing Γ_{q2} and Γ_s while the low intensity UV lamp is used as the exposure source. This is a strong indication that these two gammas are measuring the same property of the resin. From this result, we expect that these two gammas will have the highest correlation with the slopes of the working curves, presented in chapter five.

For the final comparison, figure 4.13 shows the plot of Γ_{q2} versus Γ_s with the high intensity lamp as the exposure source. The R^2 value of the data is low, at 0.05. The data point in figure 4.13 with the largest Γ_{q2} value

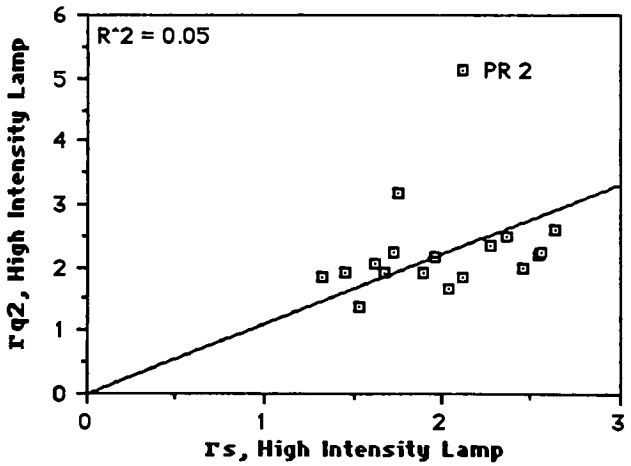

Figure 4.13: Γ_s versus Γ_{q2} using the high intensity UV lamp as the exposure source.

belongs to resin PR2. If we make the null hypothesis that there is no correlation between Γ_{q2} and Γ_s, then at the 95% confidence level, we would have to accept this hypothesis. We therefore conclude that there is no correlation between Γ_{q2} and Γ_s, when the high intensity UV lamp is used as the exposure source.

From the results presented in section 4.7, we can see that both the shrinkage and the rate sensitometers are good at producing highly correlated induction period data. This leads us to believe that the both of the sensitometers are measuring the same thing, as far as the induction period is concerned. The correlation between the shrinkage gamma and the rate gammas was not as high as expected, with the highest correlation being between Γ_{q2} and Γ_s when the low intensity UV lamp is used as the exposure source. We also find correlation between Γ_{q1} and Γ_s, when using the high intensity UV lamp as the exposure sources. As a result of finding some correlation between the shrinkage and the rate gammas, we have reason to believe that both sensitometers could be measuring the same properties of the resins.

5 Hypothesis Testing

5.1 Introduction

In this section we will test the null hypotheses as discussed in chapter one. For all sensitometers, we hypothesized that there is no correlation between the sensitometric property measured and the corresponding measure from the working curves. If the null hypothesis is rejected in favor of the alternate hypothesis, then we can say that there is some partial linear relationship between the variables.

For the shrinkage sensitometer we have two null hypotheses. The first null hypothesis is that there is no correlation between the induction period (T_{is}) and the critical exposure (E_c) as measured from the working curve. The second null hypothesis is that there is no correlation between the shrinkage gamma (Γ_s) and D_p as measured from the working curve. These hypotheses will be tested for both the high and low intensity UV lamps used as the exposure sources.

- Hypothesis tests for the shrinkage sensitometer:
  - Correlation of T_{is} and E_c:

    H_0: $\rho = 0$, for $T_{is} \propto E_c$

    H_1: $\rho \neq 0$, for $T_{is} \propto E_c$
  - Correlation of Γ_s and D_p:

    H_0: $\rho = 0$, for $\Gamma_s \propto D_p$

    H_1: $\rho \neq 0$, for $\Gamma_s \propto D_p$

The rate sensitometer has a total of three null hypotheses. The first is that there is no correlation between the induction period (T_{iq}) and the critical exposure (E_c). The second null hypothesis is that there is no correlation between the first rate gammas (Γ_{q1}) and D_p. The third null hypothesis is that there is no correlation between the second rate gamma (Γ_{q2}) and Dp. Each of these hypotheses will be tested when using both the high and low intensity UV lamps as the exposure source in the rate sensitometer.

- Hypothesis tests for the rate sensitometer:
  - Correlation of T_{iq} and E_c:

$$H_0: \quad \rho = 0, \text{ for } T_{iq} \propto E_c$$

$$H_1: \quad \rho \neq 0, \text{ for } T_{iq} \propto E_c$$

  - Correlation of Γ_{q1} and D_p:

$$H_0: \quad \rho = 0, \text{ for } \Gamma_{q1} \propto D_p$$

$$H_1: \quad \rho \neq 0, \text{ for } \Gamma_{q1} \propto D_p$$

  - Correlation of Γ_{q2} and D_p:

$$H_0: \quad \rho = 0, \text{ for } \Gamma_{q2} \propto D_p$$

$$H_1: \quad \rho \neq 0, \text{ for } \Gamma_{q2} \propto D_p$$

For the absorbancy sensitometer, there is only one hypothesis. The null hypothesis is that there is no correlation between the optical density and the inverse of the slope of the working curve, D_p. The total absorbancy of the resins is the sum of the absorbancies at each of six wavelengths used by the UV laser employed to make the working curves of the resins.

- Hypothesis tests for the absorbancy sensitometer:
  - Correlation of the optical density and $1/D_p$:

$$H_0: \quad \rho = 0, \text{ for O.D.} \propto 1/D_p$$

$$H_1: \quad \rho \neq 0, \text{ for O.D.} \propto 1/D_p$$

The flash sensitometer is a simple attempt to reproduce the working curves of the resins using an alternate exposure source. There are two hypotheses for the flash sensitometer. The first is that there will be no correlation between the critical exposure measured from the flash sensitometer (E_{cf}) and the critical exposure measured from the working curve (E_c). The second is that there is no correlation between the slopes of the working curves produced with the flash sensitometer (D_{pf}) and the slopes of the working curves produced with the laser scanner (D_p).

- Hypothesis tests for the flash sensitometer:
  - Correlation of E_{cf} and E_c:

$$H_0: \quad \rho = 0, \text{ for } E_{cf} \propto E_c$$

$$H_1: \quad \rho \neq 0, \text{ for } E_{cf} \propto E_c$$

  - Correlation of D_{pf} and D_p:

$$H_0: \quad \rho = 0, \text{ for } D_{pf} \propto D_p$$

$$H_1: \quad \rho \neq 0, \text{ for } D_{pf} \propto D_p$$

5.2 Shrinkage Sensitometer

5.2.1 Comparison of the Induction Period with E_c

Figure 5.1 is a plot of E_c versus T_{is}, where T_{is} is measured with the low intensity UV lamp as the exposure source. The R^2 value of the data, assuming an intercept of the origin, is 0.71. The line through the data in figure 5.26 is the best fit line found through simple linear regression with an intercept of the origin. We must recall that when comparing critical exposure values to induction period values that there is a lot of error (low precision) in the measurement of E_c as evidenced by table 4.6. The 95% confidence intervals for E_c have been included in figure 5.1 to demonstrate the variability of the E_c data. When testing our null hypothesis that there

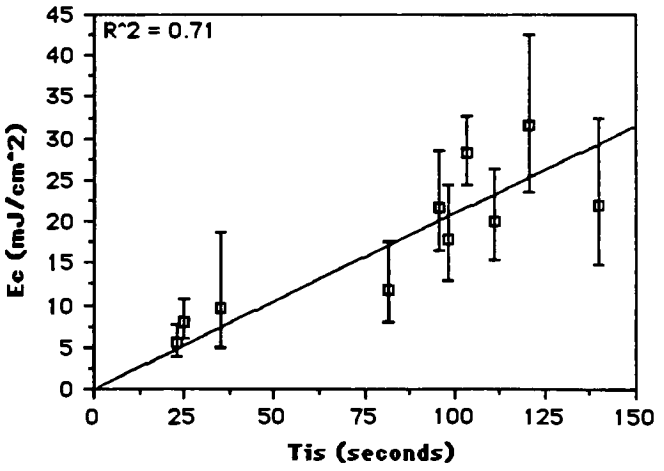

Figure 5.1: E_c versus T_{is} using the low intensity UV lamp as the exposure source.

is no correlation between E_c and T_{is}, we can state at the 95% confidence level that our hypothesis is incorrect. Therefore, we would accept that our alternate hypothesis is true, and we can conclude that there is a correlation between E_c and T_{is}, when T_{is} is measured with the low intensity UV lamp as the exposure source.

Figure 5.2 is a comparison of E_c with T_{is}, where T_{is} is measured with the high intensity UV lamp. The R^2 value, assuming an intercept of the origin, is 0.96. This is deceptively high for this plot, due to the extremely high T_{is} and E_c values for resin PR2. Without the data point for resin PR2, the scatter of the data is slightly more evident. Figure 5.3 is an enlargement of figure 5.2, where resin PR2 has been omitted from the analysis of the data. The data point for resin PR2 is not being thrown out of the analysis, but is being temporarily omitted to provide a closer look at

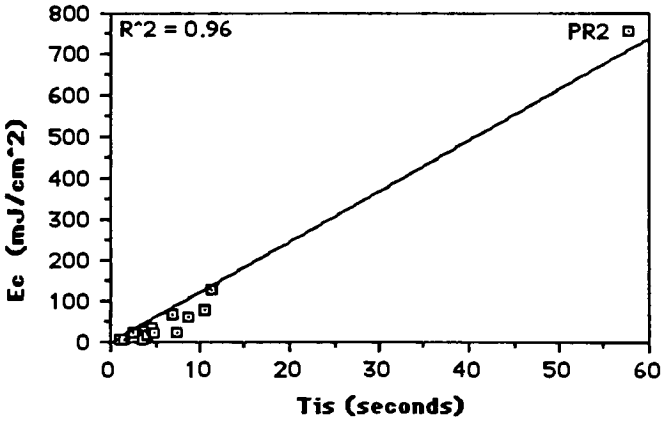

Figure 5.2: E_c versus T_{is} using the high intensity UV lamp as the exposure source.

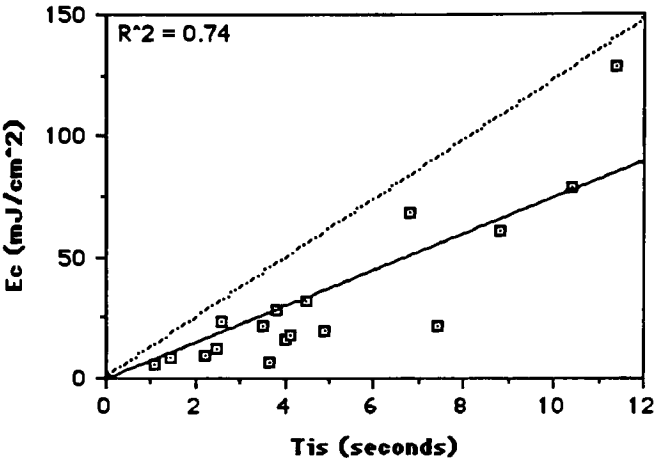

Figure 5.3: Enlargement of figure 5.2, excluding resin PR2 from the analysis

the remaining data. The dotted line in figure 5.3 is the same line from figure 5.2. The solid line is the best fit line of the remaining data with an intercept of the origin. The data in figure 5.3 has a R^2 value of 0.74, again this is assuming an intercept of the origin. When testing our null hypothesis that there is no correlation between E_c and T_{is}, we can state at the 95% confidence level that our hypothesis is incorrect. This holds true whether or not resin PR2 is included in the analysis. We would therefore accept our alternate hypothesis that E_c and T_{is} are correlated, when T_{is} is measured with the high intensity UV lamp as the exposure source.

5.2.2 Comparison of the Shrinkage Gamma with D_p

Figure 5.4 is a graph of D_p versus Γ_s, when the low intensity UV lamp is used as the exposure source in the shrinkage sensitometer. The R^2 value of the data, assuming an intercept of the origin, is 0.24, which indicates little to no correlation of the data. Included in figure 5.4 is the 95% confidence intervals for D_p. We can see from this that the majority of the scatter of the data cannot be attributed to the imprecision in the measurement of D_p. When testing our null hypothesis that there is no correlation between D_p and Γ_s, we would have to accept that our null hypothesis is correct at the 95% confidence level. We therefore conclude that there is no correlation between D_p and Γ_s, when Γ_s is measured with the low intensity UV lamp.

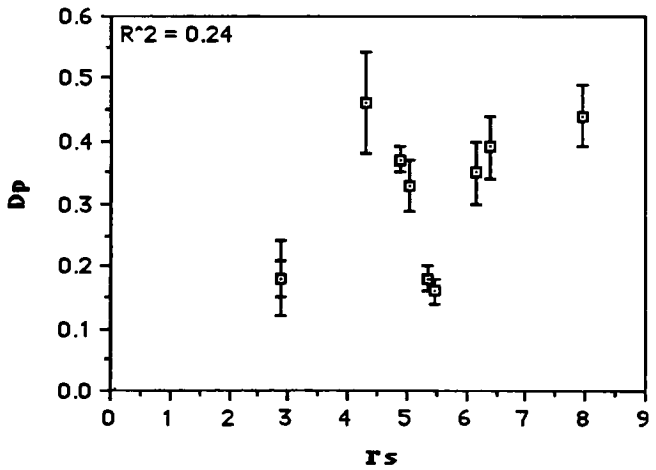

Figure 5.4: D_p versus Γ_s using the low intensity UV lamp as the exposure source.

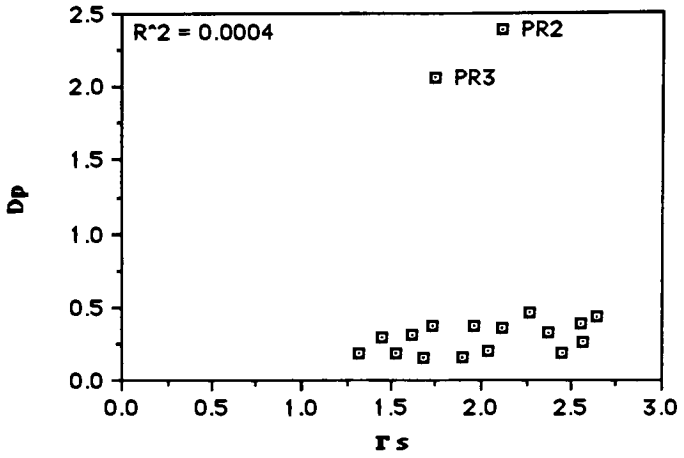

Figure 5.5: D_p versus Γ_s using the high intensity UV lamp as the exposure source.

Figure 5.5 shows the correlation between D_p and Γ_s for the high intensity lamp as the exposure source. The R^2 value of the data, again assuming an intercept of the origin, is approximately zero, at only 0.0004. When testing our null hypothesis that there is no correlation between D_p and Γ_s, we would have to accept that our null hypothesis is correct at the 95% confidence level. We therefore conclude that there is no correlation between D_p and Γ_s, when Γ_s is measured with the high intensity UV lamp.

5.3 Rate Sensitometer

5.3.1 Comparison of the Induction Period with E_c

Figure 5.6 is a plot of E_c versus T_{iq}, where T_{iq} is measured using the low intensity UV lamp as the exposure source. The R^2 value of the data, assuming an intercept of the origin, is 0.55. The line shown in the figure is the best fit line found through simple linear regression with an intercept of the origin. The error bars in figure 5.6 are the 95% confidence intervals for E_c, as given in table 4.6. When testing our null hypothesis that there is no correlation between E_c and T_{is}, we can state at the 95% confidence level that our hypothesis is incorrect. We would thus accept our alternate hypothesis that there is a correlation between E_c and T_{iq},

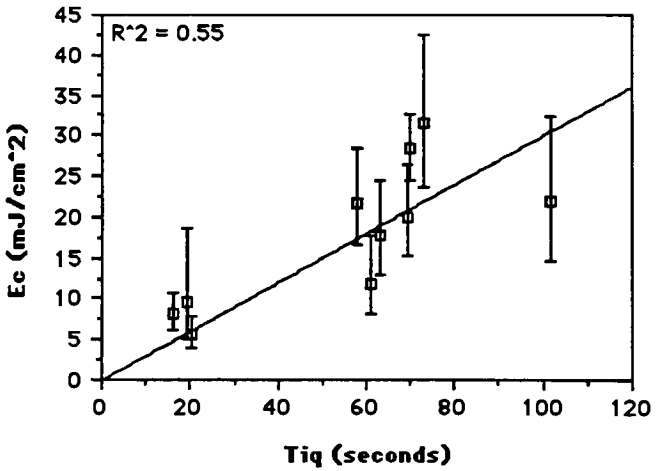

Figure 5.6: E_c versus T_{iq} using the low intensity UV lamp as the exposure source.

where T_{iq} is measured with the low intensity UV lamp as the exposure source.

Figure 5.7 shows the correlation between E_c and T_{iq} when the high intensity UV lamp is used as the exposure source. The line in the figure shows the best fit line of the data with an intercept of the origin. The R^2 value, assuming an intercept of the origin, is 0.97. This is deceptively high for this plot, due to the extremely high T_{iq} and E_c values for resin PR2. An enlargement of figure 5.7 is shown in figure 5.8, where resin PR2 has been omitted from the statistical analysis. As with the shrinkage sensitometer, resin PR2 is not being thrown out of the analysis, but is being temporarily removed to show the correlation between the remaining resins. The dotted line in figure 5.8 is the same line shown in figure 5.7, and the solid line is the best fit line of the data, excluding resin PR2. The data in figure

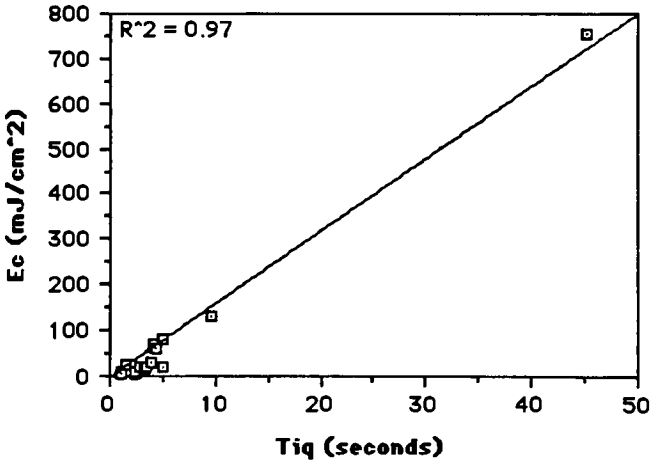

Figure 5.7: E_c versus T_{iq} using the high intensity UV lamp as the exposure source.

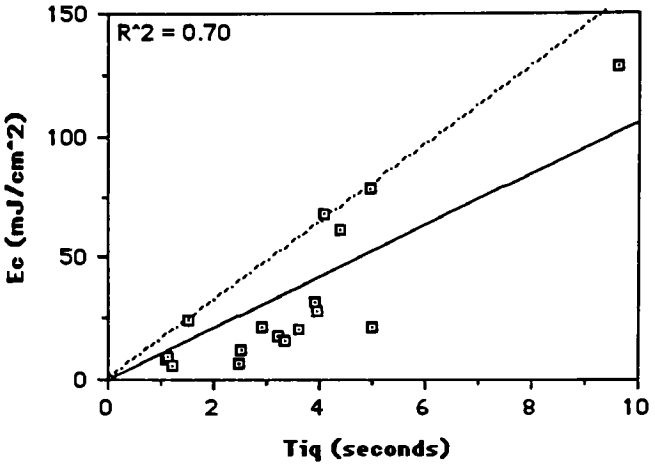

Figure 5.8: Enlargement of figure 5.7, excluding resin PR2 from the analysis.

5.8 has a R^2 value, again assuming an intercept of the origin, of 0.70. When testing our null hypothesis that there is no correlation between E_c and T_{is}, we can state at the 95% confidence level that our hypothesis is incorrect. This holds true whether or not resin PR2 is included in the analysis. We would thus accept our alternate hypothesis that there is a correlation between E_c and T_{iq}, where T_{iq} is measured with the high intensity UV lamp as the exposure source.

5.3.2 Comparison of the Rate Gammas with D_p

Figure 5.9 shows the correlation between D_p and Γ_{q1}, when the low intensity UV lamp is used as the exposure source. The R^2 value of the

data, assuming an intercept of the origin, is essentially zero, at 0.004. The error bars in the figure show the 95% confidence intervals for the D_p measurement. We can see from this graph that not all of the scatter of the data can be attributed to the error in the measurement of D_p. When testing our null hypothesis that there is no correlation between D_p and Γ_{q1}, we would have to accept that our null hypothesis is correct at the 95% confidence level. We therefore conclude that there is no correlation between D_p and Γ_{q1}, when Γ_{q1} is measured with the low intensity UV lamp.

Figure 5.10 is a plot of D_p versus Γ_{q1} when the high intensity UV lamp is used as the exposure source. The correlation of this data is low, with a R^2 value of 0.16, assuming an intercept of the origin. As with previous

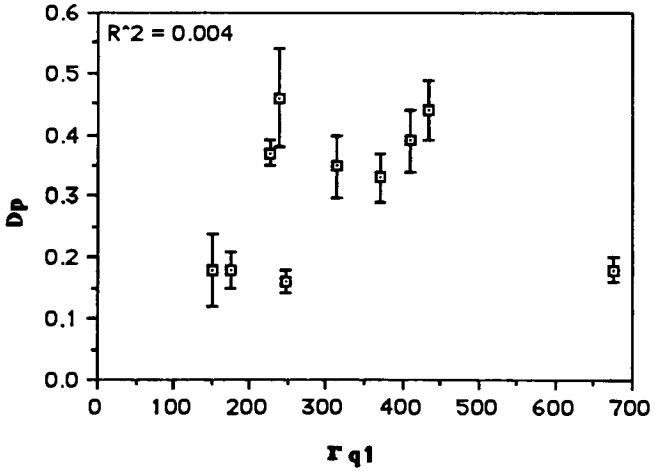

Figure 5.9: D_p versus Γ_{q1} using the low intensity UV lamp as the exposure source.

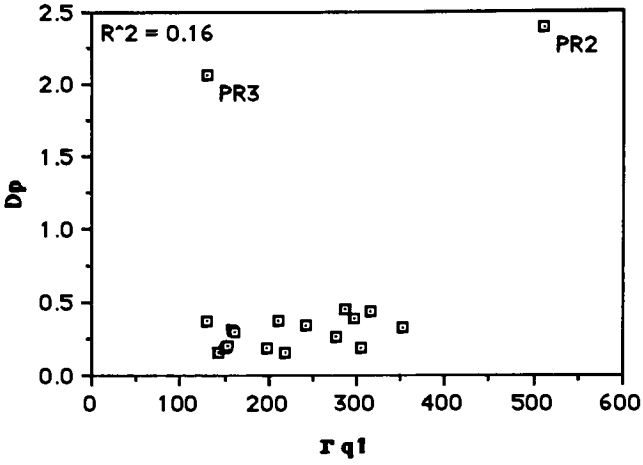

Figure 5.10: D_p versus Γ_{q1} using the high intensity UV lamp as the exposure source.

results, there appears to be some correlation of the data if the data points from resins PR2 and PR3 are eliminated from the analysis. However, if these data points are removed there is no improvement in the correlation of the data. The R^2 value remains unchanged, at 0.16. When testing our null hypothesis that there is no correlation between D_p and Γ_{q1}, we would have to accept that our null hypothesis is correct at the 95% confidence level. We therefore conclude that there is no correlation between D_p and Γ_{q1}, when Γ_{q1} is measured with the high intensity UV lamp.

Figure 5.11 shows the plot of D_p versus Γ_{q2}, where Γ_{q2} is measured using the low intensity UV lamp as the exposure source. The R^2 value of the data, assuming an intercept of the origin, is 0.24. The error bars shown in figure 5.11 are the 95% confidence intervals for D_p. Again, we can see

that not all of the scatter of the data can be attributed to the variability in the measurement of D_p. When testing our null hypothesis that there is no correlation between D_p and Γ_{q2}, we would have to accept that our null hypothesis is correct at the 95% confidence level. We therefore conclude that there is no correlation between D_p and Γ_{q2}, when Γ_{q2} is measured with the low intensity UV lamp.

Figure 5.12 shows the data plot of D_p versus Γ_{q2}, when the high intensity lamp is used as the exposure source. The R^2 value of the data, assuming an intercept of the origin, is 0.47. As with previous results, there appears to be some correlation of the data if the data points from resins PR2 and PR3 are eliminated from the analysis. However, if these data points are removed there is no improvement in the correlation of the

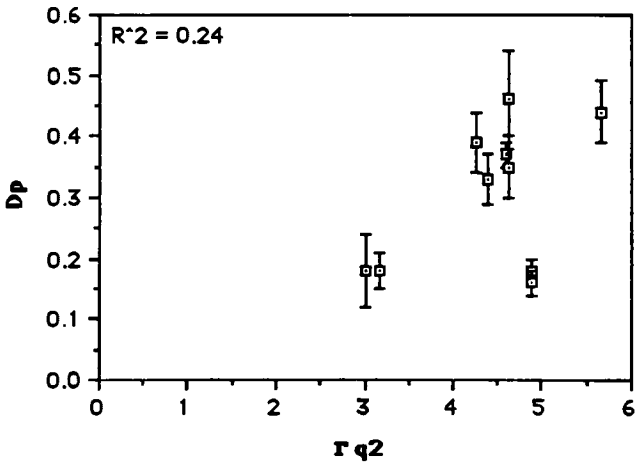

Figure 5.11: D_p versus Γ_{q2} using the low intensity UV lamp as the exposure source.

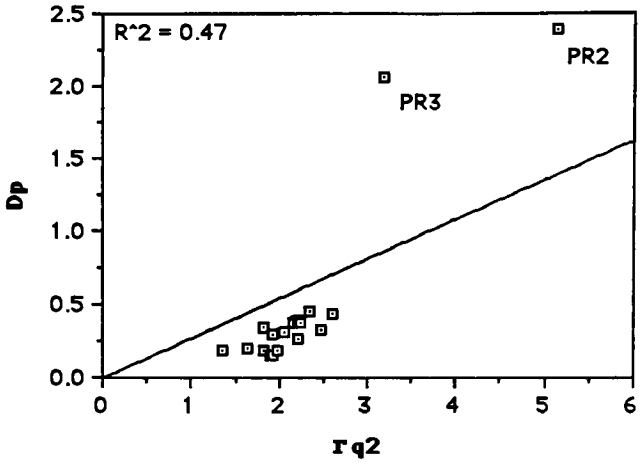

Figure 5.12: D_p versus Γ_{q2} using the high intensity UV lamp as the exposure source.

data. When these two data points are removed from the analysis, the R^2 value drops to 0.43. Again we must point out that PR2 and PR3 are not being thrown out of the analysis, the are being temporarily removed to determine the correlation of the remaining resins. When testing our null hypothesis that there is no correlation between D_p and Γ_{q2}, we can state at the 95% confidence level that our hypothesis is incorrect. We would thus accept our alternate hypothesis that there is a correlation between D_p and Γ_{q2}, where Γ_{q2} is measured with the high intensity UV lamp as the exposure source. This conclusion is reached whether or not resins PR2 and PR3 are included in the analysis.

The comparison between the optical density and the inverse of D_p is shown in figure 5.13, where the total absorbancy was tabulated in table 4.14. The R^2 value of the data, assuming an intercept of the origin, is 0.79. The line shown in figure 5.13 is the best fit line of the data, with an intercept of the origin. When testing our null hypothesis that there is no correlation between the optical density and $1/D_p$, we can state at the 95% confidence level that our hypothesis is incorrect. We would thus accept our alternate hypothesis that there is a correlation between the optical density and $1/D_p$.

From the shrinkage and the rate experiments, there was only one gamma (Γ_{q2} measured with the high intensity UV lamp) for which we could conclude that a correlation exists with D_p. This correlation, shown

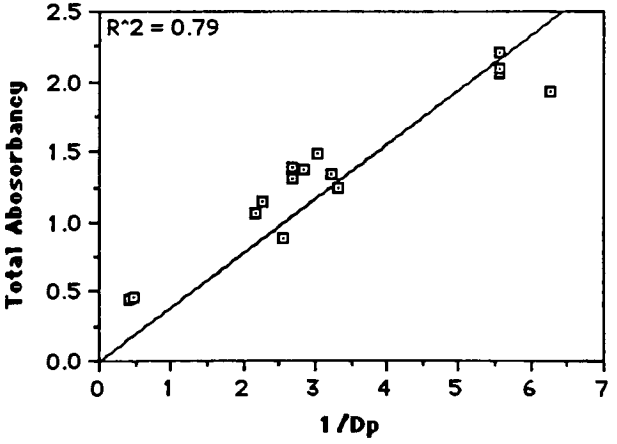

Figure 5.13: The total absorbancy versus $1/D_p$.

in figure 5.12, is not as linear as the correlation between the optical density and $1/D_p$, according to their respective R^2 values. Given the ease of measuring the optical density of the resins along with the high correlation of the optical density with the inverse of D_p, the measurement of absorbancy proves to be a much better method of indirectly determining the D_p value of a resin than using either the shrinkage or rate sensitometer.

5.5 The Flash Sensitometer

The flash sensitometer is a simple experiment to determine if the working curve data can be accurately reproduced using an alternative exposure source. If the slope (D_{pf}) and exposure axis intercept (E_{cf}) of the flash sensitometer accurately reflect the D_p and E_c data measured with the LADDER method of producing working curves, then there should be a linear correlation between D_p and D_{pf} and between E_c and E_{cf}.

Figure 5.14 shows the correlation between E_{cf} and E_c. The bold line in the figure is the best fit line of the data with an intercept of the origin. The dotted line is the line found from simple linear regression, without the required condition of an intercept of the origin. The R^2 value of the data, without the constraint on an intercept of the origin, is 0.65. The error bars in figure 5.14 are the 95% confidence intervals for E_{cf}. It is evident from this graph that not all of the non correlation can be attributed to error in the measurement of E_{cf}. When testing our null hypothesis that there is

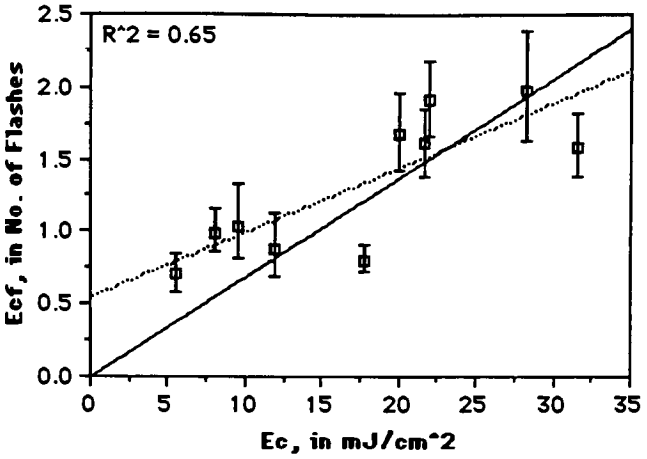

Figure 5.14: E_{cf} versus E_c.

no correlation between E_c and E_{cf}, we can state at the 95% confidence level that our hypothesis is incorrect. We would thus accept our alternate hypothesis that there is a correlation between E_c and E_{cf}.

Figure 5.15 shows the correlation graph between D_p and D_{pf}. The solid line in the figure is the best fit line with an intercept of the origin. The dotted line is the line found from simple linear regression without the required condition of an intercept of the origin. The R^2 value of the data is very low, at 0.08. It is important to recall, from chapter 3 section 5, the error that is associated in measuring the thickness of the polymer samples as produced with the flash sensitometer. However, from the 95% confidence intervals for D_{pf} (shown in figure 5.15) and the 95% confidence intervals for D_p, it is evident that the scatter of the data of figure 5.15 cannot be fully attributed to imprecision in the measurement process.

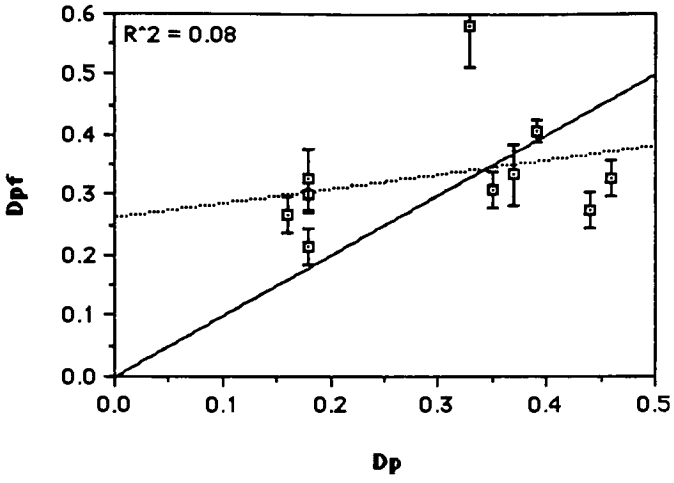

Figure 5.15: D_{pf} versus D_p.

When testing our null hypothesis that there is no correlation between D_p and D_{pf}, at the 95% confidence level we would have to accept our null hypothesis that there is no correlation between D_p and D_{pf}.

6 Conclusions and Recommendations

The shrinkage sensitometer is capable of measuring the critical exposure of the resins. The induction period (T_{is}) measured with the shrinkage sensitometer is highly correlated with the critical exposure (E_c) measured from the laser scanner. However, the slope of the shrinkage versus exposure curve (Γ_s) does not correlate with the slope of the working curve (D_p), as was predicted by Reiser's fundamental measurement of the sensitometric properties of a photopolymer. A summary of the results from the shrinkage sensitometer is listed below.

T_{is}	Correlates with E_c, using either the high or low intensity lamps as the exposure source.
Γ_s	Does not correlate with D_p, using either the high or low intensity lamps as the exposure source.

The rate sensitometer is also capable of measuring the critical exposure of the resins. The induction period (T_{iq}) measured with the rate sensitometer is highly correlated with the critical exposure (E_c) measured from the laser scanner. However, the slope of the cumulative heat output versus exposure curve (Γ_{q1}) does not correlate with the slope of the working curve (D_p). This contradicts what was predicted by Reiser's fundamental measurement of the sensitometric properties of a photopolymer. The second rate gamma (Γ_{q2}) showed a little more

promise as a potential measure of D_p. When the high intensity UV lamp was used as the exposure source, it was determined that a correlation exists between Γ_{q1} and D_p. However, no correlation was found between Γ_{q2} and D_p when the low intensity UV lamp was used as the exposure source. A summary of the results from the rate sensitometer is listed below.

T_{iq}	Correlates with E_c, using either the high or low intensity lamps as the exposure source.
Γ_{q1}	Does not correlate with D_p, using either the high or low intensity lamps as the exposure source.
Γ_{q2}	Does not correlate with D_p, using the low intensity lamp as the exposure source, but does correlate with D_p using the high intensity lamp as the exposure source.

The shrinkage and the rate sensitometers could be used to determine a resin's critical exposure. However, they would first need to be engineered for greater precision and then calibrated using an exposure source of known intensity. For more accurate results, the wavelength of the exposure source used with the shrinkage and rate sensitometer should match the wavelength used to expose the resins in a SLA.

A reason that we do not see any correlation between D_p and the shrinkage gamma and the two rate gammas could be the assumptions upon which the Reiser model was used. According to Reiser, the fundamental measurement of the sensitometric properties of a

photopolymer is the percentage of monomer converted to polymer as a function of exposure. This model was developed for thin layers of photopolymer resins for use in lithographic printing processes. It is evident that this does not carry over into the stereolithographic regime, where thick layers of photopolymer are stacked one on top the other.

The slopes of the working curves can be approximated by measuring the optical density of the resins. A correlation exists between the optical density of the resins and the inverse of D_p. This correlation was predicted by the Jacobs' model of the working curves, based on the Beer-Lambert law of absorption. The correlation between the optical density and $1/D_p$ is higher than any correlation that might exist between the three measures of gamma and D_p. Therefore, as an indirect measure of a resin's D_p value, the optical density proves to be more capable than any gamma determined from the shrinkage and rate sensitometers.

The flash sensitometer was a simple attempt to reproduce the working curves of the resins using an alternative exposure source. As was mentioned earlier, a lot of error was encountered in measuring the thickness of the polymer samples from the flash sensitometer, and this could have potentially effected the results. There is a correlation between E_c and E_{cf}, although the data is not as linear as was expected. This could be a result of the above mentioned measurement error. The slope of the flash working curve, D_{pf}, does not have any correlation with D_p. The scatter of the data is far greater than the error in the measurement process

of D_p and D_{pf}. From these results, it appears that the flash sensitometer is not a good device to use for the reproduction of the working curves.

As a recommendation for a further area of study the shrinkage sensitometer could be used as an alternate method of determining the Shrinkage Compensation Factor (SCF) used in a SLA. The SCF is entered into a SLA to compensate for the shrinkage that occurs when a resin polymerizes. Jacobs describes a rigorous method to determine the SCF, called the CHRISTMAS TREE™ diagnostic part (Jacobs, 1992 pp. 281-285). A correlation between the percent shrinkage measured by the shrinkage sensitometer and the SCF measured on a SLA could be determined. If a correlation exists, then the shrinkage sensitometer could be used as a faster and easier method of determining the SCF.

Appendix A

Resin Name	Company
PR 1	Proprietary Resin #1
PR 2	Proprietary Resin #2
PR 3	Proprietary Resin #3
PR 4	Proprietary Resin #4
PR 5	Proprietary Resin #5
PR 6	Proprietary Resin #6
Cubital 5601	Coates (England)
Loctite 8100	Loctite Corporation
SLA 5081-1*	Ciba Geigy, 3D Systems
SLR 804	DSM Desoteck Inc.
Somos 2100	DuPont
Somos 3100	DuPont
Somos 4100	DuPont
Somos 5100	DuPont
XB 5131	Ciba Geigy, 3D Systems
XB 5143	Ciba Geigy, 3D Systems
XB 5149	Ciba Geigy, 3D Systems
XB 5154	Ciba Geigy, 3D Systems

At the request of some companies, the names of the proprietary resins and the companies that manufacture them are not being published. They will be referred to as Proprietary Resins (PR) numbered 1 through 6.

* Also called XB 5081-1 in literature references.

Appendix B: Pretesting the shrinkage and rate sensitometers with HDDA.

Raw data from the measurement of shrinkage of monomer HDDA using the shrinkage sensitometer. At the bottom of each column is the average and standard deviation of each measurement. The %Error listed is found by dividing the standard deviation by the mean and multiplying by 100 (different than the calculation found in the text). The second set of averages, standard deviations and %Errors is for the data excluding the highlighted point.

X_f = final thickness (measured with micrometer)

Δx = change in thickness (measured from output).

Sample#	T_{is}	T_{hs}	X_f (mm)	Δx (mm)	%S	Γ_s
1	3.36	7.92	121	20.28	14.35	2.69
2	3.36	7.20	118	19.11	13.94	3.02
3	2.64	6.48	111	18.17	14.07	2.56
4	2.40	6.24	110	18.72	14.54	2.41
5	2.40	6.72	121	19.19	13.69	2.24
6	3.36	8.40	133	21.53	13.93	2.51
7	2.88	7.20	113	18.95	14.36	2.51
8	2.40	6.48	124	20.83	14.38	2.32
9	2.40	7.20	120	20.28	14.46	2.10
10	2.40	6.72	114	19.50	14.61	2.24
11	2.40	6.72	125	19.81	13.68	2.24
12	2.88	6.24	114	18.72	14.10	2.98
13	2.16	6.48	114	19.50	14.61	2.10
14	5.28	11.04	115	18.33	13.75	3.12
15	2.40	7.20	132	23.01	14.84	2.10
16	2.40	6.72	124	21.84	14.98	2.24
17	2.40	6.24	113	18.33	13.96	2.41
18	2.40	6.72	127	20.98	14.18	2.24
19	2.88	6.48	116	18.33	13.65	2.84
20	2.16	6.72	133	22.62	14.54	2.03
21	2.40	6.72	123	22.00	15.17	2.24
22	3.36	6.24	124	20.28	14.06	3.72
23	2.16	6.48	130	20.59	13.67	2.10
24	2.64	6.72	123	22.62	15.53	2.46
25	2.40	6.24	128	21.14	14.17	2.41
Average:	2.72	6.94	121.04	20.19	14.29	2.47
St. Dev. :	0.66	1.00	7.05	1.49	0.49	0.40
%Error:	24.29	14.43	5.82	7.38	3.45	16.22
Average:	2.61	6.77	121.29	20.26	14.31	2.44
St. Dev. :	0.40	0.53	7.09	1.47	0.49	0.39
%Error:	15.17	7.89	5.84	7.25	3.42	15.77

Raw data from the measurement of rate of reaction of monomer HDDA using the rate sensitometer.

Sample #	T_{iq}	T_{hq}	Height (cm)	Γ_{q1}	Γ_{q2}
1	1.80	5.10	14.30	167.96	2.21
2	1.95	5.85	16.40	220.95	2.10
3	3.60	8.40	13.75	266.00	2.72
4	4.35	9.30	7.40	158.49	3.03
5	2.10	5.55	11.85	151.46	2.37
6	1.95	5.10	11.80	138.59	2.40
7	2.10	5.40	16.90	210.17	2.44
8	3.90	8.70	11.75	235.42	2.87
9	4.20	8.70	9.40	188.34	3.16
10	1.95	5.40	14.40	179.08	2.26
11	1.80	4.95	15.90	181.26	2.28
12	1.95	5.10	15.90	186.75	2.40
13	1.95	5.10	15.60	183.23	2.40
14	1.95	5.25	12.95	156.58	2.32
15	1.95	5.40	16.70	207.68	2.26
16	3.30	7.20	8.50	140.94	2.95
17	1.80	5.10	15.20	178.53	2.21
18	1.80	5.10	16.50	193.80	2.21
19	1.80	5.10	16.10	189.10	2.21
20	2.10	5.40	14.00	174.11	2.44
21	1.80	4.95	14.70	167.58	2.28
22	1.50	4.95	14.00	159.60	1.93
23	1.80	5.40	14.50	180.32	2.10
24	1.80	5.25	16.70	201.92	2.15
25	2.10	5.40	14.75	183.43	2.44
Average:	2.29	5.89	14.00	184.05	2.40
St. Dev. :	0.83	1.37	2.60	28.96	0.31
%Error:	36.41	23.22	18.61	15.73	12.86
Average:	1.90	5.24	14.96	180.60	2.27
St. Dev. :	0.15	0.23	1.53	20.52	0.14
%Error:	7.81	4.40	10.22	11.36	5.98

Appendix C: The working curves of the resins.

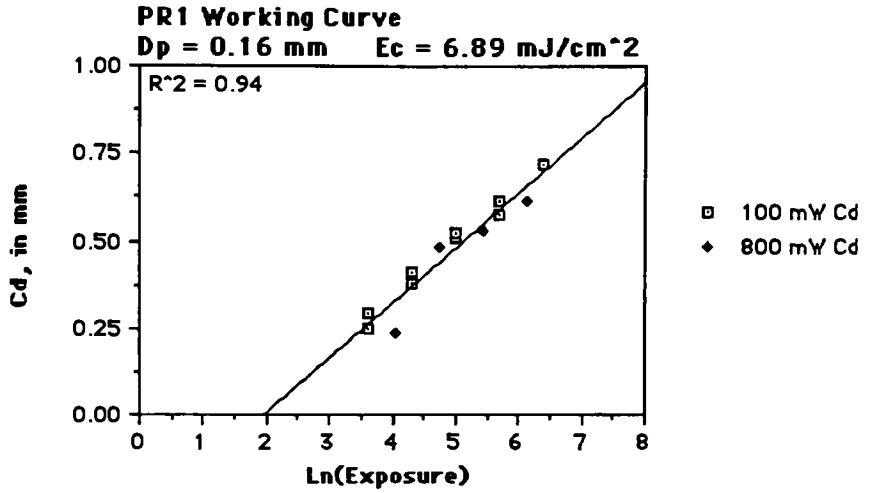

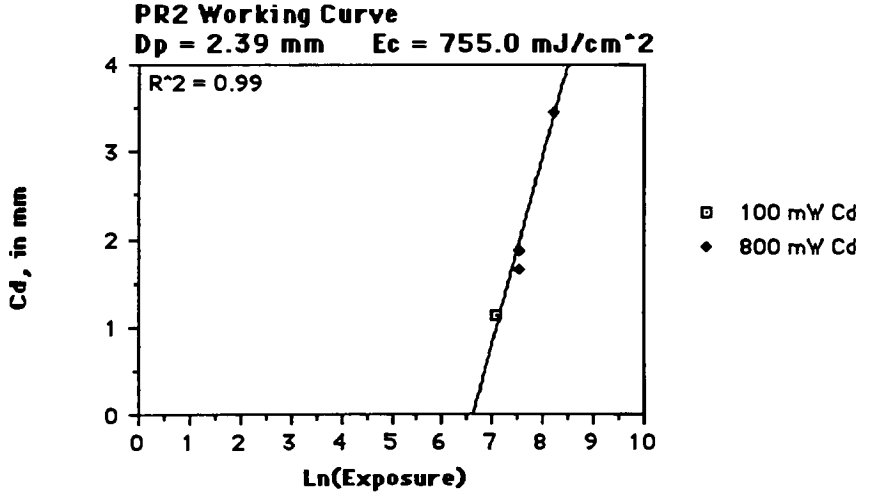

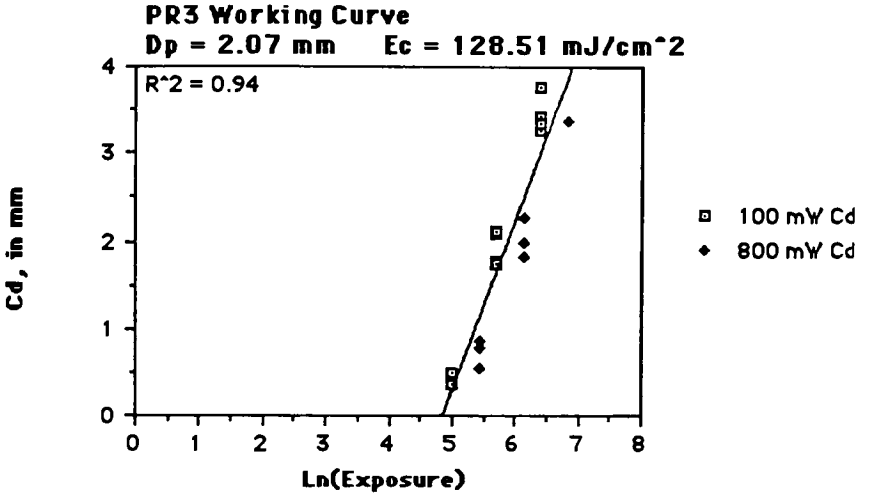
PR3 Working Curve
Dp = 2.07 mm Ec = 128.51 mJ/cm^2
R^2 = 0.94
Cd, in mm
Ln(Exposure)
100 mW Cd
800 mW Cd

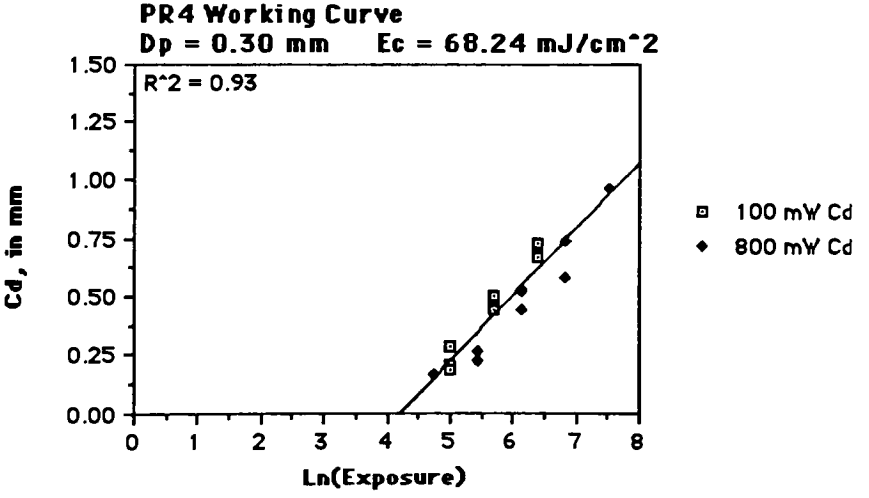
PR4 Working Curve
Dp = 0.30 mm Ec = 68.24 mJ/cm^2
R^2 = 0.93
Cd, in mm
Ln(Exposure)
100 mW Cd
800 mW Cd

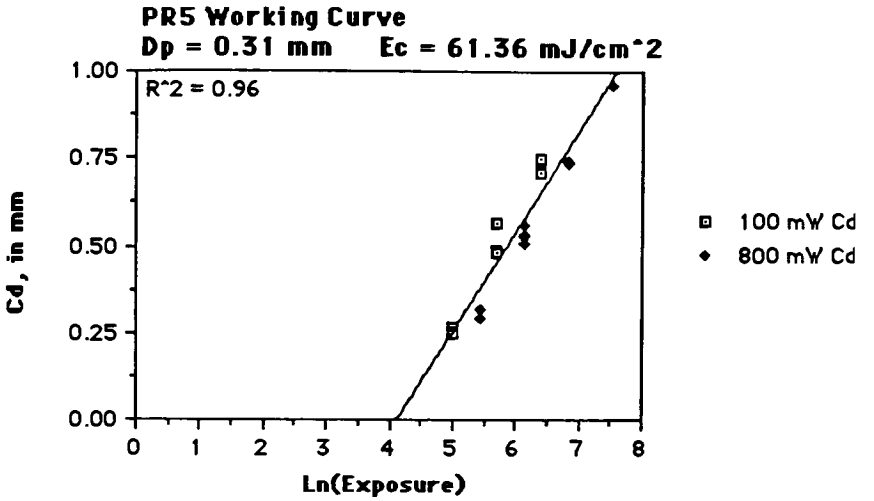
PR5 Working Curve
Dp = 0.31 mm Ec = 61.36 mJ/cm^2
R^2 = 0.96
Cd, in mm
1.00
0.75
0.50
0.25
0.00
0 1 2 3 4 5 6 7 8
Ln(Exposure)
100 mW Cd
800 mW Cd

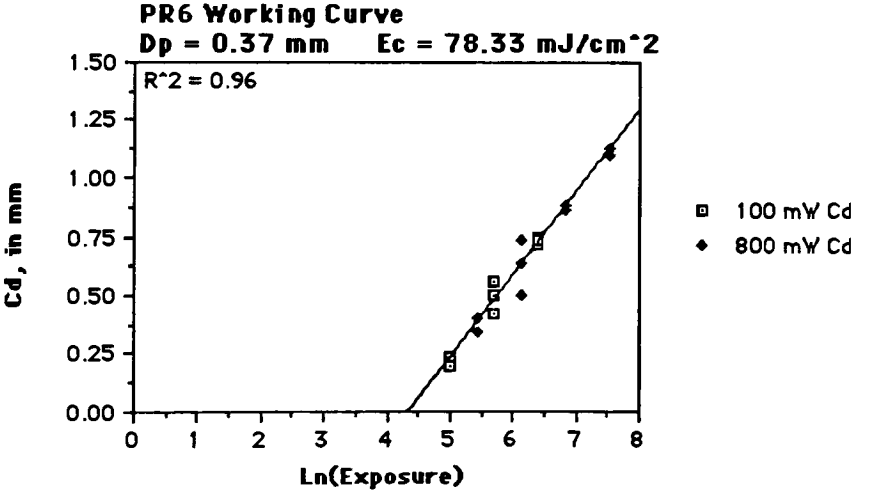
PR6 Working Curve
Dp = 0.37 mm Ec = 78.33 mJ/cm^2
R^2 = 0.96
Cd, in mm
1.50
1.25
1.00
0.75
0.50
0.25
0.00
0 1 2 3 4 5 6 7 8
Ln(Exposure)
100 mW Cd
800 mW Cd

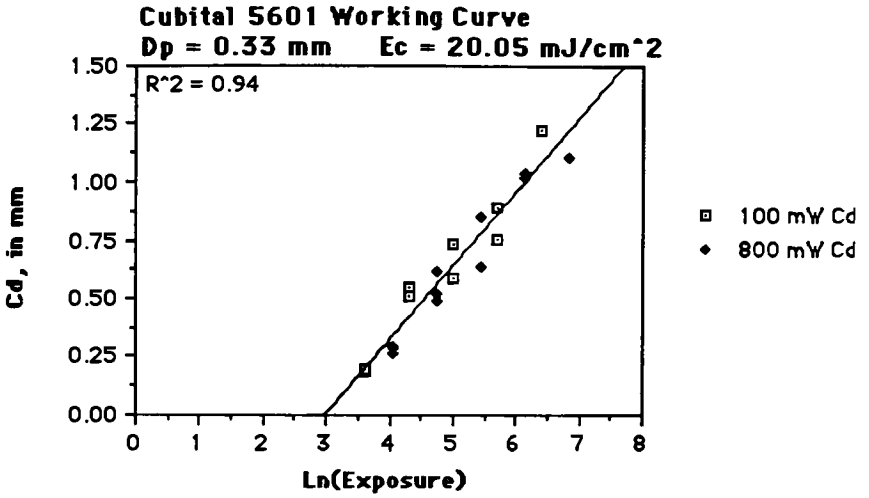
Cubital 5601 Working Curve
Dp = 0.33 mm Ec = 20.05 mJ/cm^2
R^2 = 0.94
Cd, in mm
Ln(Exposure)
100 mW Cd
800 mW Cd

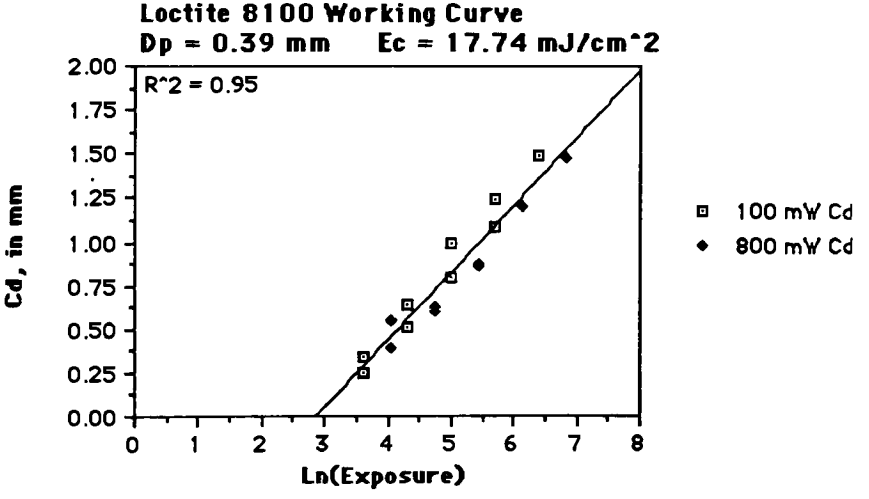
Loctite 8100 Working Curve
Dp = 0.39 mm Ec = 17.74 mJ/cm^2
R^2 = 0.95
Cd, in mm
Ln(Exposure)
100 mW Cd
800 mW Cd

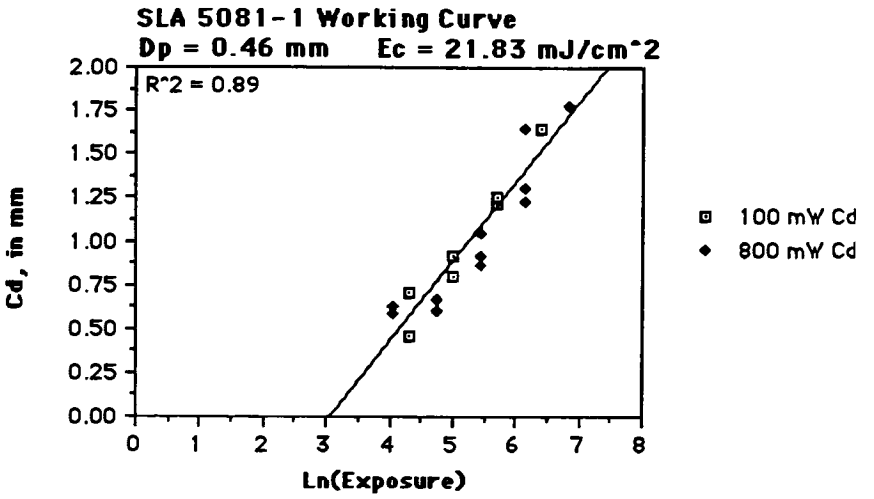
SLA 5081-1 Working Curve
Dp = 0.46 mm Ec = 21.83 mJ/cm^2
R^2 = 0.89
Cd, in mm
Ln(Exposure)
100 mW Cd
800 mW Cd

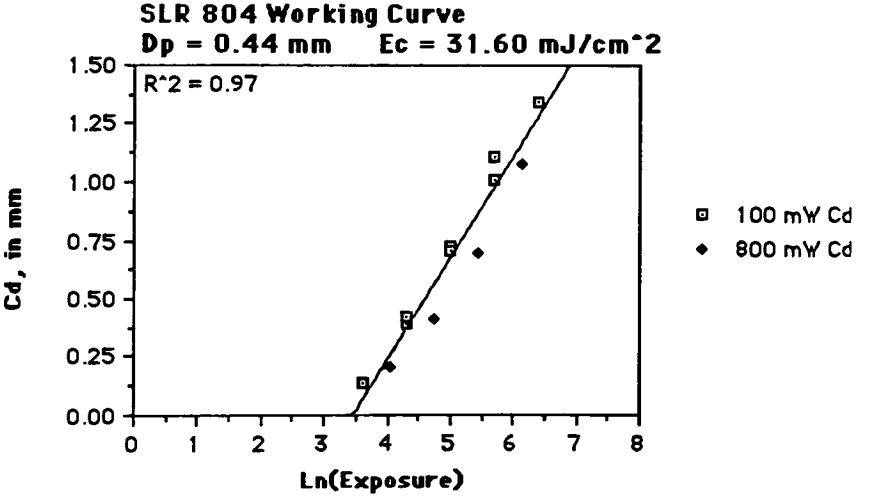
SLR 804 Working Curve
Dp = 0.44 mm Ec = 31.60 mJ/cm^2
R^2 = 0.97
Cd, in mm
Ln(Exposure)
100 mW Cd
800 mW Cd

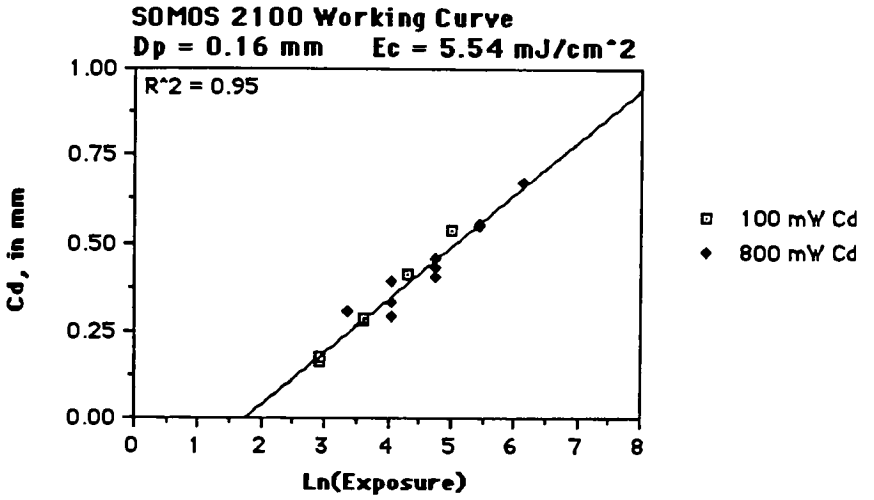
SOMOS 2100 Working Curve
Dp = 0.16 mm Ec = 5.54 mJ/cm^2
R^2 = 0.95
Cd, in mm
Ln(Exposure)
100 mW Cd
800 mW Cd

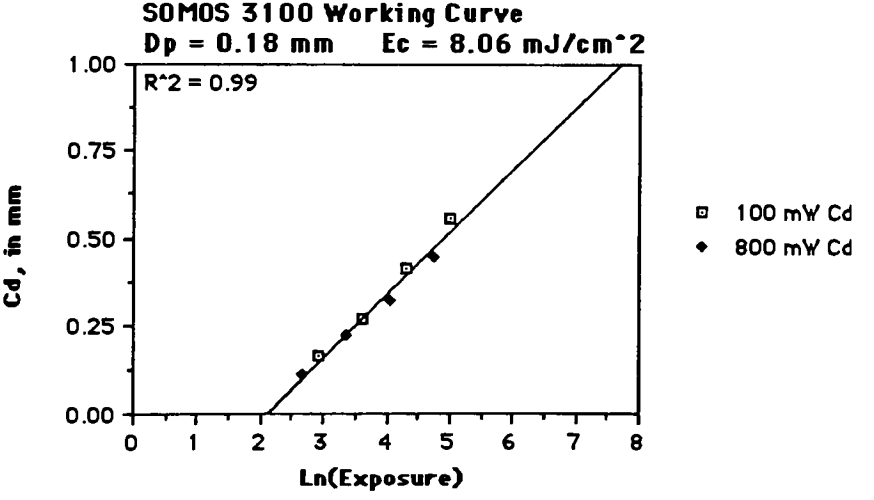
SOMOS 3100 Working Curve
Dp = 0.18 mm Ec = 8.06 mJ/cm^2
R^2 = 0.99
Cd, in mm
Ln(Exposure)
100 mW Cd
800 mW Cd

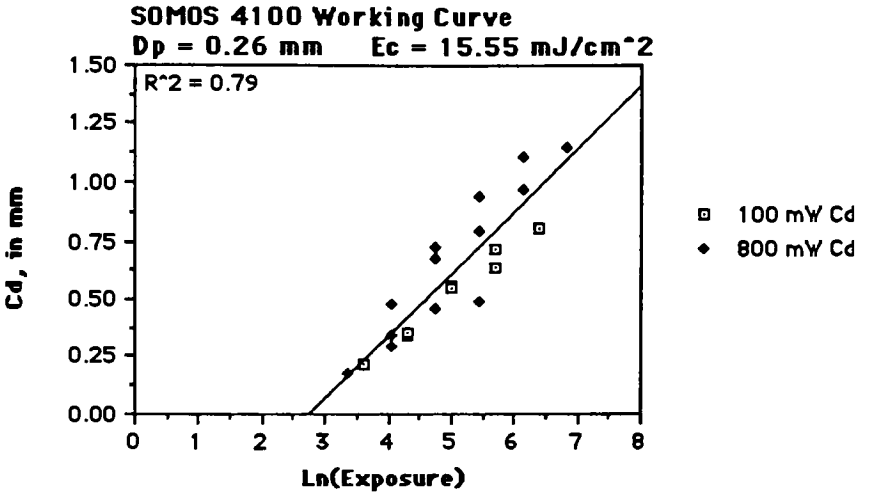
SOMOS 4100 Working Curve
Dp = 0.26 mm Ec = 15.55 mJ/cm^2
R^2 = 0.79
Cd, in mm
Ln(Exposure)
100 mW Cd
800 mW Cd

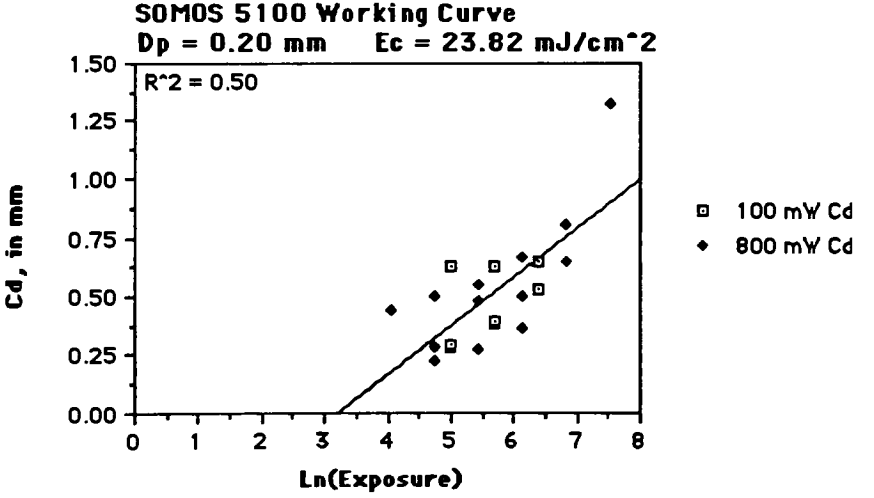
SOMOS 5100 Working Curve
Dp = 0.20 mm Ec = 23.82 mJ/cm^2
R^2 = 0.50
Cd, in mm
Ln(Exposure)
100 mW Cd
800 mW Cd

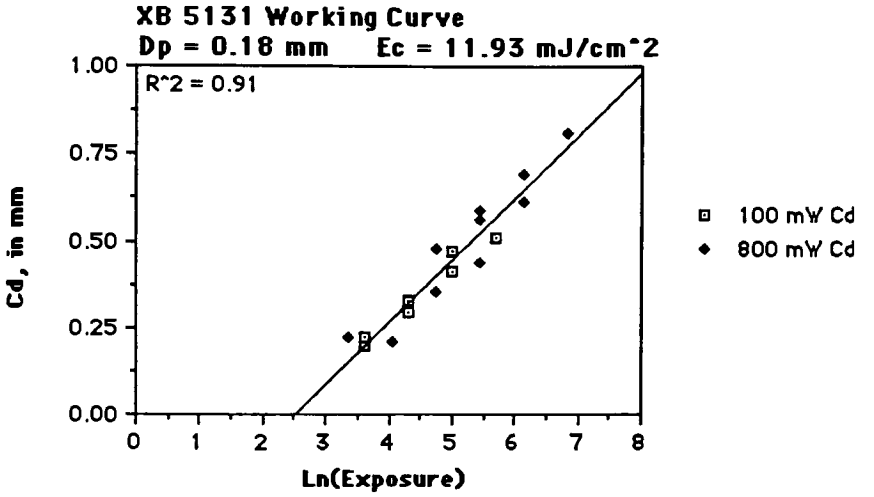
XB 5131 Working Curve
Dp = 0.18 mm Ec = 11.93 mJ/cm^2
R^2 = 0.91
Cd, in mm
Ln(Exposure)
100 mW Cd
800 mW Cd

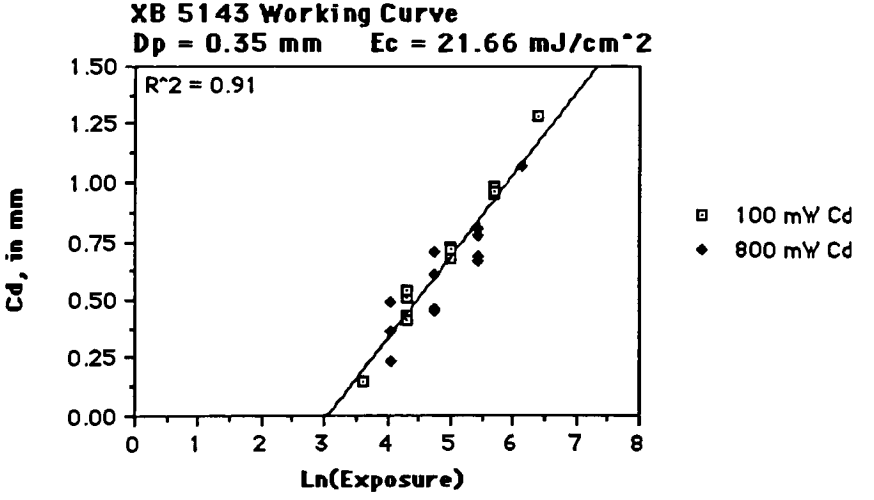
XB 5143 Working Curve
Dp = 0.35 mm Ec = 21.66 mJ/cm^2
R^2 = 0.91
Cd, in mm
Ln(Exposure)
100 mW Cd
800 mW Cd

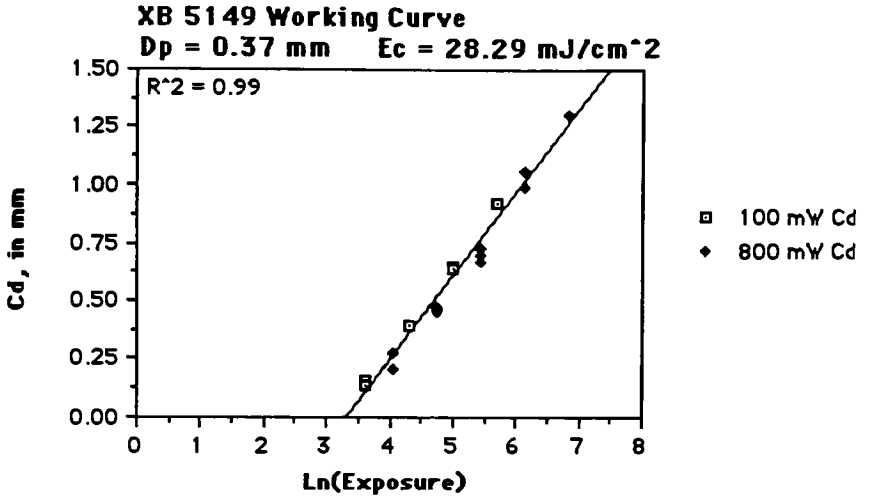
XB 5149 Working Curve
Dp = 0.37 mm Ec = 28.29 mJ/cm^2
R^2 = 0.99
Cd, in mm
Ln(Exposure)
100 mW Cd
800 mW Cd

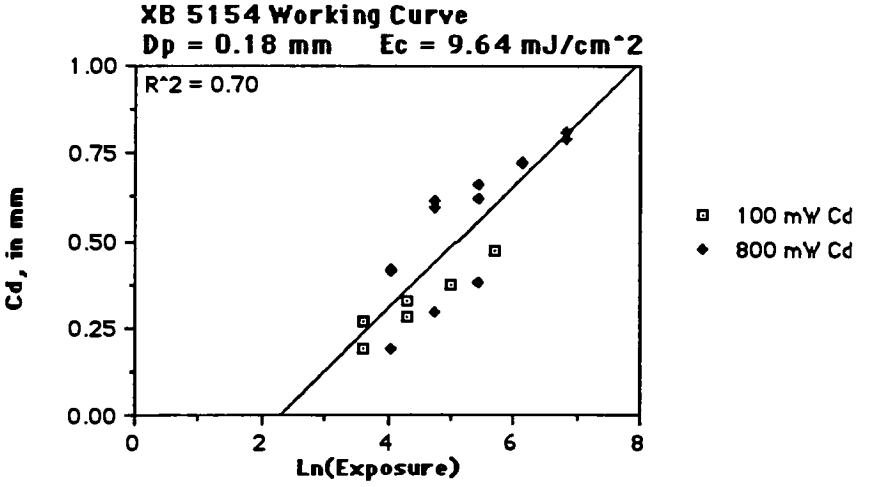
XB 5154 Working Curve
Dp = 0.18 mm Ec = 9.64 mJ/cm^2
R^2 = 0.70
Cd, in mm
Ln(Exposure)
100 mW Cd
800 mW Cd

Appendix D: Absorbancy plots of all of the resins.
PR1

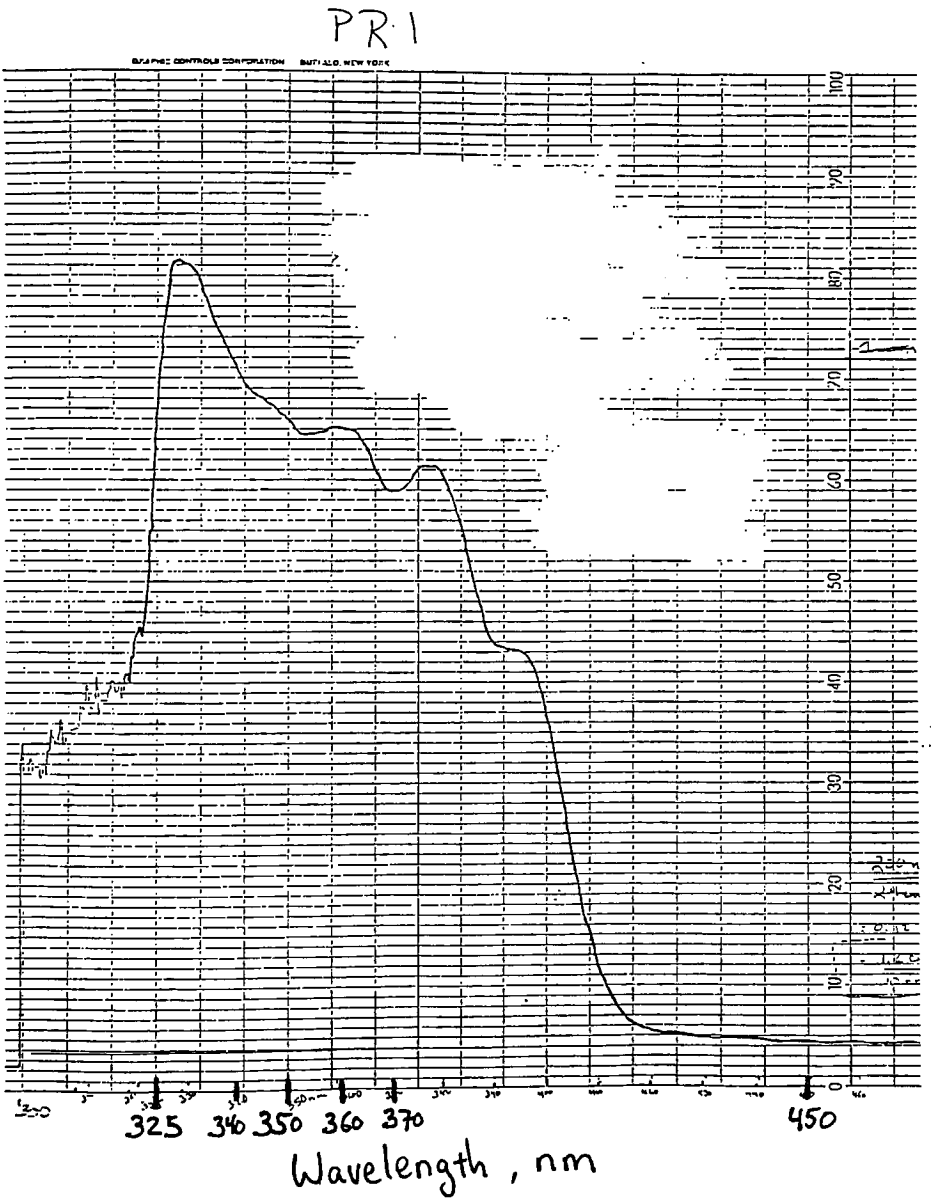

PR2

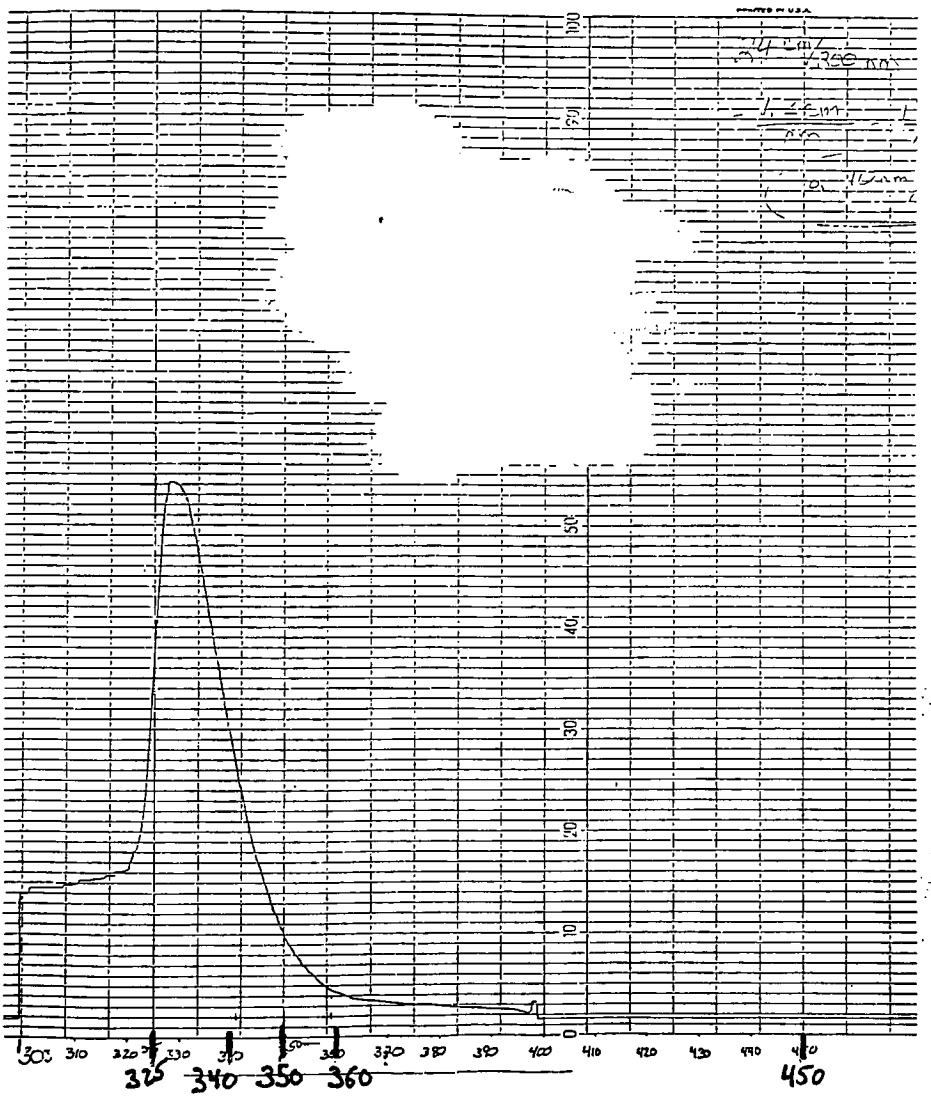
PR2
100
90
50
40
30
20
10
0
300 310 320 325 330 340 350 360 370 380 390 400 410 420 430 440 450
325 340 350 360
450
Wavelength, nm

PR3

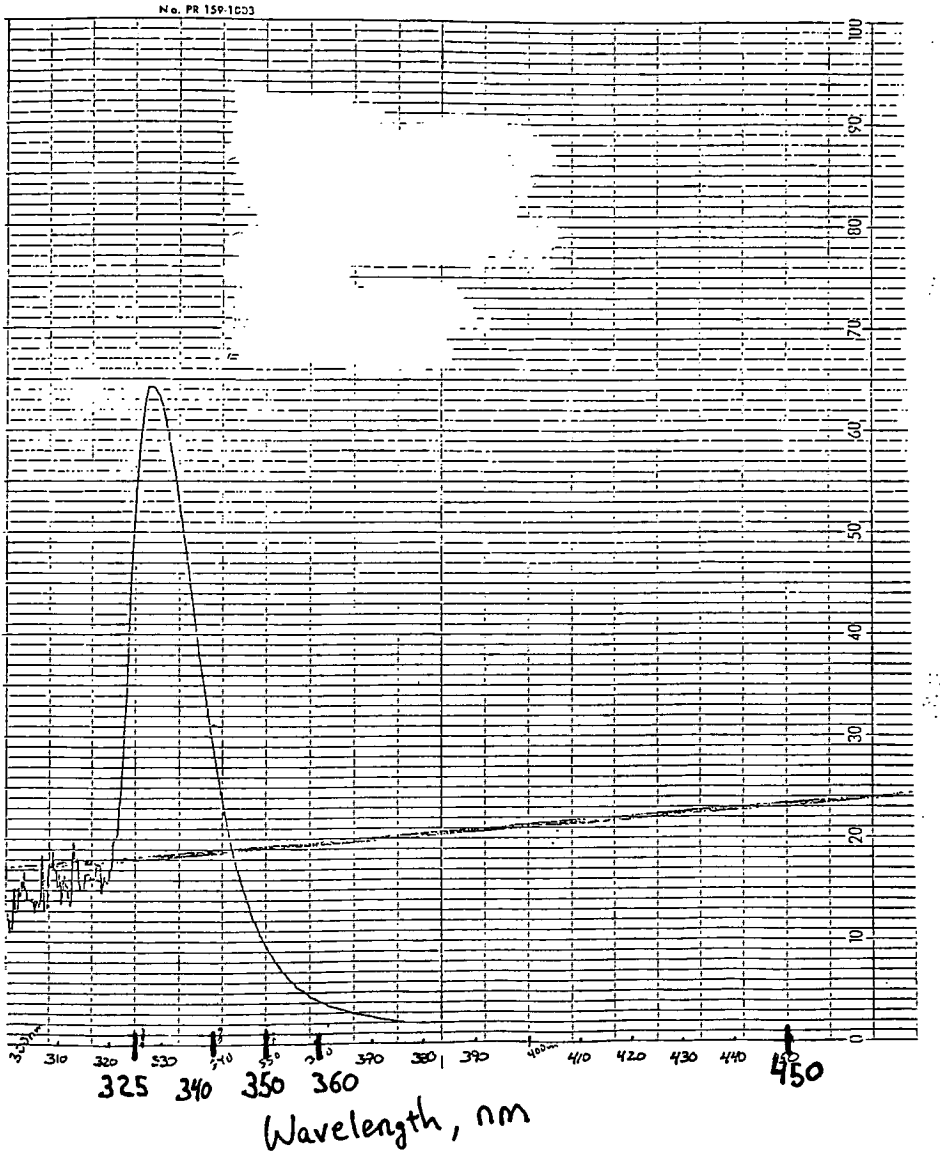
PR3
No. PR 159-1003
100
90
80
70
60
50
40
30
20
10
0
310
320
330
340
350
360
370
380
390
400
410
420
430
440
450
325
340
350
360
Wavelength, nm

PR4

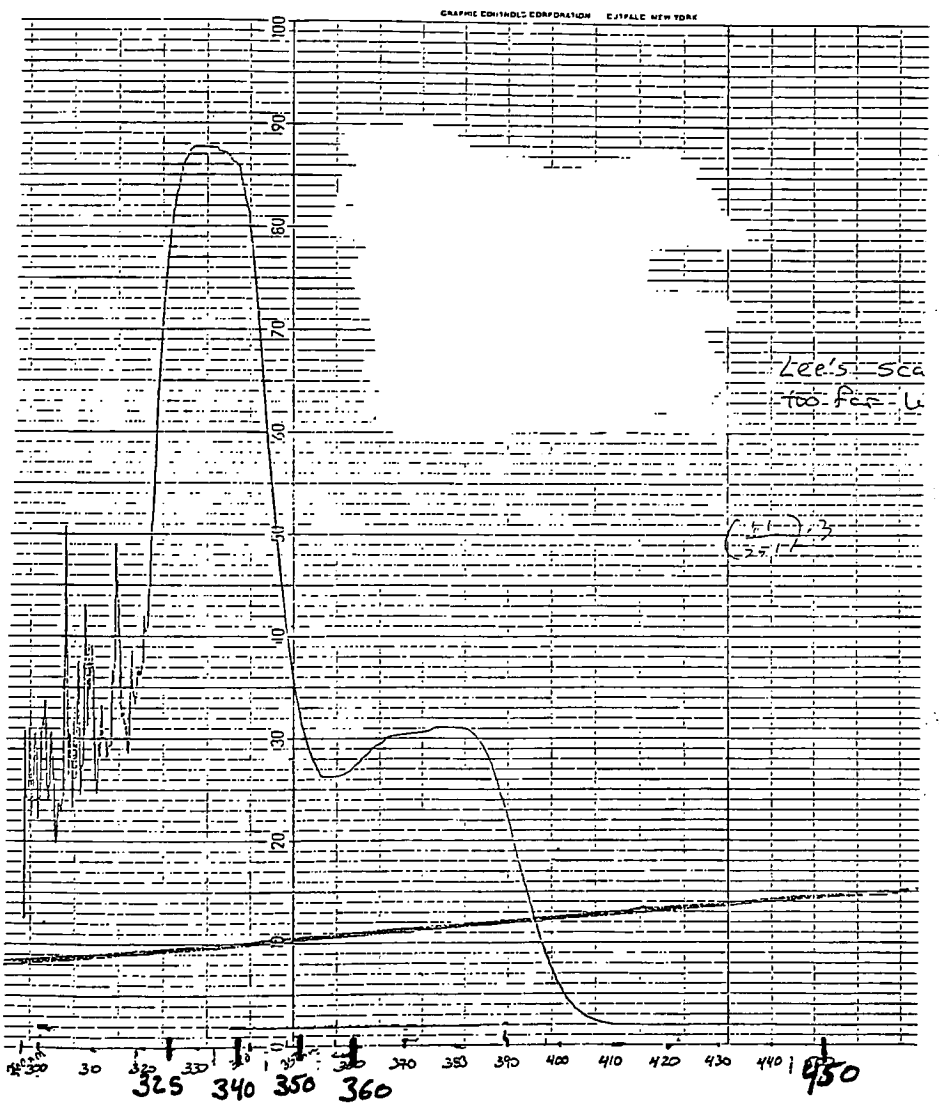
PR4
GRAPHIC CONTROLS CORPORATION
100
90
80
70
60
50
40
30
20
10
0
325
340
350
360
450

PR5

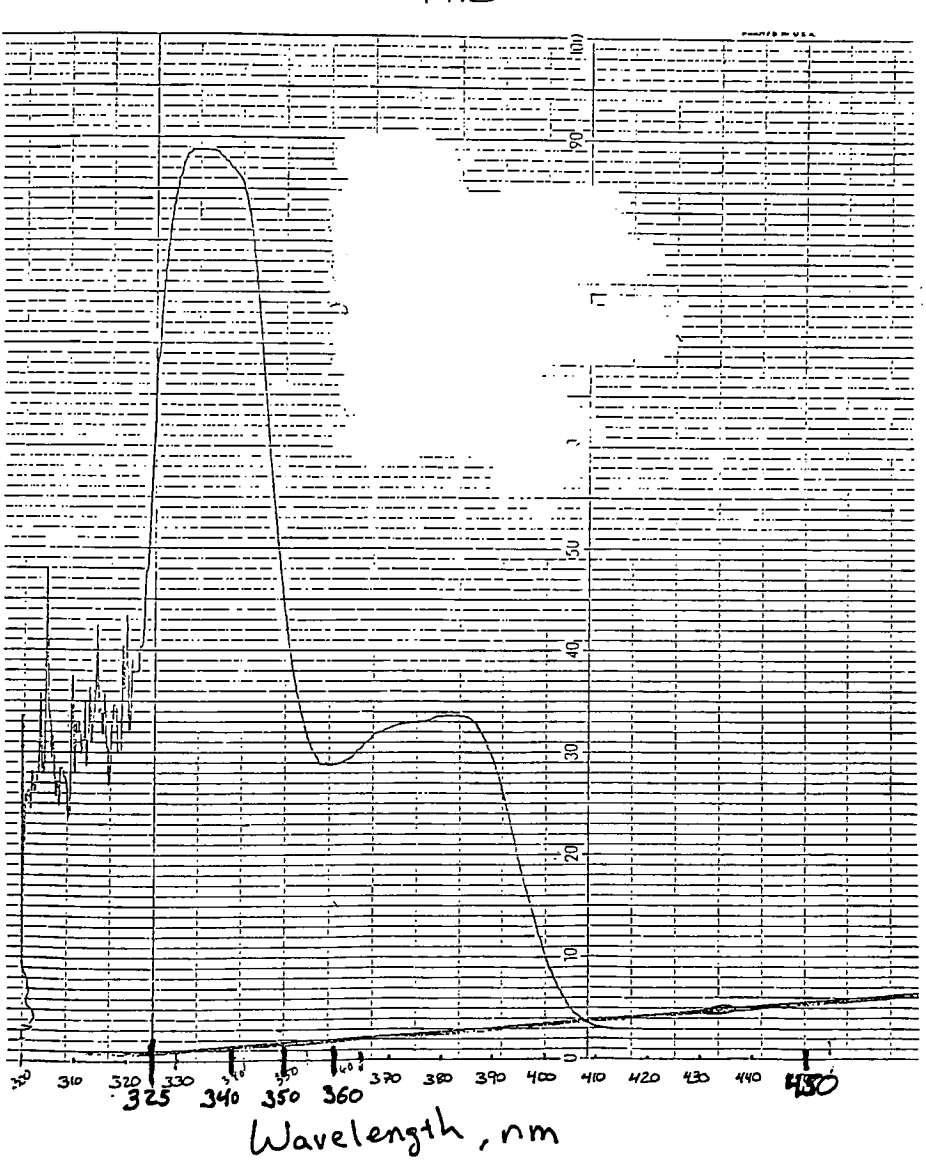
PR5
100
90
70
50
40
30
20
10
0
310
320
330
340
350
360
370
380
390
400
410
420
430
440
450
325
340
350
360
Wavelength, nm

PR6

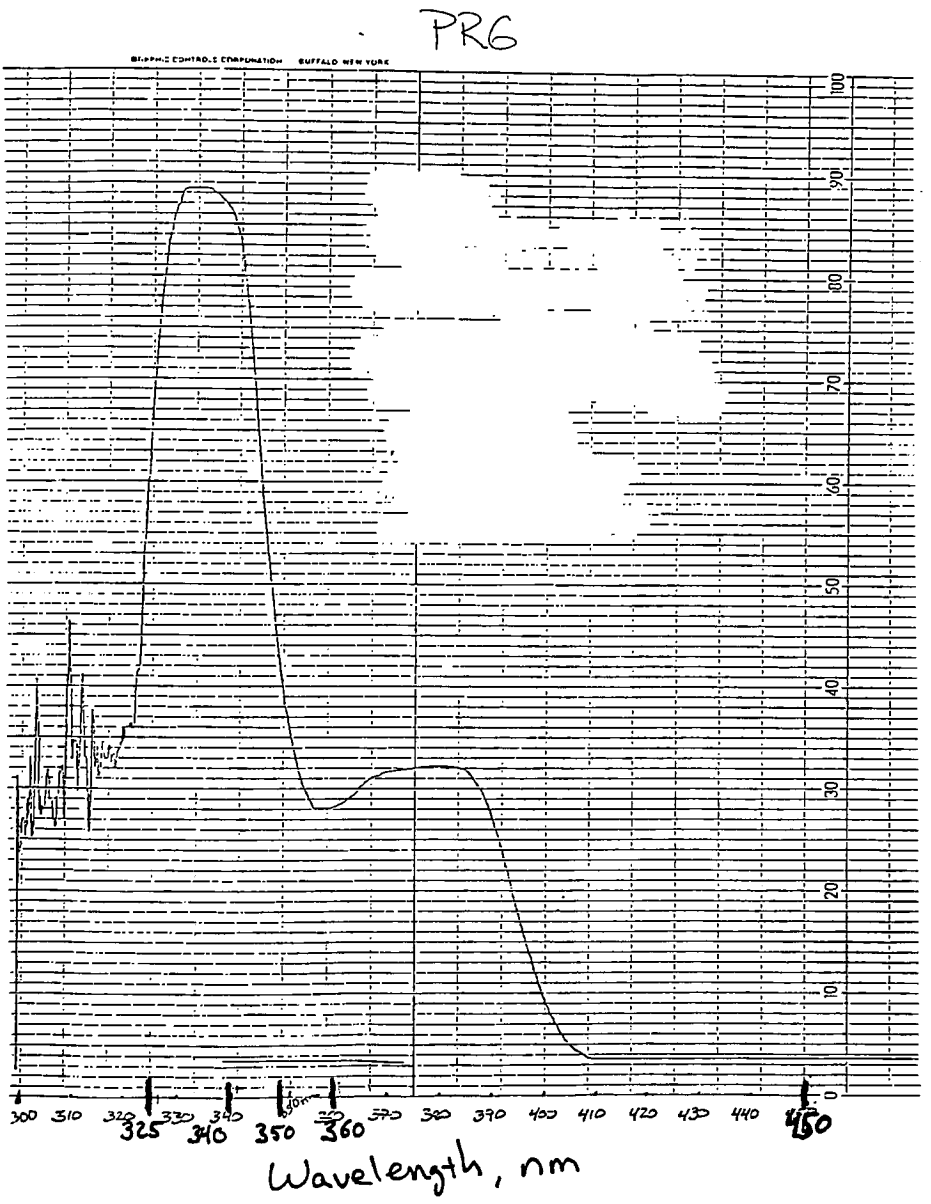
PR6
BECKMAN INSTRUMENTS, INC. BUFFALO NEW YORK
100
90
80
70
60
50
40
30
20
10
0
300 310 320 325 330 340 340 350 360 370 380 390 400 410 420 430 440 450
Wavelength, nm

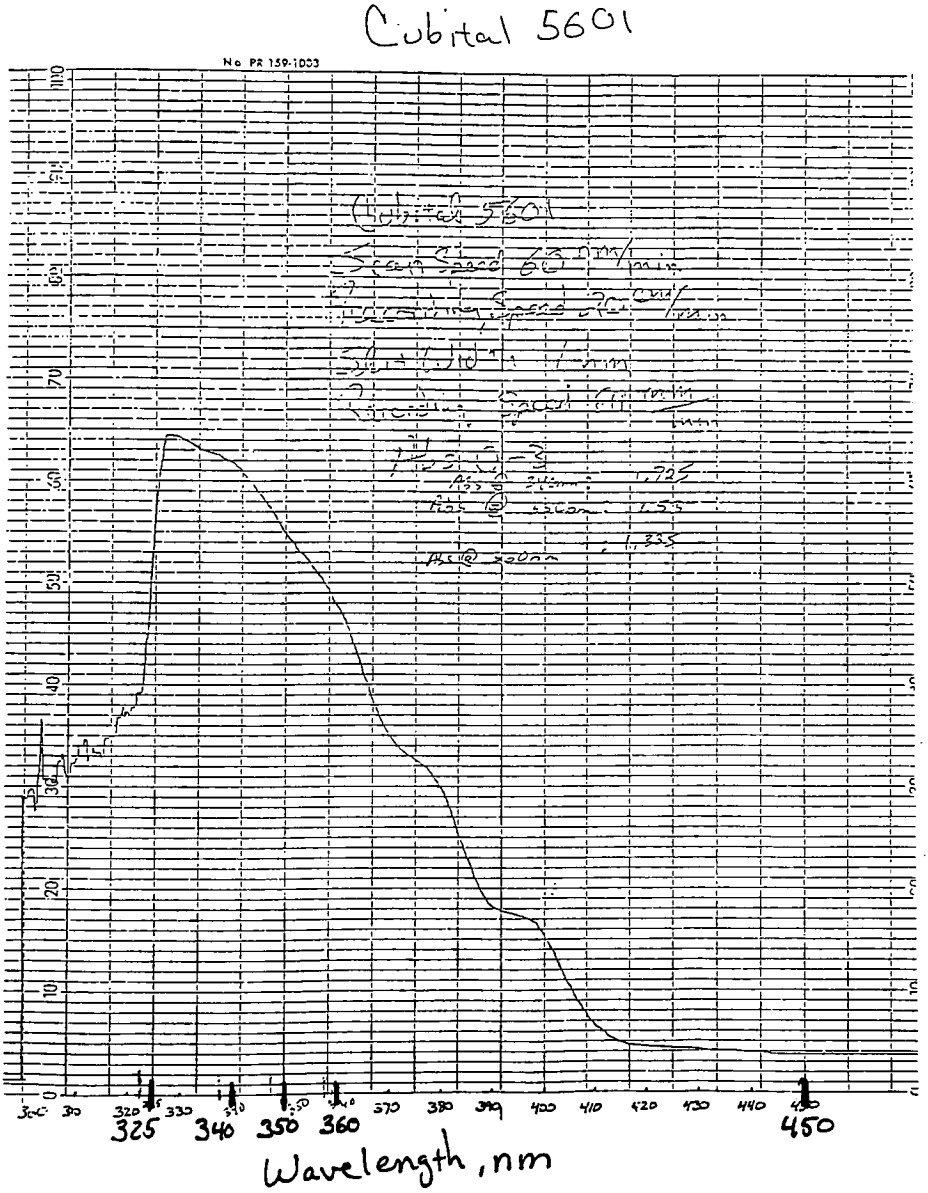
Cubital 5601
No PR 159-1003
325
340
350
360
450
Wavelength, nm

Loctite 8100

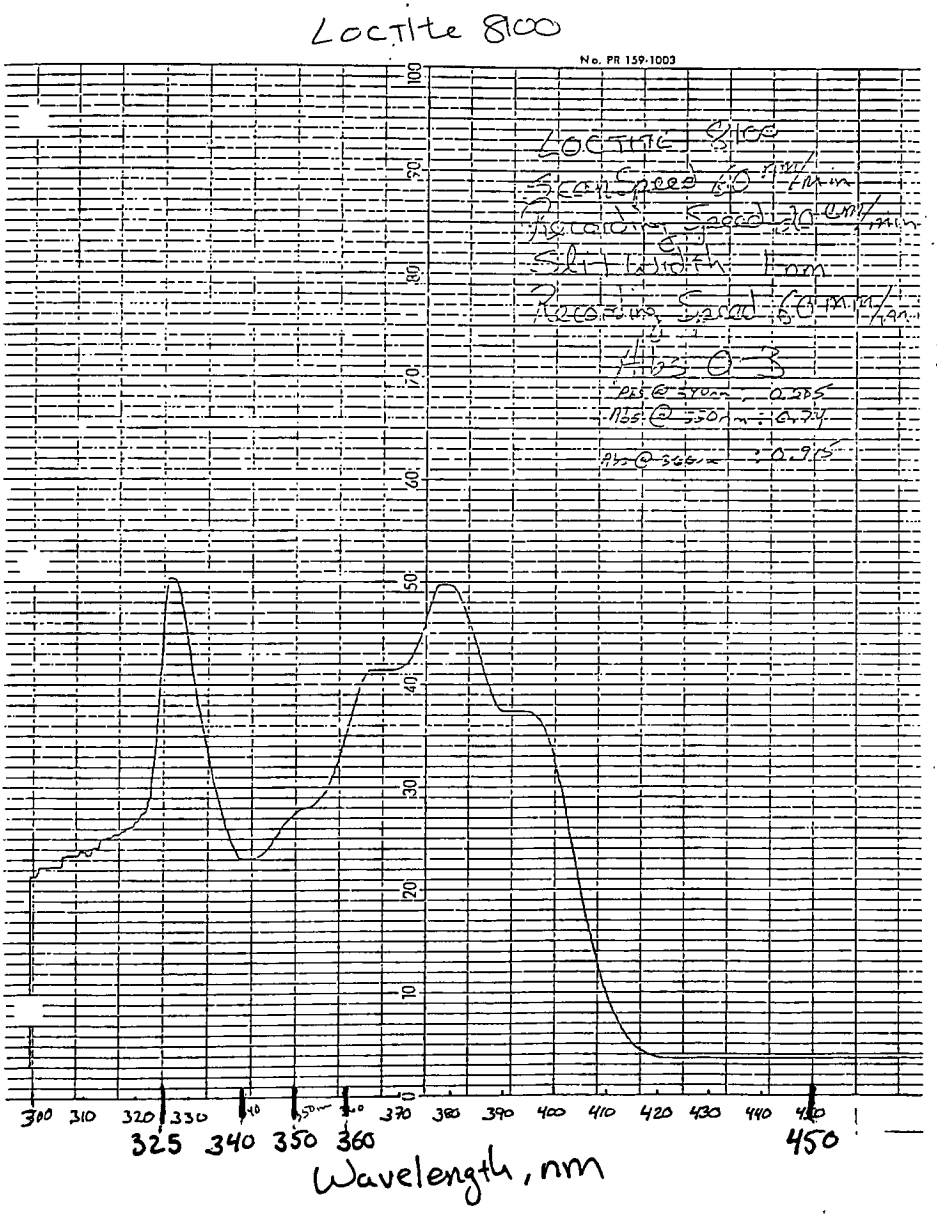

SLA 5081-1

SLA 5081-1

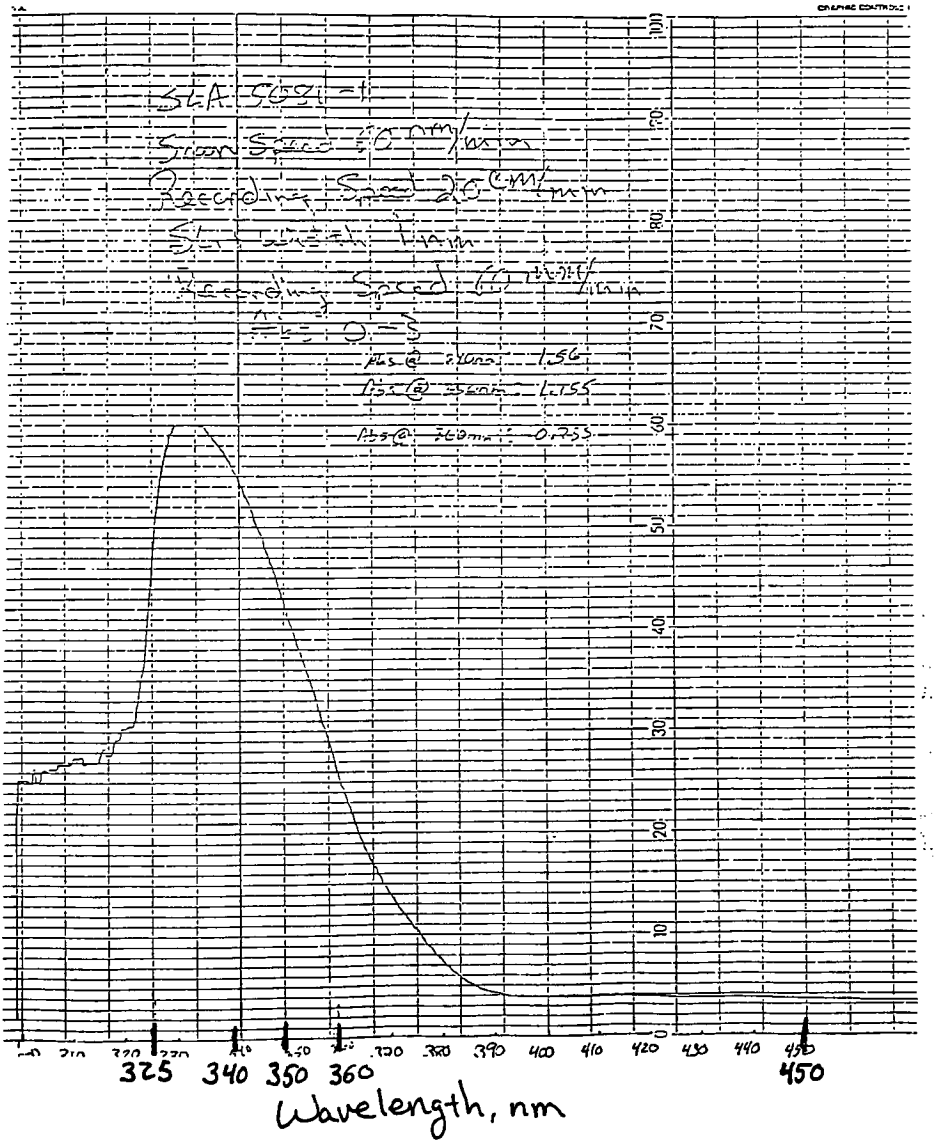

SLR 804

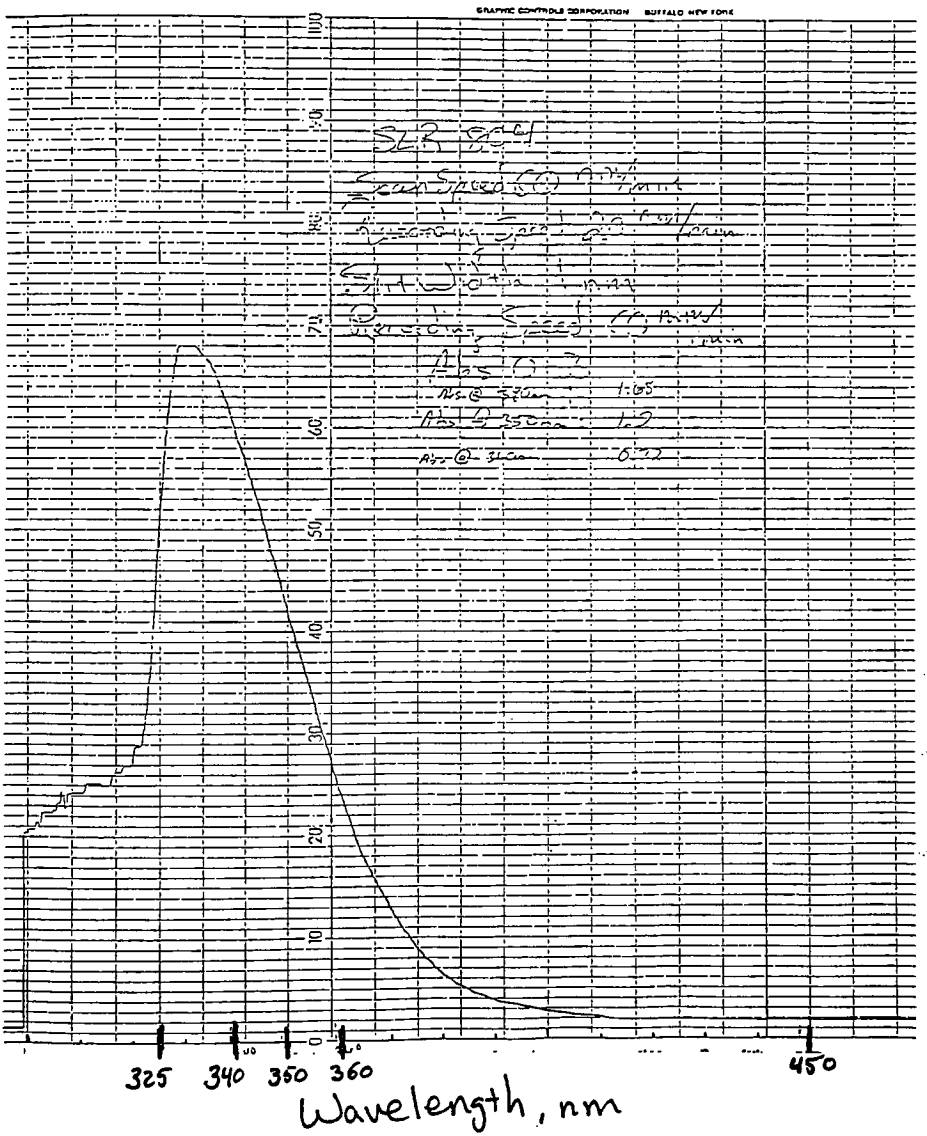
GRAPHIC CONTROLS CORPORATION BUFFALO NEW YORK
100
90
80
70
60
50
40
30
20
10
0
325
340
350
360
450
Wavelength, nm

Somos 2100

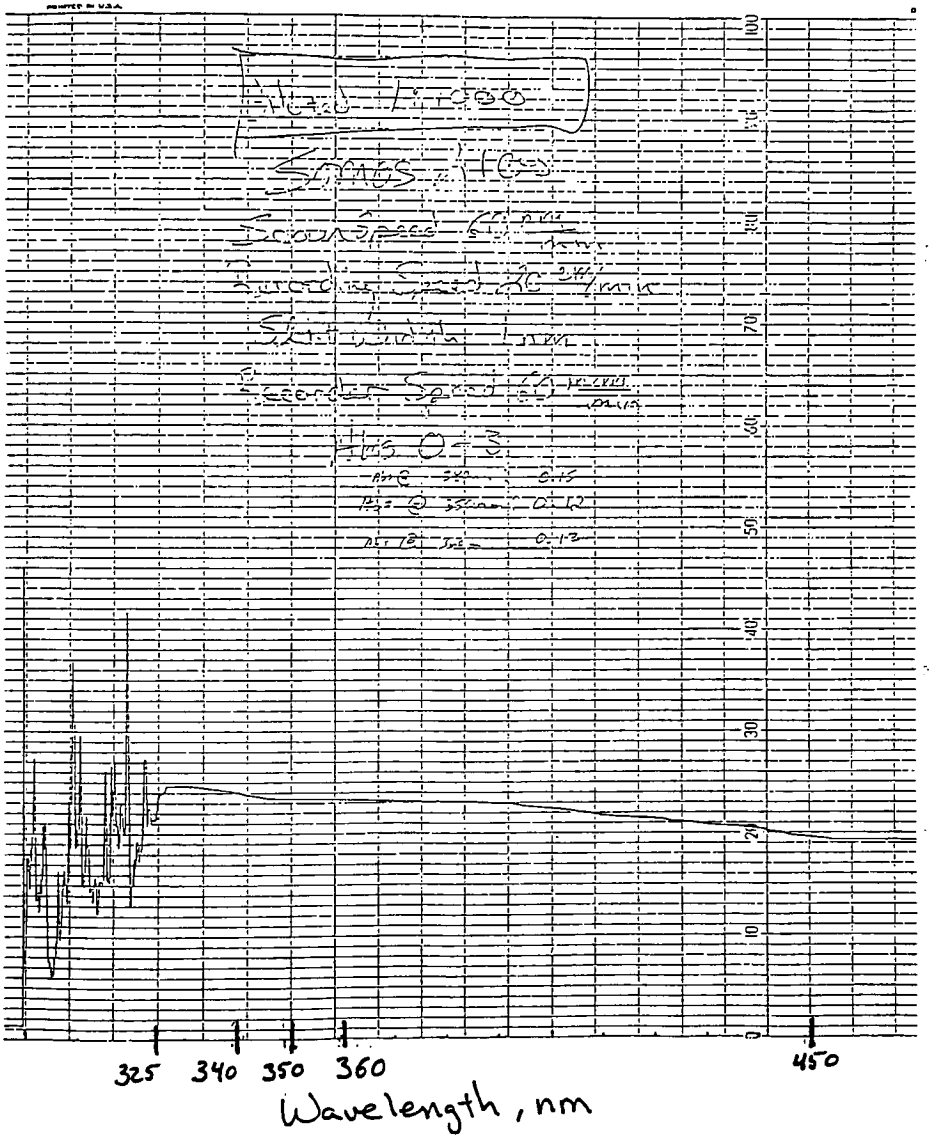

Somos 3100

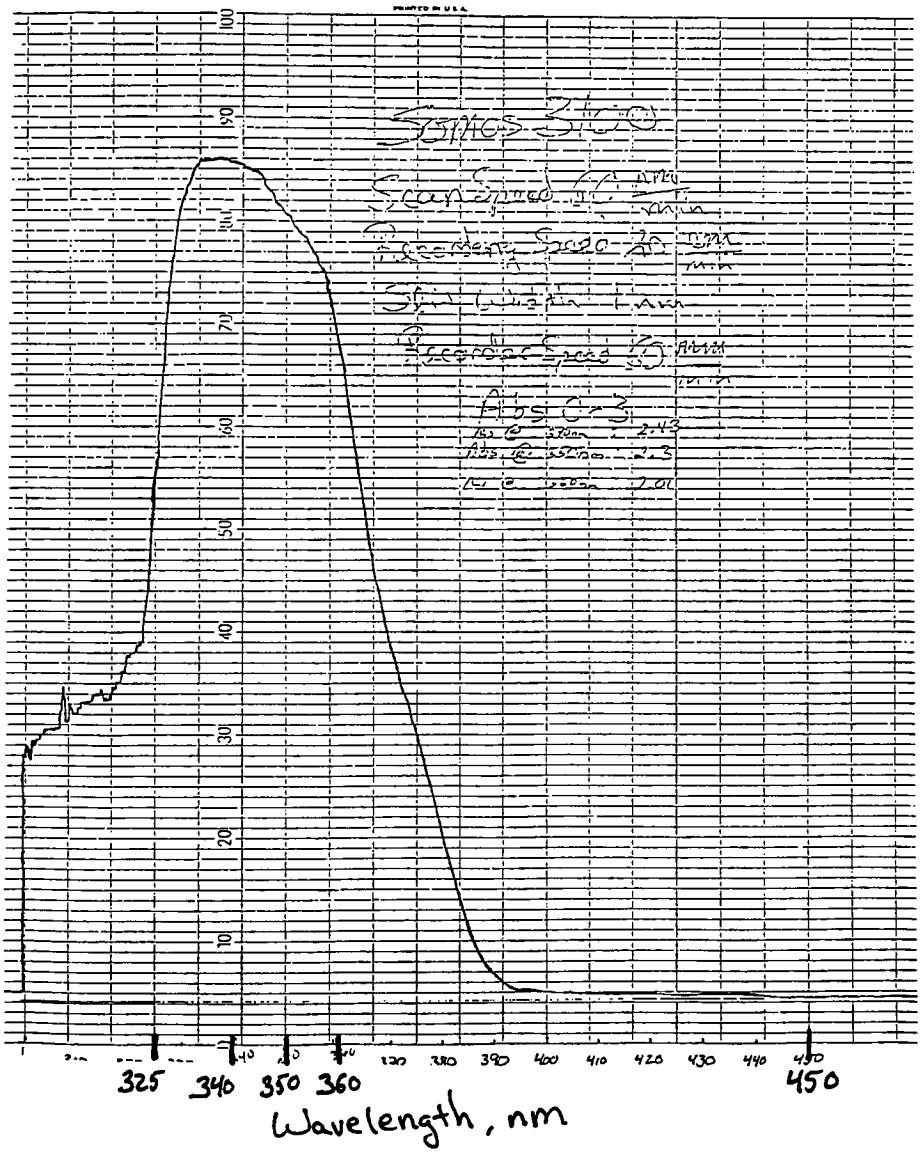

Somos 4100

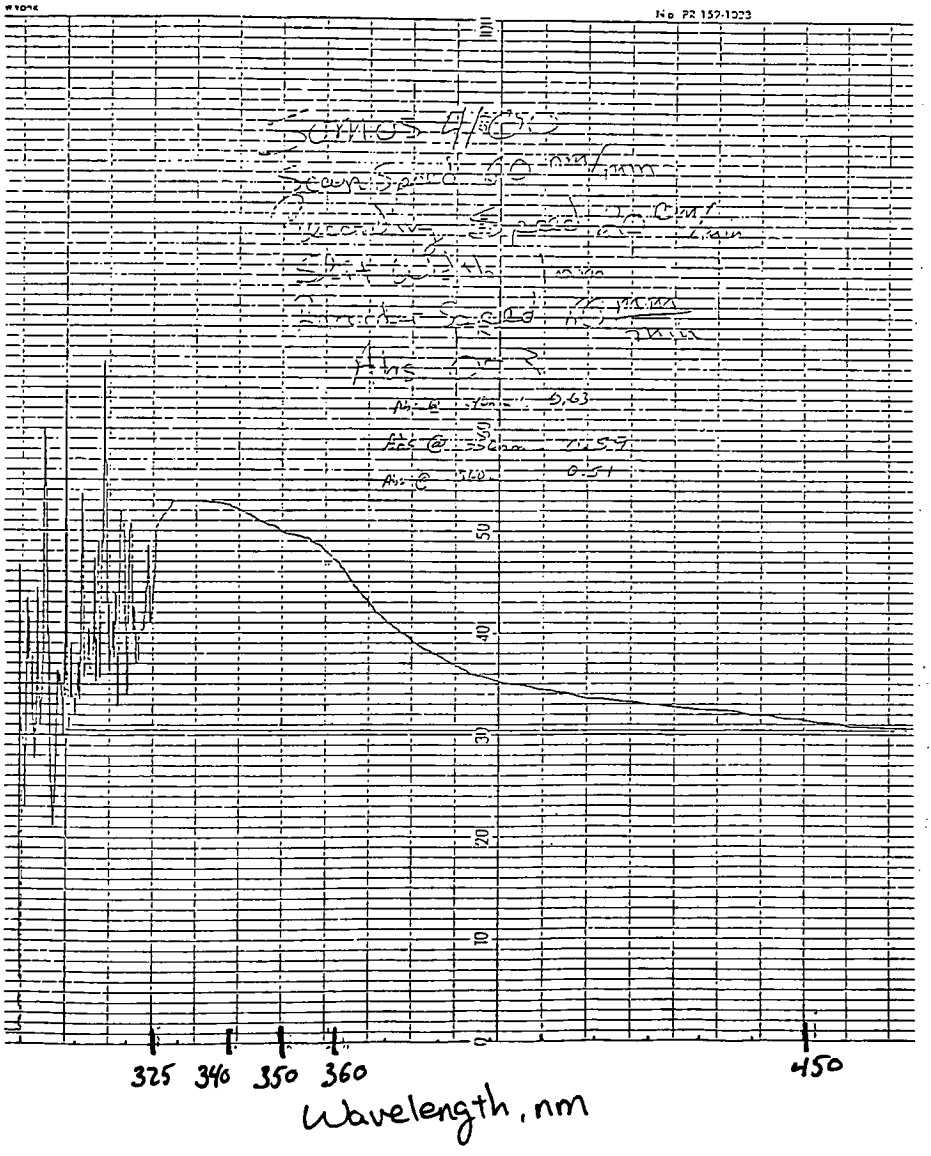

Somos 5100

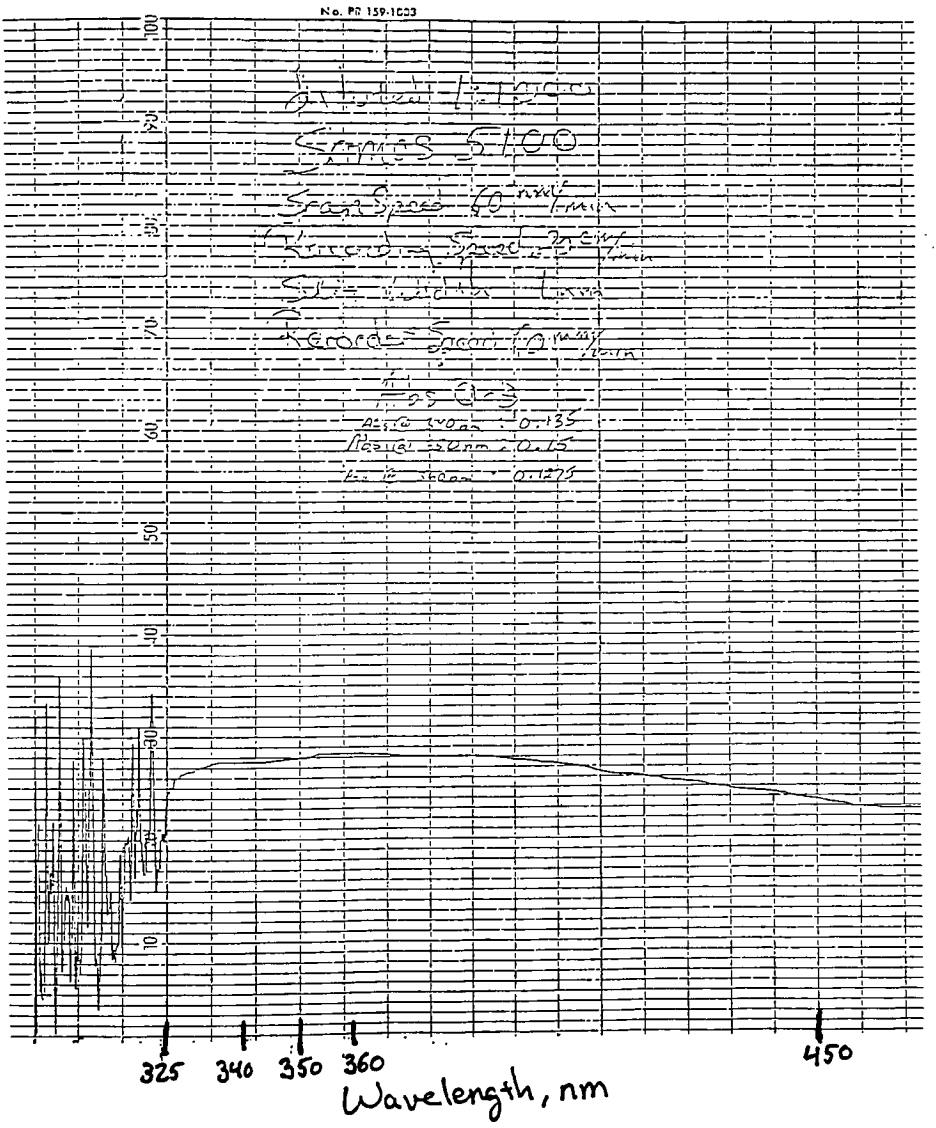
No. PR 159-1003
100
90
80
70
60
50
40
30
20
10
325
340
350
360
450
Wavelength, nm

XB 5131

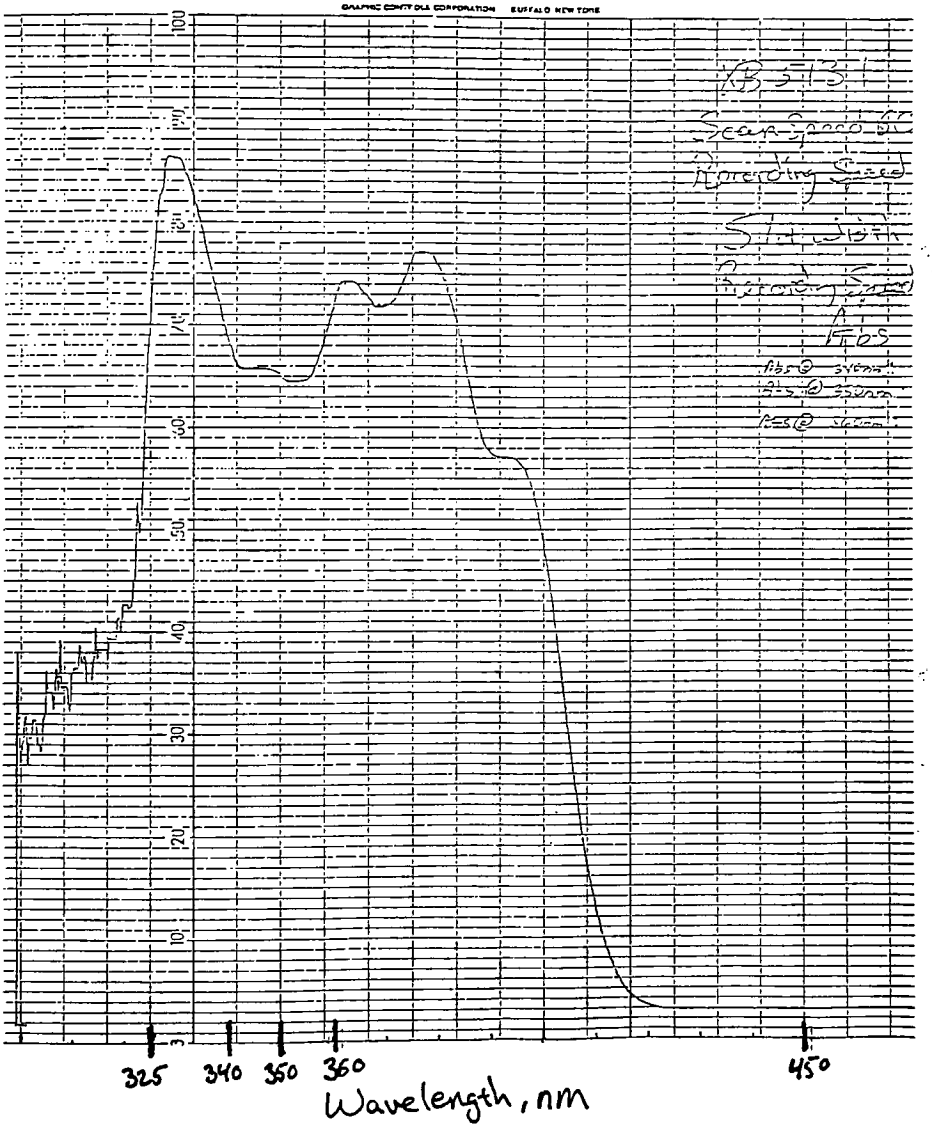
GRAPHIC CONTROLS CORPORATION BUFFALO NEW YORK
100
90
80
70
60
50
40
30
20
10
0
325
340
350
360
450
Wavelength, nm

XB 5143

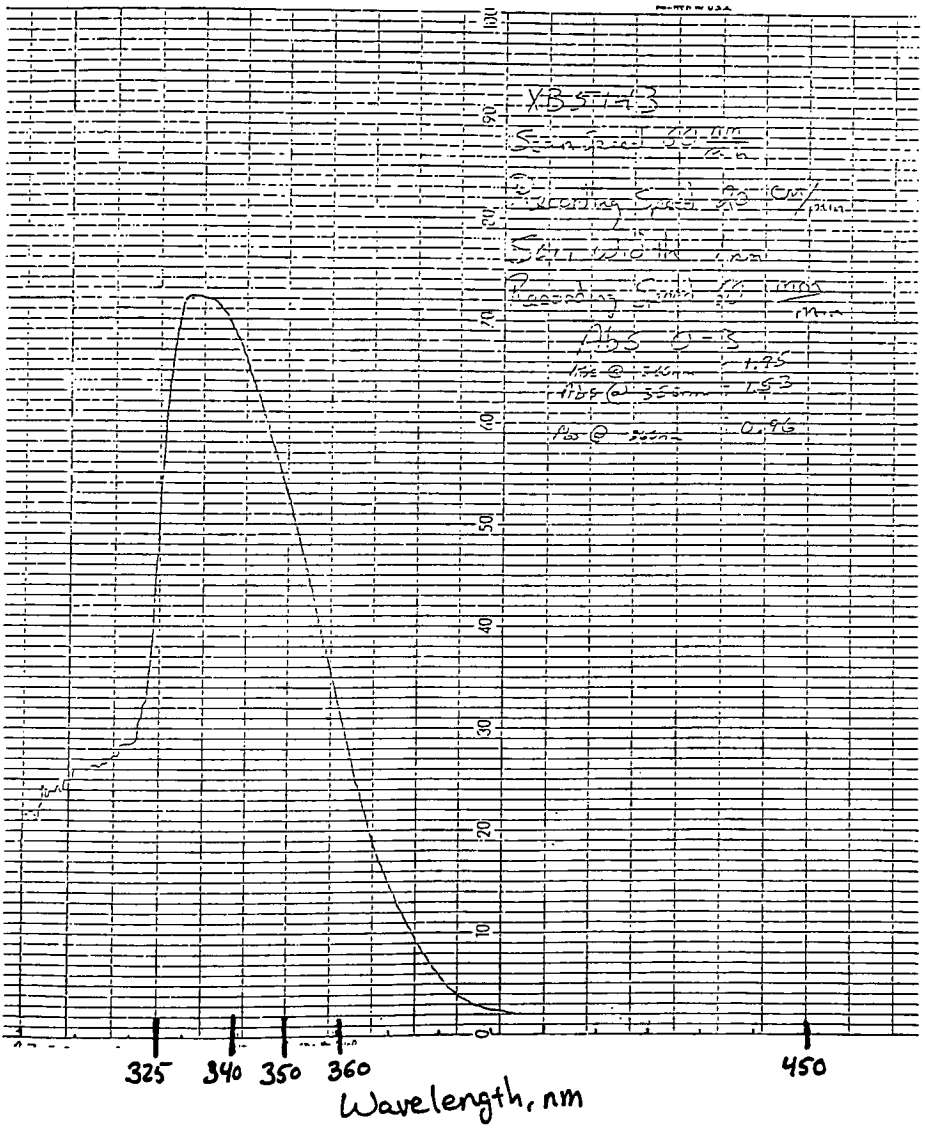
XB 5143
100
90
80
70
60
50
40
30
20
10
0
325
340
350
360
450
Wavelength, nm

XB 5149

XB 5149

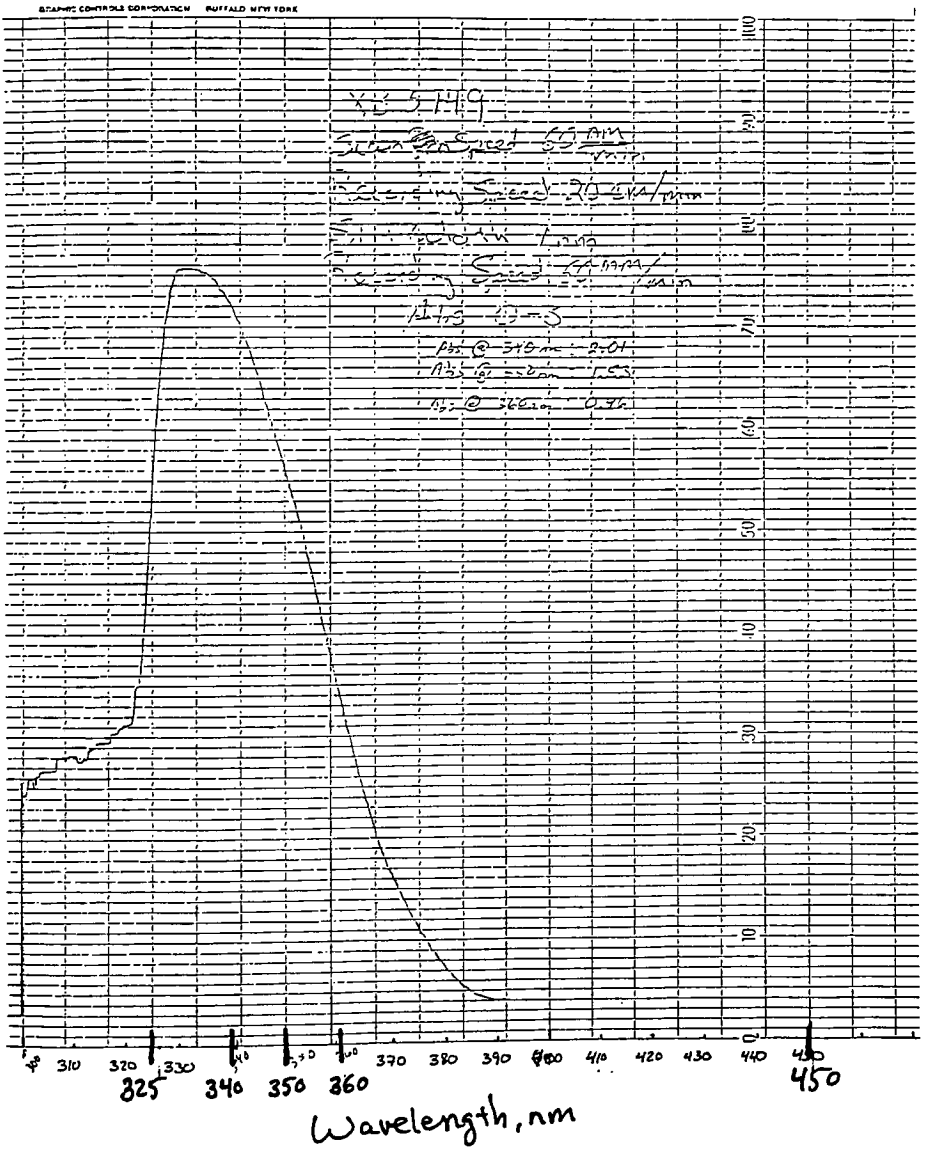

XB 5154

XB 5154

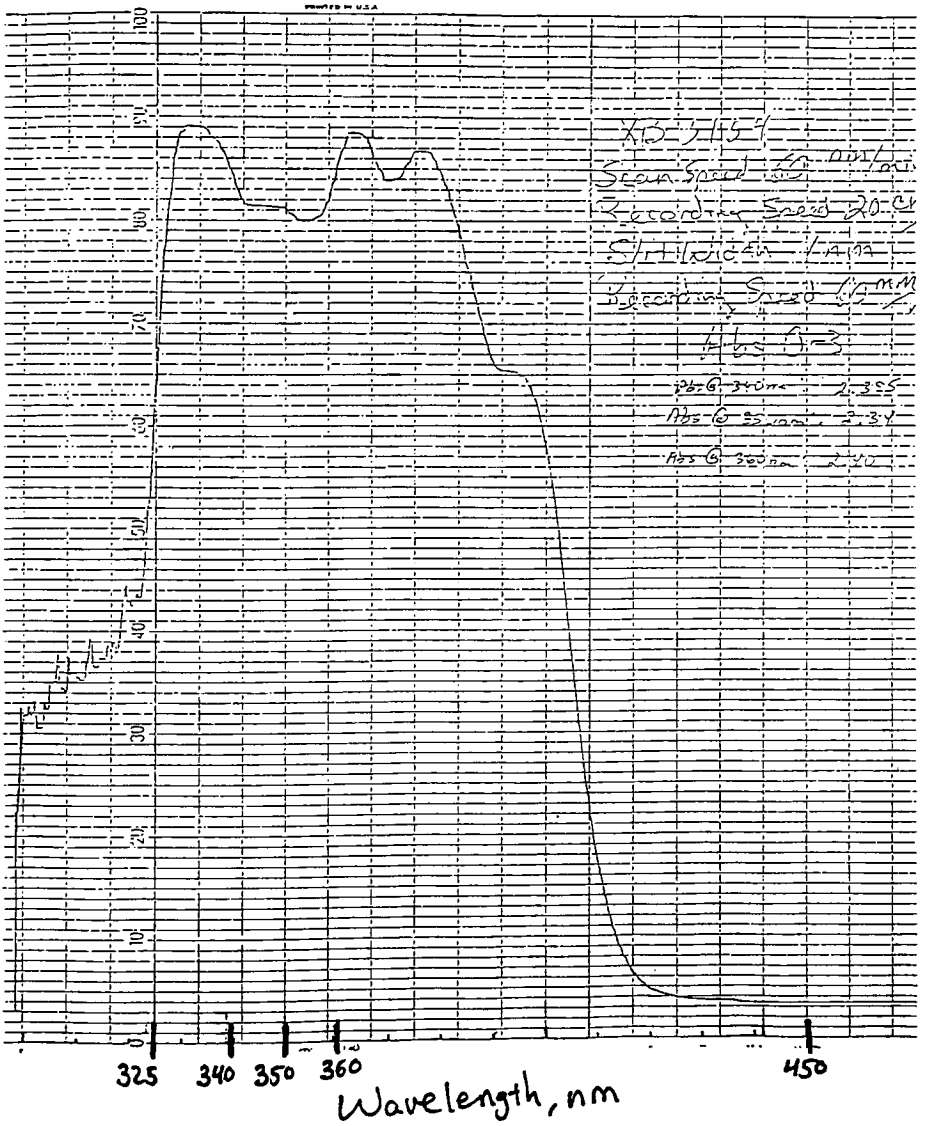

Appendix E: The flash working curves of the resins.

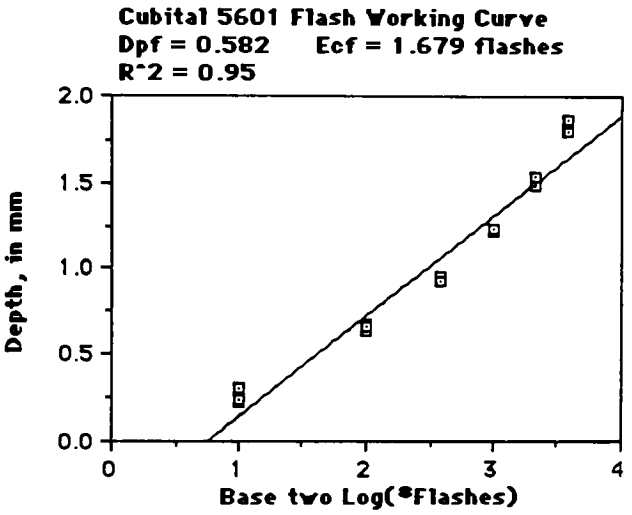

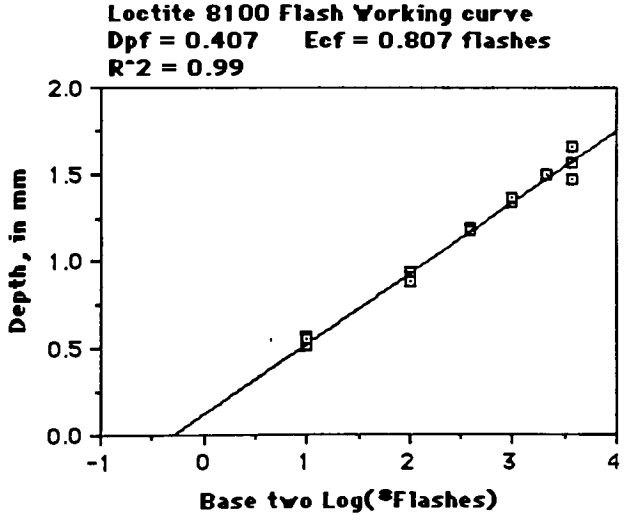

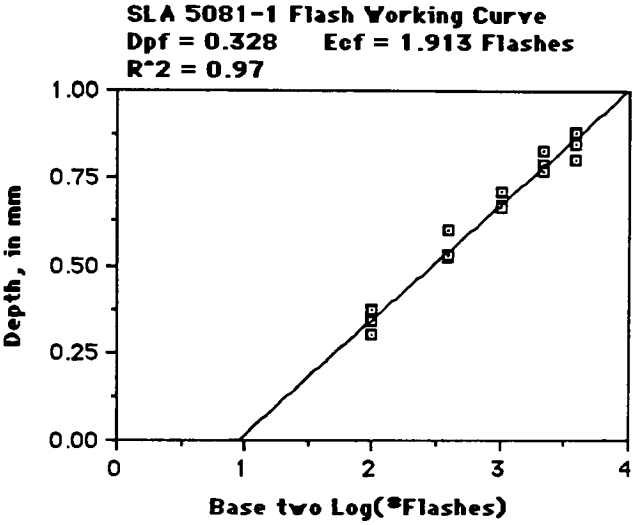
SLA 5081-1 Flash Working Curve
Dpf = 0.328 Ecf = 1.913 Flashes
R^2 = 0.97
1.00
0.75
0.50
0.25
0.00
Depth, in mm
0
1
2
3
4
Base two Log(#Flashes)

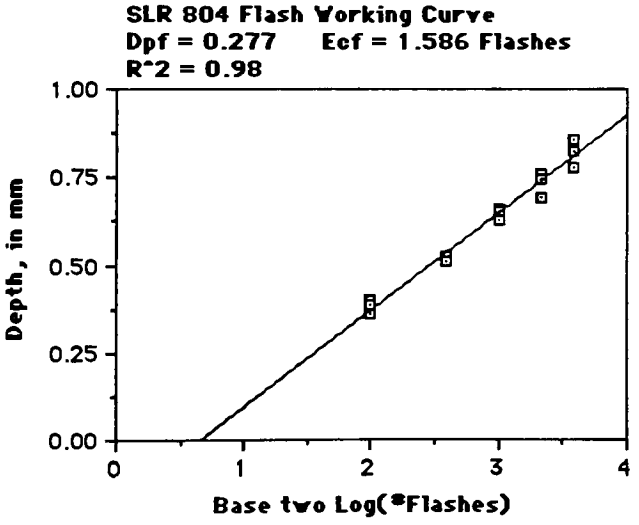
SLR 804 Flash Working Curve
Dpf = 0.277 Ecf = 1.586 Flashes
R^2 = 0.98
1.00
0.75
0.50
0.25
0.00
Depth, in mm
0
1
2
3
4
Base two Log(#Flashes)

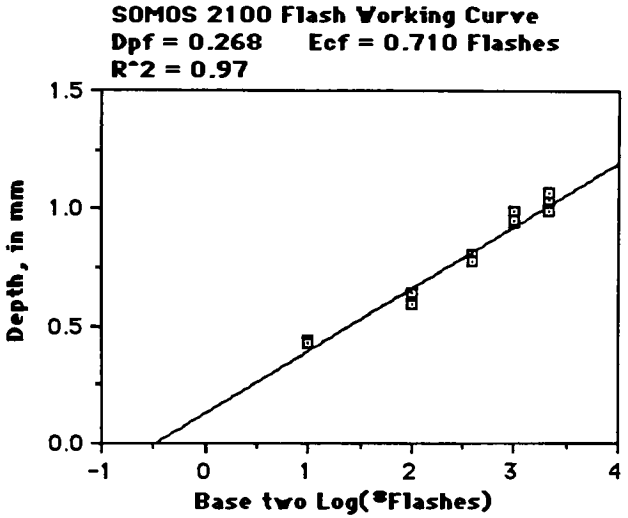
SOMOS 2100 Flash Working Curve
Dpf = 0.268 Ecf = 0.710 Flashes
R^2 = 0.97
Depth, in mm
1.5
1.0
0.5
0.0
-1
0
1
2
3
4
Base two Log(#Flashes)

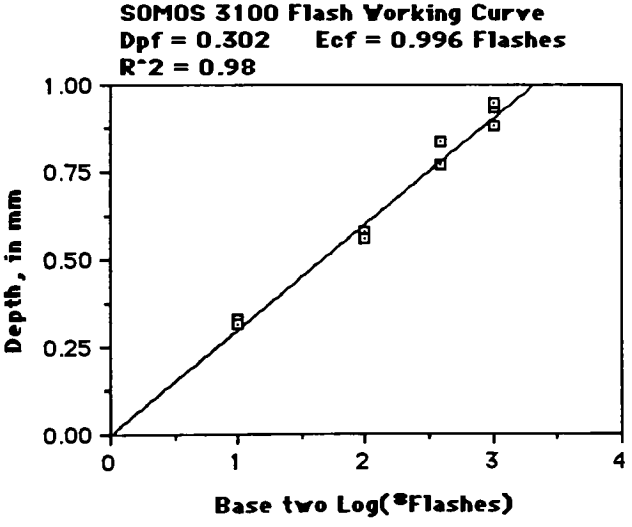
SOMOS 3100 Flash Working Curve
Dpf = 0.302 Ecf = 0.996 Flashes
R^2 = 0.98
Depth, in mm
1.00
0.75
0.50
0.25
0.00
0
1
2
3
4
Base two Log(#Flashes)

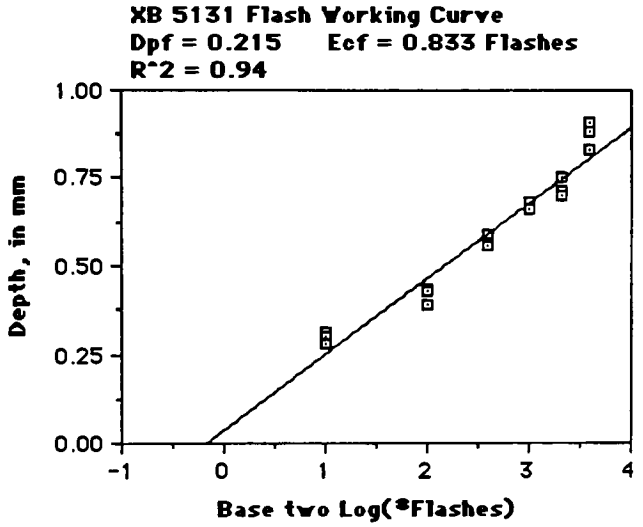
XB 5131 Flash Working Curve
Dpf = 0.215 Ecf = 0.833 Flashes
R^2 = 0.94
1.00
0.75
0.50
0.25
0.00
Depth, in mm
-1
0
1
2
3
4
Base two Log(*Flashes)

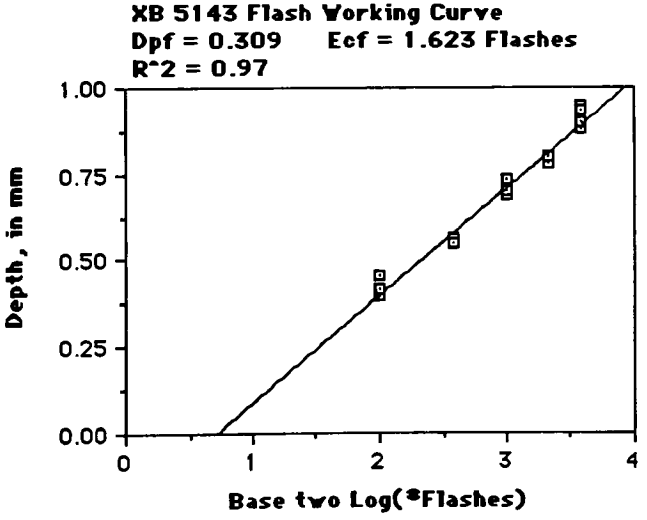
XB 5143 Flash Working Curve
Dpf = 0.309 Ecf = 1.623 Flashes
R^2 = 0.97
1.00
0.75
0.50
0.25
0.00
Depth, in mm
0
1
2
3
4
Base two Log(*Flashes)

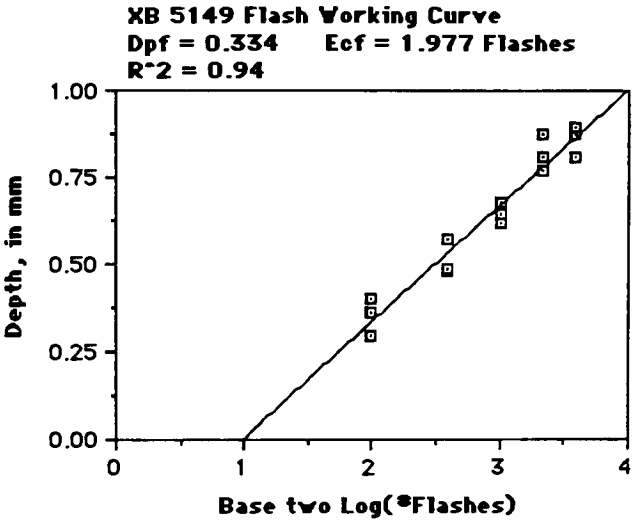
XB 5149 Flash Working Curve
Dpf = 0.334 Ecf = 1.977 Flashes
R^2 = 0.94
1.00
0.75
0.50
0.25
0.00
Depth, in mm
0
1
2
3
4
Base two Log(#Flashes)

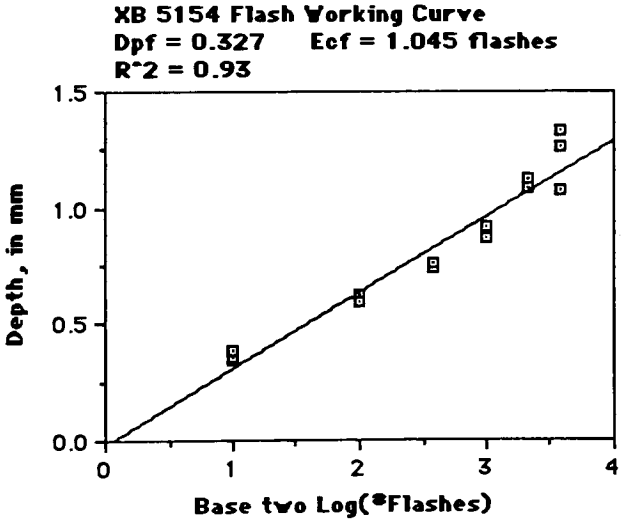
XB 5154 Flash Working Curve
Dpf = 0.327 Ecf = 1.045 flashes
R^2 = 0.93
1.5
1.0
0.5
0.0
Depth, in mm
0
1
2
3
4
Base two Log(#Flashes)

Reference List:

André, J.C.; Duclos, A.M.; Jézéquel, J.Y. "Industrial Photochemistry XX. Three-dimensional machining with laser: polymer deformation induced by shrinkage phenomena" J. Photochem. Photobiol. A: Chem., Vol. 70, pp. 285-299 (1993)

deBoer, J.; Visser, R.J.; Melis, G.P. "Time-resolved determination of volume shrinkage and refractive index change of thin polymer films during photopolymerization" Polymer, Vol. 33, No. 6, pp. 1123-1126 (1992)

Flory, P.; Orwoll, R.A.; Vrij, A. "title" Journal of American Chemical Society, Vol. 86, pp 3507 (1964)

Gozzelino, G.; Priola, A.; Mantegna, M. "Analysis of Thermal Curves Obtained During Radiation Curing of Polymeric Films" Journal of Applied Polymer Science, Vol. 44, pp. 927-931 (1992)

Herbert, Alan J. "Solid Object Generation" Journal of Applied Photographic Engineering, Vol. 6, No. 4, pp. 185-188 (1982)

Hoyle, C.E.; Sundell, P.E.; Trapp, M.; Kang, D.M.; Sheng, D.; Nagarajan, R. "Polymerization kinetics of mono-and multifunctional monomers initiated by high intensity laser pulses: dependence of rate on peak pulse intensity and chemical structure" SPIE Vol 1559 Photopolymer Device Physics, Chemistry and Applications II (1991)

Hoyle, C.E.;, Wantanabe, T.; Whitehead, J. " " Proceedings SPIE-International Society of Optical Engineers 1665 (Liquid Crystal Materials) Vol. 35, pp. 212 (1992)

Hug, William F.; Jacobs, Paul F. "Laser Technology Assessment for Stereolithographic Systems" Second International Conference on Rapid Prototyping, Sponsored by The Rapid Prototype Development Laboratory (RPDL) Center for Advanced Manufacturing, University of Dayton, at the University of Dayton, June 23-26, 1991, pp 29-38.

Jacobs Ph.D, Paul F. "Rapid Prototyping and Manufacturing, Fundamentals of Stereolithography" Published by Society of Manufacturing Engineers, 1992

(a) Kloosterboer, J.G. "Network Formation by Chain Crosslinking Photopolymerization and its Applications in Electronics" Advances in Polymer Science, Vol. 84 "Polymers in Electronics" pp. 1-61 (1988)

(b) Kloosterboer, J.G.; Lijten, G.F.C.M. "Chain Cross-Linking Photopolymerization of Tetraethyleneglycol Diacrylate" ACS Symp. Ser., Vol. 367, pp 409-26 (1988)

Kloosterboer, J.G.; van de Hei, G.M.M.; Boots, H.M.J. "Inhomogeneity during the photopolymerization of diacrylates: d.s.c. experiments and percolation theory" Polymer Communications, Vol. 25, pp. 354-357 (1984)

van Krevelen, D.W. "Properties of Polymers" Elsevier Publishing Company., NY (1990) p. 102

Neckers, D.C. "Architecture With Photopolymerization" Polymer Engineering and Science, Vol. 32, No. 20, pp. 1481-89 (1992)

Nichols, Frank S.; Flowers, Ralph G. "Prediction of Shrinkage in Addition Polymerizations" Industrial and Engineering Chemistry. Vol. 42, No. 2, pp 292-95 (1950)

Park, Chan S. "Contemporary Engineering Economics" Addison-Wesley Publishing Co., Inc., Reading, Massachusetts (1993)

Reiser, Arnost "Photoreactive Polymers. The Science and Technology of Resists" John Wilen & Sons, Inc. Publishers. New York (1989)

Trapp, M.A.; Hoyle, C.E. "The effect of laser parameters on the kinetic factors which influence the polymerization of multifunctional acrylates" Polym. Mater. Sci. Eng., Vol. 60

Watts, D.C.; Cash, A.J. "Determination of polymerization shrinkage kinetics in visible-light-cured materials: methods development" Dent. Mater. Vol. 7, pp. 281-287 (1991)

Watts, D.C.; Cash, A.J. "Kinetic measurements of photo-polymerization contraction in resins and composites" Measurement Sciences and Technology, Vol. 2, No. 8, pp. 788-794 (1991)

Statistical References:

Dougherty, Edward R. "Probability and Statistics for the Engineering , Computing, and Physical Sciences" Prentice Hall, Inc, New Jersey (1990)

Volk, William "McGraw-Hill Series in Chemical Engineering: Applied Statistics for Engineers" McGraw-Hill Book Company, Inc., New York (1958)